

DETAILING DAPPED ENDS OF PRETENSIONED  
CONCRETE BEAMS

by

DONNA J. MADER, B.S.

THESIS

Presented to the Faculty of the Graduate School of  
The University of Texas at Austin  
in Partial Fulfillment  
of the Requirements  
for the Degree of  
MASTER OF SCIENCE IN ENGINEERING

THE UNIVERSITY OF TEXAS AT AUSTIN

May, 1990

To my parents and family for  
their constant faith in me.

## ACKNOWLEDGEMENTS

The research described herein has been made possible through funding provided by the Texas State Department of Highways and Public Transportation.

The author wishes to express appreciation to Dr. John E. Breen for his guidance and encouragement. Thanks also to Dr. James Jirsa and Dr. Ned Burns for their advice and technical assistance.

Thanks is also given to the staff of Ferguson Structural Engineering Laboratory whose assistance was essential to this project: Pat Ball, Jennifer Batson, Sharon Cunningham, Wayne Fontenot, Laurie Golding, Wayne Little, Dick Marshall, Irene Moore, Blake Stassney, and Alec Tahmassebi.

A special thanks goes out to Brian Falconer for performing an initial finite element analysis on the test specimens and to Alfredo SantoLamazza for all his hard work and advice. Thanks is also given to the concrete crew whose assistance was essential to this research: Asit Baxi, Jim Ernzen, Cliff Hall, Tony Powers, David Sanders, Alfredo SantoLamazza, Gregor Wollman, and Les Zumbrunnen.

The author also wishes to express gratitude for the advice, friendship, and support of Hakim B., Brian F., Cliff H., Traci H., Azez H., Sara M., Theresa R., and Karen W. A special thank you goes to Tony P. for providing solutions to existing problems and new problems to consider.

A separate thank you goes to Chris H. for all the abuse so freely offered.

And last but not least, thank you Mom and Dad.

## TABLE OF CONTENTS

CHAPTER 1	INTRODUCTION . . . . .	1
1.1	<u>General</u> . . . . .	1
1.2	<u>Objective and Scope</u> . . . . .	1
CHAPTER 2	LITERATURE REVIEW . . . . .	3
2.1	<u>Introduction</u> . . . . .	3
2.2	<u>Design Methods for Dapped Beams</u> . . . . .	3
2.2.1	<b>Non-prestressed Beams</b> . . . . .	3
2.2.1.1	<u>Prestressed Concrete Institute</u> <u>Design Method</u> . . . . .	3
2.2.1.2	<u>Strut-and-Tie Design Procedure</u> . . . . .	4
2.2.2	<b>Prestressed Beams</b> . . . . .	7
2.2.2.1	<u>Menon/Furlong Design Procedure</u> . . . . .	7
2.3	<u>Implementing Prestress Forces into the Strut-</u> <u>and-Tie-Model</u> . . . . .	9
CHAPTER 3	TEST PROGRAM . . . . .	15
3.1	<u>Introduction</u> . . . . .	15
3.2	<u>Design of Specimens</u> . . . . .	15
3.2.1	<b>General Description</b> . . . . .	15
3.2.2	<b>Prestressed Concrete Institute Detail</b> <b>(PCI)</b> . . . . .	17
3.2.3	<b>Menon/Furlong Detail (M/F)</b> . . . . .	21
3.2.4	<b>Orthogonal Strut-and-Tie Detail (OST)</b> . . . . .	25
3.2.5	<b>Inclined Strut-and-Tie Detail (IST)</b> . . . . .	25
3.3	<u>Materials</u> . . . . .	30
3.4	<u>Fabrication</u> . . . . .	32
3.5	<u>Test Procedure</u> . . . . .	36
3.6	<u>Instrumentation</u> . . . . .	36
CHAPTER 4	EXPERIMENTAL RESULTS . . . . .	41
4.1	<u>Introduction</u> . . . . .	41

4.2	<u>Overall Specimen Behavior</u>	41
4.2.1	General	41
4.2.2	PCI Detail	43
4.2.3	M/F Detail	46
4.2.4	OST Detail	46
4.2.5	IST Detail	48
4.3	<u>Evaluation of End Reinforcement</u>	48
4.4	<u>Behavior of Prestressing Strand</u>	52
4.5	<u>Behavior of Stirrups</u>	56
4.6	<u>Behavior of Beam Flexural Reinforcement</u>	56
4.7	<u>Overall Comparison of End Details</u>	58
4.8	<u>Design Recommendations for Implementing the Strut-and-Tie Model</u>	64
4.8.1	General	64
4.8.2	Orthogonal Strut-and-Tie	64
4.8.3	Inclined Strut-and-Tie	69
CHAPTER 5	SUMMARY AND CONCLUSIONS	73
5.1	<u>Summary</u>	73
5.2	<u>Conclusions</u>	73
5.2.1	Ultimate Capacity	74
5.2.2	Cracking Patterns	74
5.2.3	Efficiency	74
5.2.4	Comparison of Strut-and-Tie Models to Observed Behavior	74
APPENDIX A		76
REFERENCES		89

## LIST OF TABLES

<u>Table</u>		<u>Page</u>
3.1	Concrete Mix Proportions . . . . .	34
4.1	Design, Cracking, Predicted, and Failure Loads From all Tests . . . . .	42
4.2	Loads at First Measured Yielding . . . . .	51
4.3	Load at First Web Crack . . . . .	57
4.4	Volume of Steel in "D" Region of All Specimens (Excluding Main Flexural Reinforcement) . . . . .	61
4.5	Cost Rating Units for Construction Tasks . . . . .	62
4.6	Total Construction Operation Cost Rating for all Specimens . . . . .	62
4.7	Compression Forces and Angles for Orthogonal Strut-and-Tie Model . . . . .	67
4.8	Calculated and Measured Tension Forces for Orthogonal Strut-and-Tie . . . . .	67
4.9	Compression Forces and Angles for Inclined Strut-and-Tie Model . . . . .	71
4.10	Calculated and Measured Tension Forces for Inclined Strut-and-Tie . . . . .	71

## LIST OF FIGURES

<u>Figure</u>	<u>Page</u>
2.1 Prestressed Concrete Institute Reinforcement Pattern . . . . .	5
2.2 PCI Design Method Anchorage Requirements . . .	5
2.3 Strut-and-Tie Models . . . . .	6
2.4 Placement of Tie Reinforcement . . . . .	8
2.5 Menon/Furlong Design Method . . . . .	10
2.6 Menon/Furlong Anchorage Requirements . . . .	11
2.7 Strut-and-Tie Model For Transfer of Prestress to Concrete - from Ref. 13. . . . .	14
2.8 Simplified Strut-and-Tie Model Showing Corresponding Reinforcement - from Ref. 13. .	14
3.1 Test Specimen Dimensions . . . . .	16
3.2 Layout of Prestressing Strand . . . . .	18
3.3 #3 Vertical Stirrups . . . . .	18
3.4 #5 Hoops for PCI Detail . . . . .	19
3.5 Bearing Plate . . . . .	20
3.6 Reinforcement Layout for PCI Detail . . . . .	22
3.7 Photograph of PCI Reinforcement Layout . . .	22
3.8 Steel Strap in M/F Detail . . . . .	23
3.9 Reinforcement Layout for M/F Detail . . . . .	24
3.10 Photograph of M/F Reinforcement Layout . . .	24
3.11 OST Design Model . . . . .	26
3.12 Reinforcement Layout for OST Detail . . . . .	27
3.13 Photograph of OST Reinforcement Layout . . .	27
3.14 Strut-and-Tie Models Combined to Design IST Detail . . . . .	28
3.15 IST Detail Design Model . . . . .	29
3.16 Reinforcement Layout for IST Detail . . . . .	31

3.17	Photograph of IST Reinforcement Layout . . . . .	31
3.18	Stress-Strain Curve of Prestressing Strand . . . . .	33
3.19	Stress-Strain Curve of #5 Reinforcing Bar . . . . .	33
3.20	Concrete Strength vs. Time . . . . .	34
3.21	End Plate of Prestressing Bed . . . . .	35
3.22	Draping Hardware . . . . .	35
3.23	Test Set-Up . . . . .	37
3.24	PCI Gage Location . . . . .	39
3.25	M/F Gage Location . . . . .	39
3.26	OST Gage Location . . . . .	40
3.27	IST Gage Location . . . . .	40
4.1	Cracking, Predicted, and Ultimate Failure Loads For All Specimens . . . . .	42
4.2	Load vs. Deflection Curve For All Specimens . . . . .	44
4.3	PCI Specimen at Failure . . . . .	44
4.4	Restrained #5 Hoop . . . . .	45
4.5	M/F Specimen at Failure . . . . .	47
4.6	OST Specimen at Failure . . . . .	47
4.7	IST Specimen at Failure . . . . .	49
4.8	Applied Load vs. Strain in Yielded Vertical Reinforcement of All Tests . . . . .	49
4.9	Applied Load vs. Strain in Main Horizontal Dap Reinforcement of All Tests . . . . .	51
4.10	Applied Load vs. Strain in Inclined Bars of IST Test . . . . .	53
4.11	Applied Load vs. Strain in Local Vertical Dap Reinforcement of All Tests . . . . .	53
4.12	Applied Load vs. Strain in Straight Strand of OST Test . . . . .	55
4.13	Applied Load vs. Straight Strand Slip of All Tests . . . . .	55



4.14	Applied Load vs. Stirrup Strain of All Tests . . . . .	57
4.15	Applied Load vs. Strain in Main Flexural Reinforcement (Gage 10) of All Tests . . . . .	59
4.16	Discontinuity Zone at Beam End . . . . .	59
4.17	Ultimate Load per Volume of Steel of All Tests . . . . .	61
4.18	Ultimate Load per Construction Rating Unit of All Tests . . . . .	63
4.19	Final Strut-and-Tie Model - Orthogonal . . . . .	65
4.20	Percent Difference Between Measured and Calculated Tie Forces at Ultimate of OST Model . . . . .	68
4.21	Final Strut-and-Tie Model - Inclined . . . . .	70
4.22	Percent Difference Between Measured and Calculated Tie Forces at Ultimate of IST Model . . . . .	72
A.1	Applied Load vs. Strain in Tie 2 of PCI Test.	77
A.2	Applied Load vs. Strain in Tie 2 of M/F Test.	77
A.3	Applied Load vs. Strain in Tie 2 of OST Test.	78
A.4	Applied Load vs. Strain in Tie 2 of IST Test.	78
A.5	Applied Load vs. Strain in Horizontal Dap Reinforcement of PCI Test . . . . .	79
A.6	Applied Load vs. Strain in Horizontal Dap Reinforcement of M/F Test . . . . .	79
A.7	Applied Load vs. Strain in Horizontal Dap Reinforcement of OST Test . . . . .	80
A.8	Applied Load vs. Strain in Horizontal Dap Reinforcement of IST Test . . . . .	80
A.9	Applied Load vs. Strain in Tie 3 of PCI Test.	81
A.10	Applied Load vs. Strain in Tie 3 of M/F Test.	81
A.11	Applied Load vs. Strain in Tie 3 of OST Test.	82
A.12	Applied Load vs. Strain in Tie 3 of IST Test.	82

A.13	Applied Load vs. Straight Strand Strain of PCI Test . . . . .	83
A.14	Applied Load vs. Straight Strand Strain of M/F Test . . . . .	83
A.15	Applied Load vs. Straight Strand Strain of IST Test . . . . .	84
A.16	Applied Load vs. Draped Strand Strain of PCI Test . . . . .	84
A.17	Applied Load vs. Draped Strand Strain of M/F Test . . . . .	85
A.18	Applied Load vs. Draped Strand Strain of OST Test . . . . .	85
A.19	Applied Load vs. Draped Strand Strain of IST Test . . . . .	86
A.20	Applied Load vs. Draped Strand Slippage of All Tests . . . . .	86
A.21	Applied Load vs. Main Flexural Reinforcement Strain of PCI Test . . . . .	87
A.22	Applied Load vs. Main Flexural Reinforcement Strain of M/F Test . . . . .	87
A.23	Applied Load vs. Main Flexural Reinforcement Strain of OST Test . . . . .	88
A.24	Applied Load vs. Main Flexural Reinforcement Strain of IST Test . . . . .	88

## CHAPTER I INTRODUCTION

### 1.1 General

As time progresses, there is an increasing need for building and maintaining a better national transportation system. Economical longer span bridges are essential in reaching this goal. The Texas State Department of Highways and Public Transportation (TSDHPT) has made substantial progress in this direction through the use of high-strength and prestressed concrete as well as the use of "drop-in" beams which stretch span length when combined with cantilever spans.

Several design methods are currently being used to determine the internal forces occurring within the dapped-ends of these "drop-in" concrete beams. The TSDHPT now uses a method which requires the construction of a steel strap within the end of the beam. This is a time consuming and expensive task which can possibly be avoided through use of better design methods. The strut-and-tie method suggested by Schlaich et al. [17] is becoming a more effective design tool. However, it needs experimental verification and economic evaluation to be adopted for use in American design practices.

### 1.2 Objective and Scope

The research described within this thesis is part of a larger study sponsored by the TSDHPT on detailing concrete beams used in Texas highway bridges. In this portion of the project, methods used for detailing the

discontinuity in the ends of dapped pretensioned beams were investigated with emphasis on incorporating prestressing forces into the design.

Two design methods which had primarily been developed for non-pretensioned beams and one method developed specifically for pretensioned beams were studied and compared: 1) Prestressed Concrete Institute (PCI) design method [14], 2) Menon/Furlong design method [11], and 3) the strut-and-tie model [17]. These three methods were evaluated through tests to determine how prestressing forces effect the load path in a beam.

The physical tests consisted of two beams with four different end details. By studying the behavior, recommendations for future design models can be made.

## CHAPTER 2

### LITERATURE REVIEW

#### 2.1 Introduction

Several different design methods have been shown by tests, to be safe for the design of reinforcement for dapped beams. Two of these, the PCI procedure [9,10,14] and the strut-and-tie procedure [7], when originally developed did not account for prestressing forces. Subsequent to its original development, recommendations have been made for implementing prestress forces into the strut-and-tie model [17]. The third design method, the Menon/Furlong procedure [11], was developed especially for pretensioned beams. This chapter includes an outline of each of these design methods as well as suggestions that have been made for implementing prestress forces into the strut-and-tie model.

#### 2.2 Design Methods for Dapped Beams

##### 2.2.1 **Non-prestressed Beams.**

2.2.1.1 Prestressed Concrete Institute Design Method. This design method is based on research conducted at the University of Washington [9,10] and is presented in the Prestressed Concrete Institute Design Handbook [14]. The basic design procedure will be outlined herein. For a more thorough description of the PCI method see Reference 2.

The basic reinforcement layout proposed by the PCI procedure is shown in Figure 2.1. Hanger reinforcement,

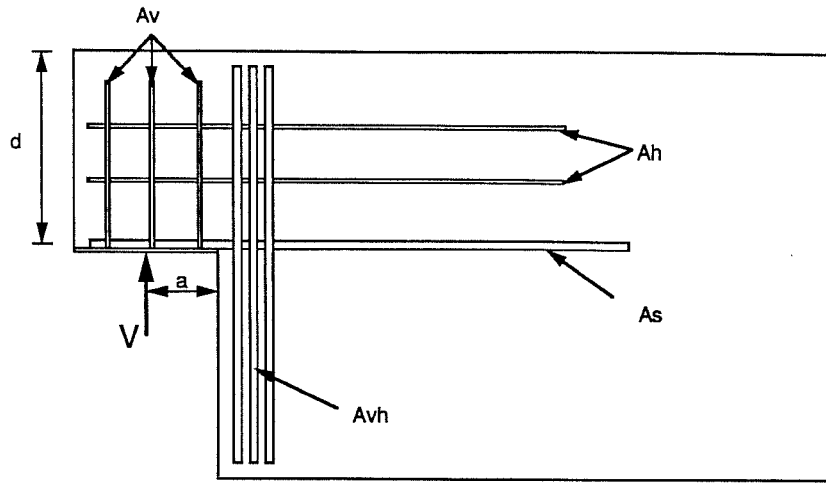
$A_{vh}$ , is designed to carry the total shear due to factored loads. These bars should be placed as close to the re-entrant corner as possible. Required flexural reinforcement within the dap,  $A_s$ , is determined by the moment  $M = V \cdot a$ . Additional horizontal reinforcement,  $A_h$ , in the dapped end is based on shear friction analysis. A minimum area equal to one-half of the flexural reinforcement,  $A_s$ , must be provided for shear friction reinforcement. Local shear reinforcement,  $A_v$ , is also required to resist a possible diagonal tension crack in the dap.

The PCI design procedure also specifies reinforcement anchorage requirements. These are shown in Figure 2.2.

2.2.1.2 Strut-and-Tie Design Procedure. Based on applications of the theory of plasticity, concrete members can be modeled as a series of struts, ties, and nodes as suggested by Schlaich et al. [17], Marti [7,8], and others. By replacing a complex system with a strut-and-tie model, internal forces within the system can be estimated. Barton [2] thoroughly covers the strut-and-tie model application to dapped beams so only a brief summary is presented in this thesis.

Dapped beams can be modeled using several different strut-and-tie models (Fig. 2.3). The model of Fig 2.3a includes only orthogonal ties to transfer forces through the beam. The model of Fig. 2.3b contains a diagonal tie across the re-entrant corner of the dap. The third model shown in Fig. 2.3c is a combination of the first two.

The strut-and-tie design process is initiated by choosing a basic model and assuming a compression strut angle. It normally ensures satisfactory crack control at service load levels if this angle coincides with the



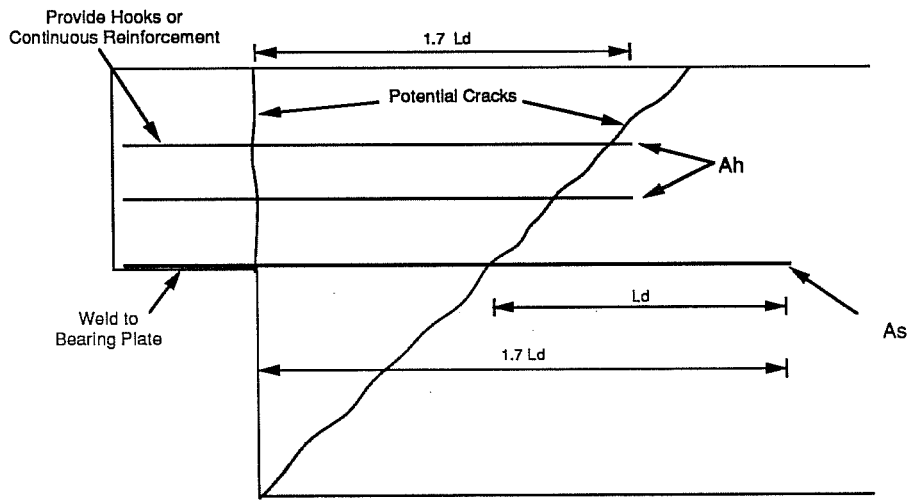
$$A_{vh} > V/f_y$$

$$A_s > (V \cdot a) / (f_y \cdot d)$$

$$A_h > V / f_y - A_s$$

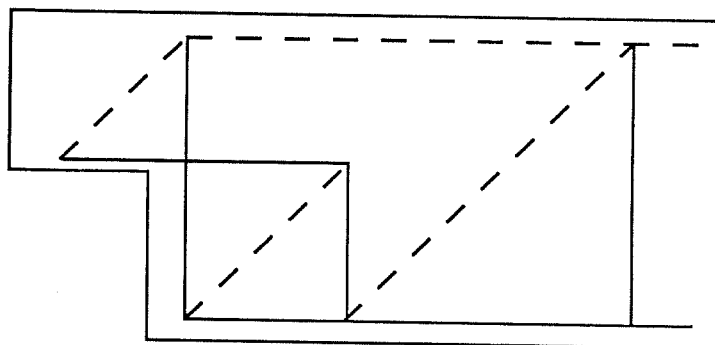
$$A_v > 1/2 f_y (V - 2 \sqrt{f'_c} b d)$$

Figure 2.1 Prestressed Concrete Institute Reinforcement Pattern

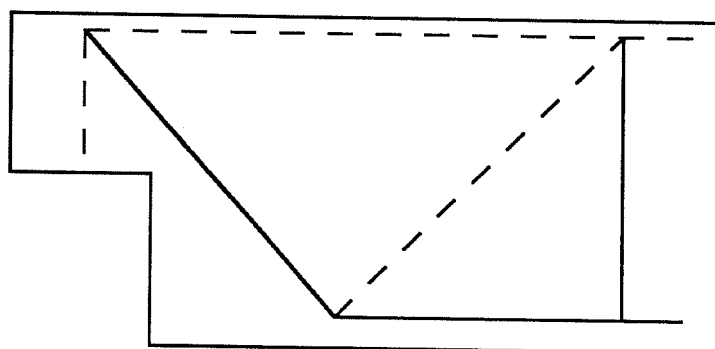


Ld = ACI Development Length

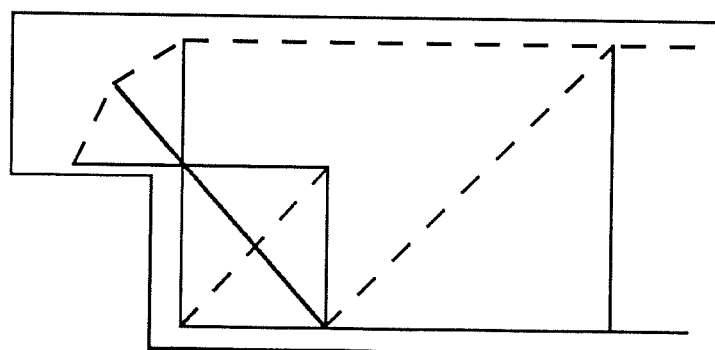
Figure 2.2 PCI Design Method Anchorage Requirements



a. Orthogonal Strut-and-Tie Model



b. Diagonal Strut-and-Tie Model



c. Combined Strut-and-Tie Model

--- compression strut  
 ——— tension tie

Figure 2.3 Strut-and-Tie Models



angle of the elastic principal stress. Strut angles are limited to a range of 30 to 60 degrees in the CEB code [4].

After a strut angle is chosen, tie forces are calculated from geometry. Required reinforcement areas, based on the tie forces, must be placed within boundaries of zones in which the ties are considered to act (Fig. 2.4).

The final step in the strut-and-tie design process is to check the concrete compressive stresses. Compressive stresses are limited to some value less than  $f_c'$ . Diagonal cracks are typically steeper at first cracking than at failure due to force redistribution. Therefore, compressive struts at failure often cross initial cracks and tensile reinforcement. These two factors lead to a reduced or effective strength at failure.

The effective concrete strength limit is expressed as  $\nu_e f_c'$  where  $\nu_e$  is an efficiency factor and  $f_c'$  is the 28-day compressive strength. Much research has been conducted to determine the value of  $\nu_e$  [5,12,15,16,17]. As shown by Powers [13], values for  $\nu_e$  compared closely to those calculated using the following equation proposed by Bergmeister et al. [3].

$$\nu_e = 0.6 [0.5 + 15/\sqrt{f_c'}]$$

The units of  $f_c'$  must be in psi for this equation to be valid.

## 2.2.2 Prestressed Beams.

2.2.2.1 Menon/Furlong Design Procedure. This design method is based on research conducted at the University of Texas at Austin [11]. The TSDHPT currently

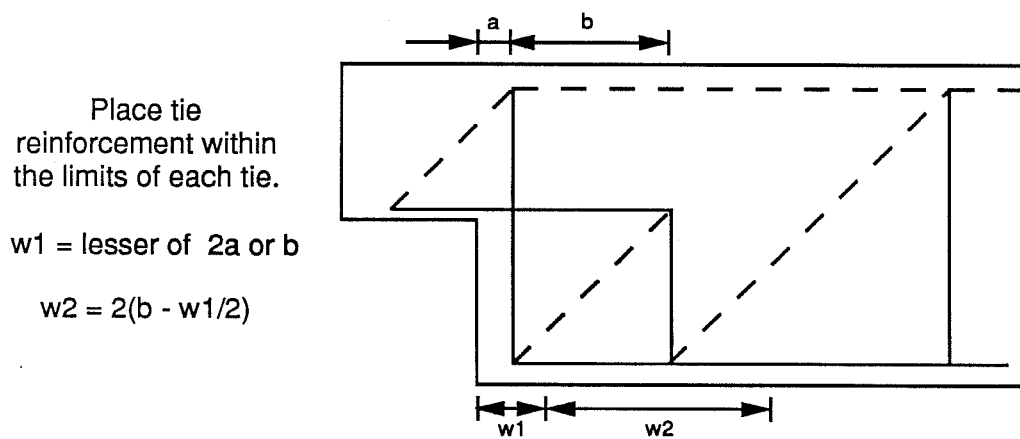


**Figure 2.4 Placement of Tie Reinforcement**

uses the Menon/Furlong method for design of highway bridges. The basic reinforcement layout, including a steel strap, is shown in Figure 2.5a.

The first step in the Menon/Furlong design method is to determine the amount of horizontal shear reinforcement required based on shear friction analysis. A crack is assumed to form parallel to the hanger strap as shown in Figure 2.5b. Required reinforcement,  $A_s$ , is determined by the following equation:

$$A_s = 1/f_y (V_u/\mu' - P_u)$$

where  $f_y$  = yield stress of reinforcement

$V_u$  = applied shear force at crack

$P_u$  = applied normal force at crack

$\mu'$  = weighted coefficient of friction based on relative steel and concrete areas.

Determining the required strap area is the second step in the Menon/Furlong procedure. This is accomplished by analyzing a section of the end of the beam defined by an assumed diagonal crack (Fig 2.5c). This crack begins at the re-entrant corner of the dap and is assumed to extend with a horizontal projection equal to twice the height of the dap. The height of the section at the far end is taken as the depth of the neutral axis at that point. Required strap area is determined by summing moments about point A in Figure 2.5c.

Reinforcement anchorage recommendations are shown in Figure 2.6. The Menon/Furlong design procedure is presented in Reference 2 in more detail.

### 2.3 Implementing Prestress Forces into the Strut-and Tie Model.

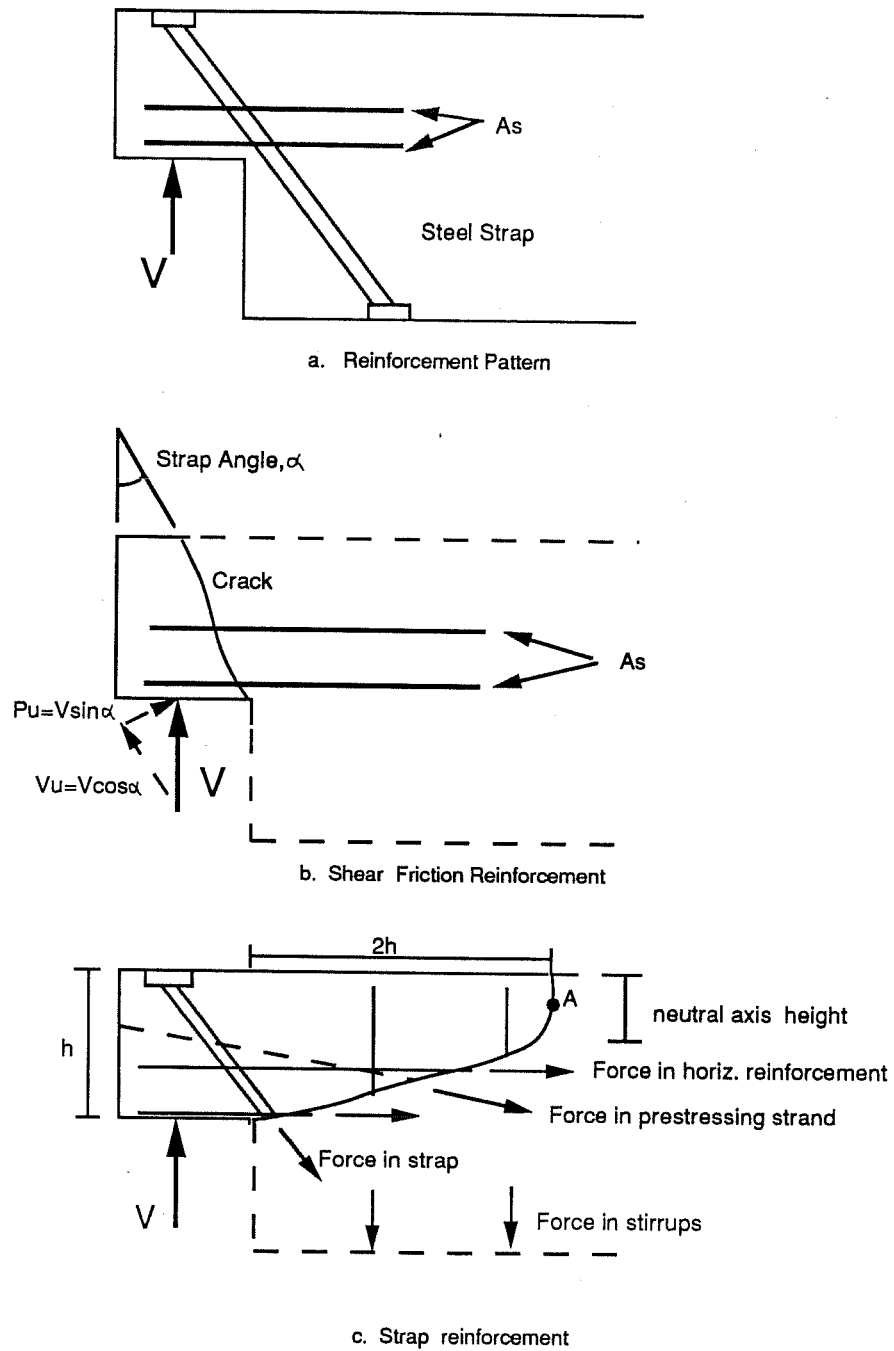
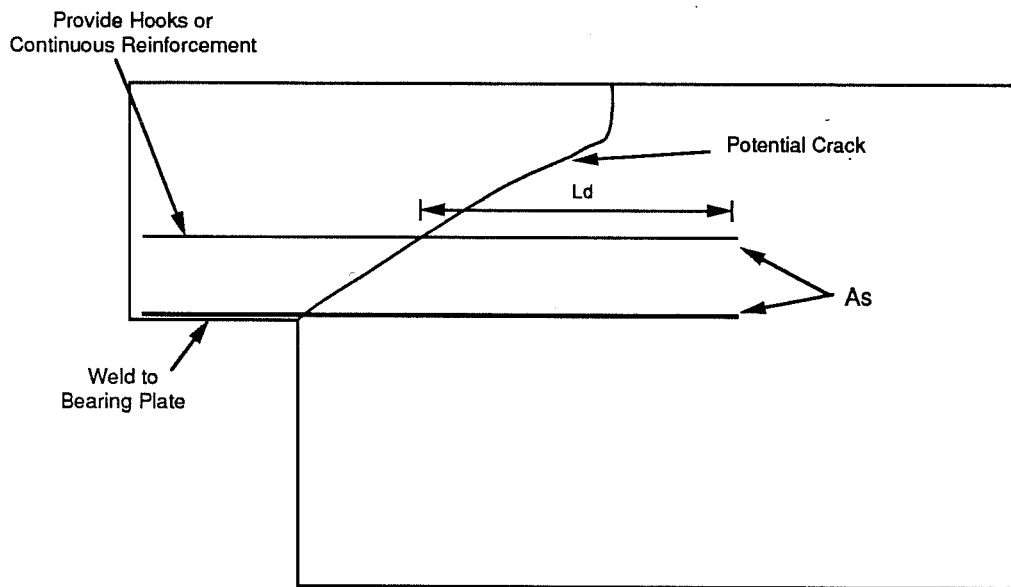


**Figure 2.5 Menon/Furlong Design Method**



$L_d$  = ACI Development Length

**Figure 2.6 Menon/Furlong Anchorage Requirements**

Much literature is available on the strut-and-tie design model for reinforced concrete, but very little is available on applying this model to prestressed concrete. Schlaich et al. [17] suggested that a prestressed beam be treated exactly the same as a non-prestressed beam except that the prestress force should be modeled as an additional axial load applied to the ends of the beam at the centroid of the strands. Any harped or draped strands would have the vertical component applied as forces wherever they occur.

Based on such models, the major difference between prestressed and non-prestressed reinforcement is that part of the capacity of a prestressed strand is applied as a force to the beam before external load is applied to the beam. Therefore, the resisting load-carrying capacity of a tendon is limited to the residual capacity defined as the tendon capacity minus the applied effective prestress force. This available tendon residual capacity is added to the capacity of any non-prestressed reinforcement to provide the total flexural capacity of the tension chord. Thurliman [18] noted that generally the available prestress tendon residual capacity is approximately equal to the capacity of non-prestressed reinforcement. Therefore, as the beam is loaded, both steels should reach their yield strains simultaneously.

The model proposed by Schlaich et al. [17] is not completely applicable to pretensioned beams because it does not account for the transfer length of the prestressing strand since the prestress force is zero at the end of the beam. Bergmeister [3] suggested applying the prestress force in three equal increments along the

transfer length taken as  $50d_b$  [6], where  $d_b$  is the diameter of the prestressing strand. This results in the simple strut-and-tie model shown in Figure 2.7.

In research conducted by Powers [13], prestress forces were assumed to be applied at the third points of the  $50d_b$  transfer lengths and applied at the centroid of all strands (Fig 2.8). Vertical forces from draped strands were applied at the drape point only. The loading pattern assumed by Powers resulted in a conservative strut-and-tie model design in all but two cases. These two cases were unconservative by less than 1% so it can be effectively termed a conservative model.

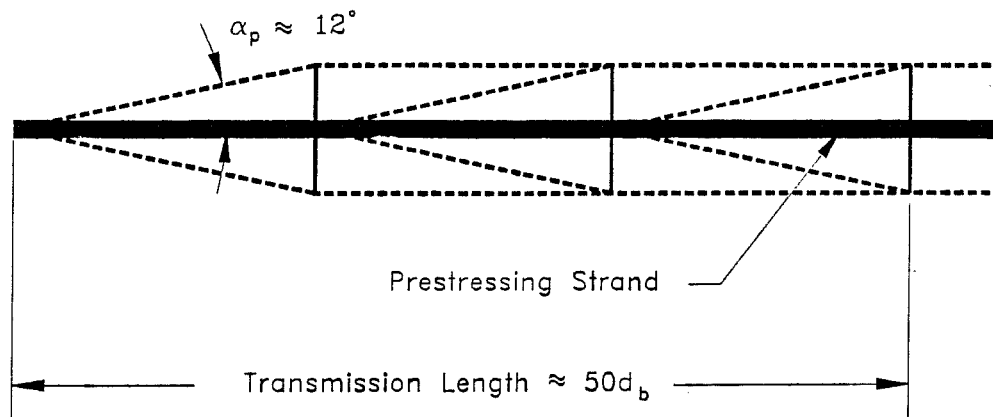


**Figure 2.7 Strut-and-Tie Model For Transfer of Prestress to Concrete - from Ref. 13.**

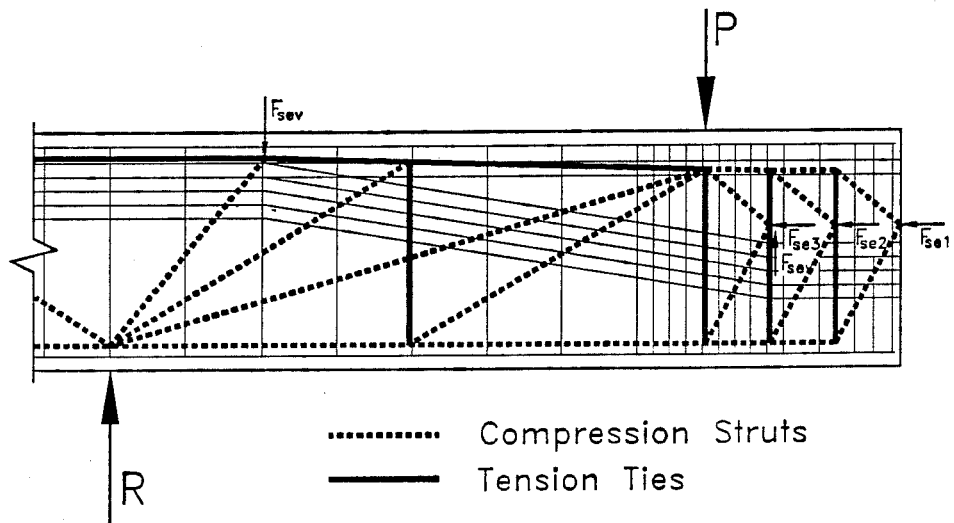


**Figure 2.8 Simplified Strut-and-Tie Model Showing Corresponding Reinforcement - from Ref. 13.**



CHAPTER 3  
TEST PROGRAM

3.1 Introduction

Four pretensioned dapped beam end details were tested in order to evaluate the different design methods. The details designed using different strut-and-tie models were compared to details designed using other design methods to determine the most efficient placement of reinforcing steel.

Within this paper the test specimens are referred to with the following abbreviations:

Prestressed Concrete Institute - PCI

Menon/Furlong - M/F

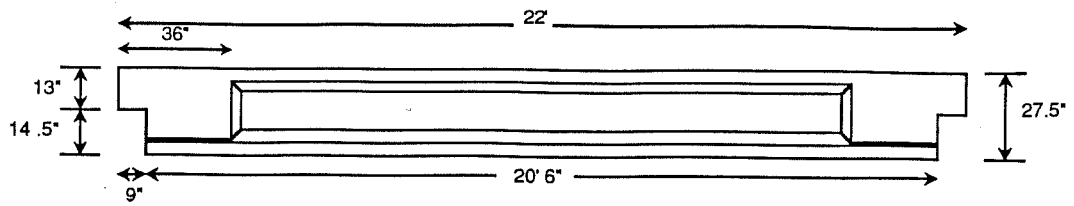
Orthogonal Strut-and-Tie - OST

Inclined Strut-and-Tie - IST

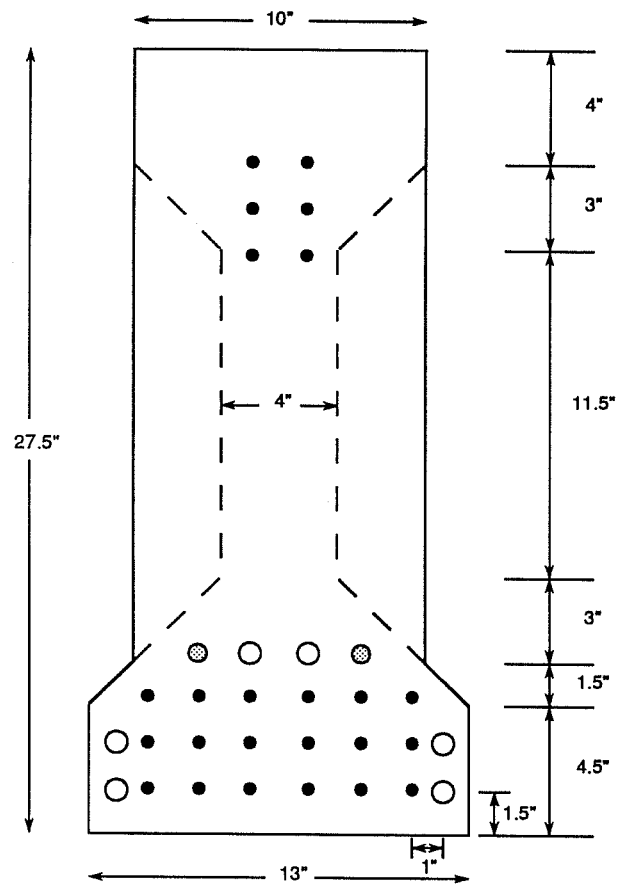
3.2 Design of Specimens

**3.2.1 General Description.** A total of two test beams were constructed. The beams used in this study were approximately half scale models of the Texas type IV beams used in many highway bridges. The overall geometry of the specimens and their cross-section is shown in Figures 3.1a and b. All specimens were designed for an ultimate load of 175 kips which produced an end shear of 100 kips.

An initial study was performed using the prestressing forces and loads in prototype Type IV beams to determine the level of combined stresses in the dap region. The test beams were designed so that the stresses in the test



a. Side View



- 3/8" prestressing strand
- #6 reinforcing bar
- ⊗ #5 reinforcing bar

\*All reinforcement is 1 5/8" on center unless otherwise labeled.

b. Cross-Section

Figure 3.1 Test Specimen Dimensions

beam daps would match those in the full scale beams. The inclination angle of the draped prestressing strand was also consistent with the angle in the actual beams. Total prestressed reinforcement consisted of twenty-four 3/8" pretensioned strands. Eighteen straight strands were placed in the bottom flange of the beams. The other six strands were inclined through the top flange near the ends of the beams and horizontal through the middle section (Fig 3.2). Each strand was stressed to 18 kips for an overall prestressing force of 432 kips.

Non-prestressed flexural reinforcement consisted of six #6 and two #5 bars arranged around the prestressing strand in the bottom flange. Flexural capacity of the beams was designed to be 25% greater than shear capacity to ensure a shear failure at the dapped end. One #2 bar was placed in the top flange in order to help in constructing the cage. Away from the ends of the beams, #3 stirrups (see Fig 3.3) were placed at six inches on center to provide the necessary shear strength. Details of reinforcement in the end regions are given later.

### **3.2.2 Prestressed Concrete Institute Detail (PCI).**

The first test detail was designed using the Prestressed Concrete Institute method [14] described in Section 2.2.1.1. The main hanger reinforcement consisted of three #5 hoops which looped around the prestressed reinforcement (Fig 3.4). Three #5 bars welded to a bearing plate provided auxiliary flexural reinforcement in the dap. The development length of these bars is shown in Figure 3.5.

Horizontal shear reinforcement across the dap interface was provided by one #3 and one #4 closed ties. Local vertical shear reinforcement within the dap

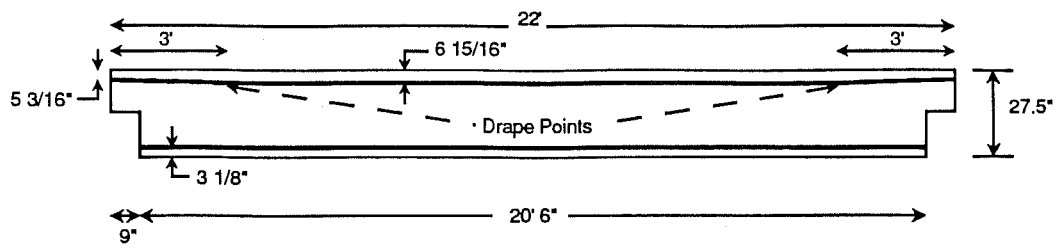


Figure 3.2 Layout of Prestressing Strand

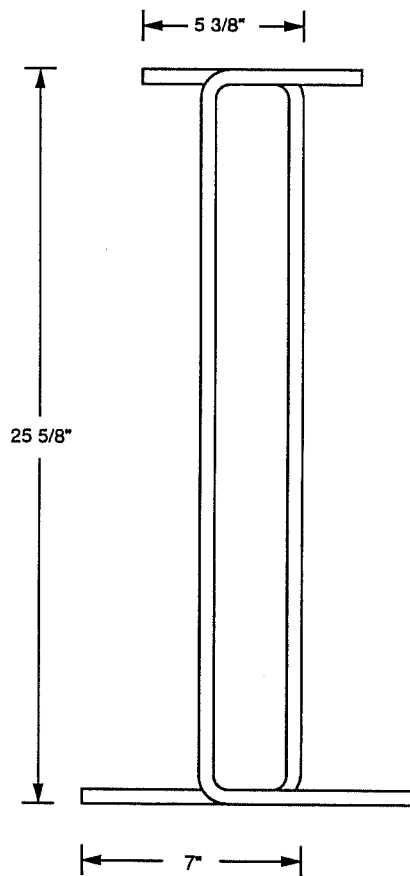
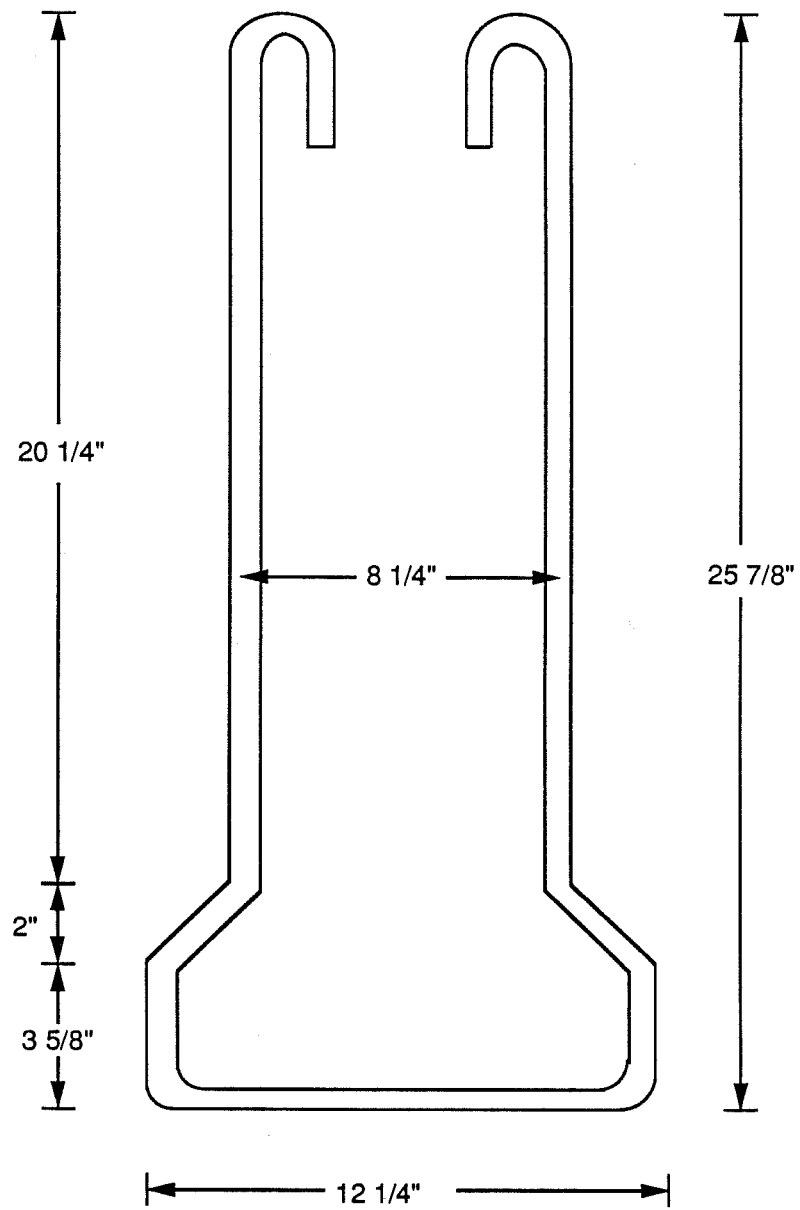
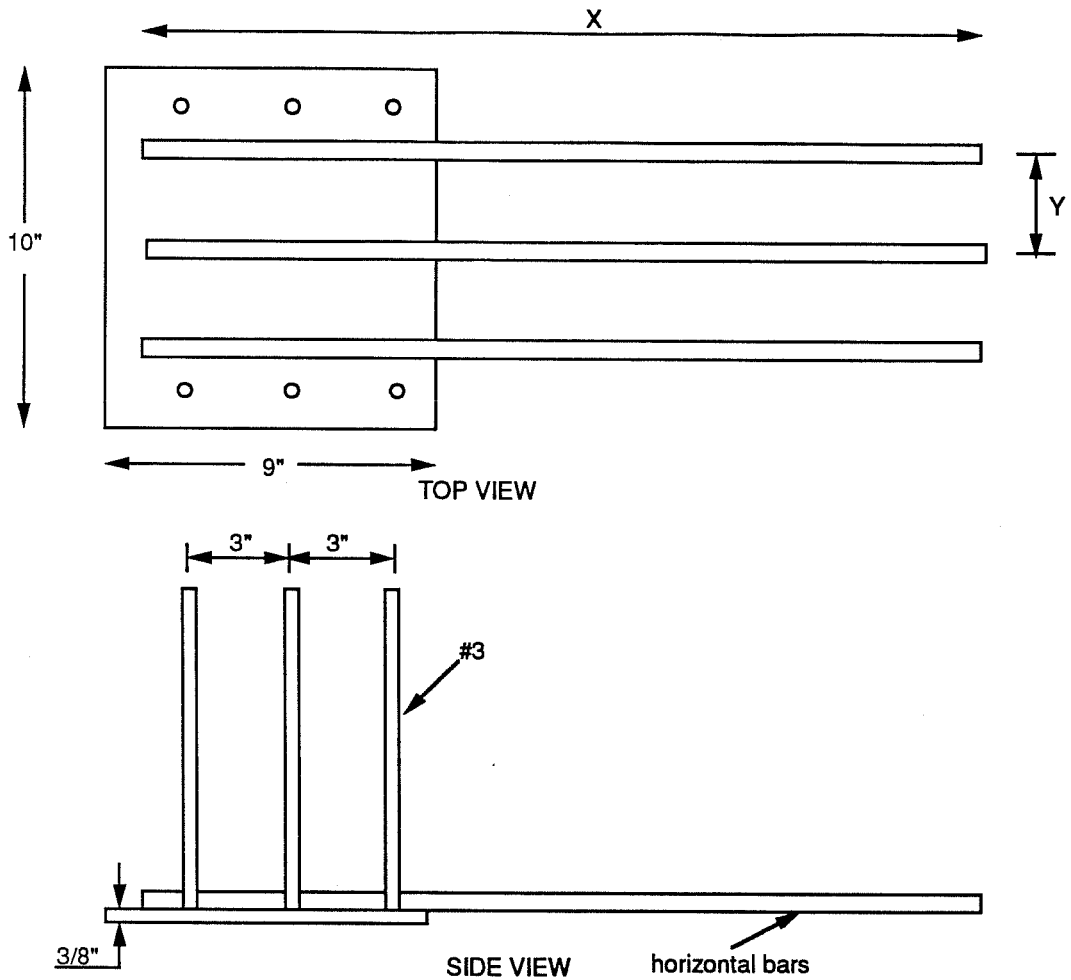


Fig. 3.3 #3 Vertical Stirrups



**Figure 3.4 #5 Hoops for PCI Detail**



Detail	Horizontal Bar Size	Number of Bars	Length of Bars (X)	Spacing of Bars (Y)
PCI	#5	3	35 "	2.5 "
M/F	#4	3	23"	2.5"
OST	#5	4	34.5"	2.25"
	#4	1	34.5"	1.75"
IST	#6"	2	34.75"	1.5"

\* Not welded to plate

Figure 3.5 Bearing Plate

consisted of three #3 closed hoops. The PCI procedure [14] does not state how this local vertical reinforcement should be positioned with respect to the normal beam shear reinforcement. According to the ACI Building Code [1], maximum stirrup spacing is 20.6 inches for these beams. One #3 stirrup was spaced approximately midway between the #5 stirrups which were at the end of the full depth section and the normal #3 stirrups which began at the cross-section change 36 inches from the end of the beam. The detailing layout is shown in Figure 3.6 with a photograph in Figure 3.7.

**3.2.3 Menon/Furlong Detail (M/F).** The Menon/Furlong design procedure [11] is currently used by the TSDHPT and is described in Section 2.2.2.1. To begin the design, the steel strap was assumed to be at an angle as close as possible to that in the Texas Type IV beams as shown in Figure 3.8.

The horizontal steel across the dap interface required by shear friction analysis (shown in Figure 3.9) consisted of three #4 bars welded to a bearing plate similar to the PCI detail (Fig 3.5) and one #3 hoop above the bearing plate in the dap.

By summing moments according to the Menon/Furlong method, a strap of four 3/8"x1" steel plates was found to provide adequate strength. Two #3 stirrups were placed within the end 36 inches of the beam (Fig 3.9) and were included when summing moments. A detailed drawing of this strap is shown in Figure 3.8. Local shear strength within the dap was provided for using #3 hoops identical to those used for the PCI procedure.

The overall reinforcement layout is shown in Figure 3.9 and pictured in Figure 3.10.

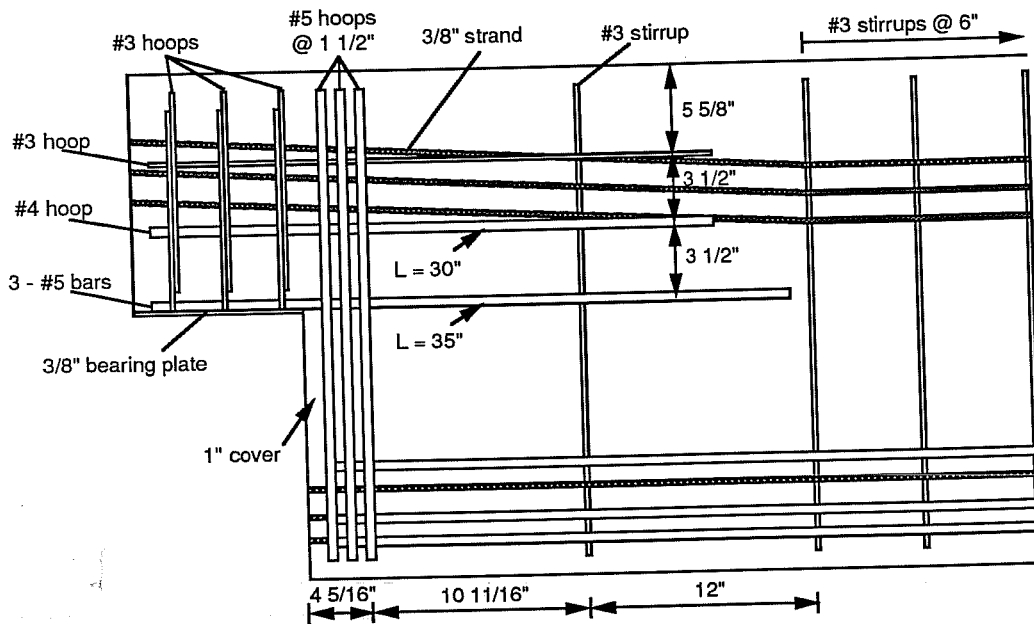


Figure 3.6 Reinforcement Layout for PCI Detail

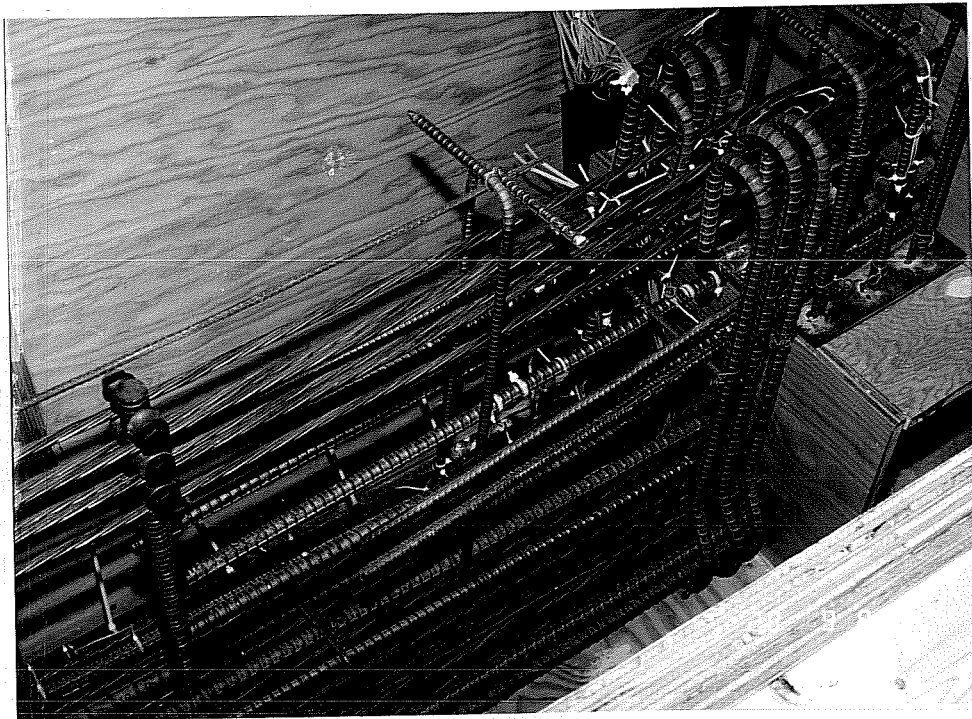


Figure 3.7 Photograph of PCI Reinforcement Layout



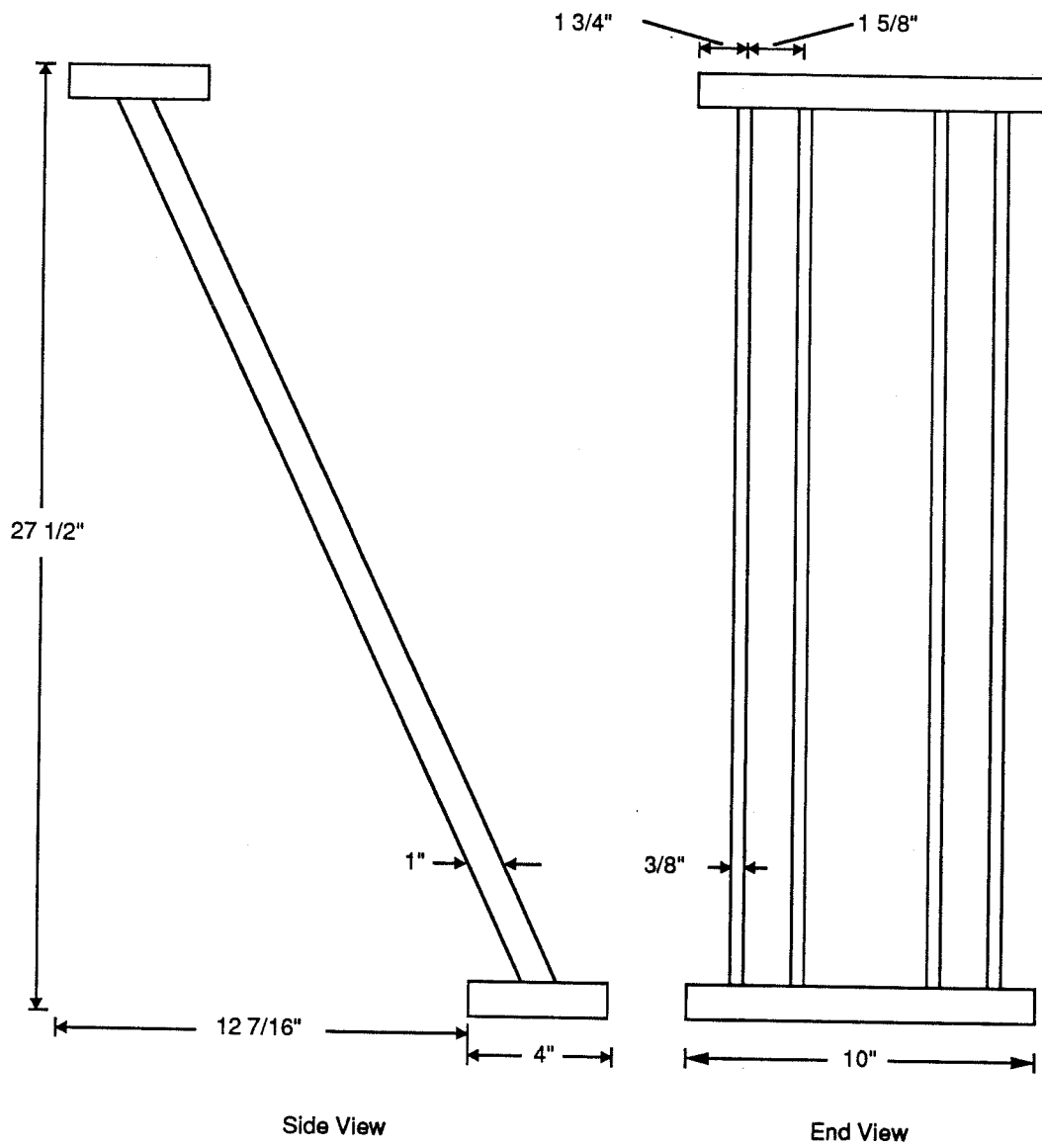


Figure 3.8 Steel Strap In M/F Detail

**3.2.4 Orthogonal Strut-and-Tie Detail (OST).** The third specimen was designed using the strut-and-tie model [7,17] shown in Figure 3.11. A compression strut angle of 49.6 degrees was chosen based on the geometry of the test specimen. Horizontal tension tie 6 was positioned at the center of gravity of the straight prestressing strand. The non-stressed flexural reinforcement was included to provide a 25% safety margin against flexural failure.

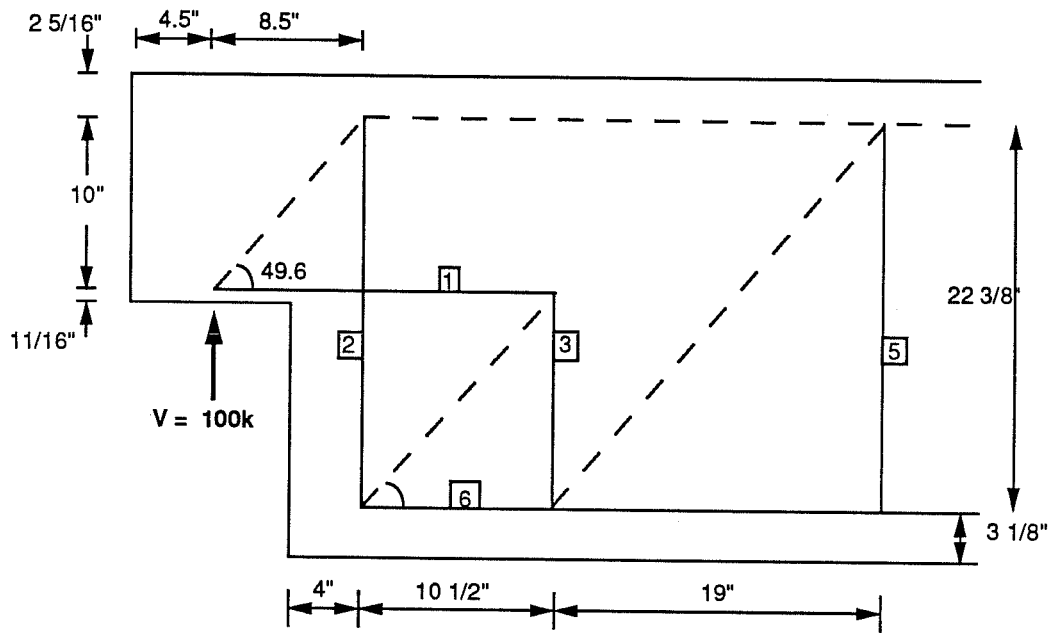
Four #5 and one #4 bar provided the steel necessary for tension tie 1 in the dapped end. These bars were welded to a bearing plate similar to the one used in the PCI method (Fig 3.5).

Vertical tension tie forces were determined from the geometry of the strut-and-tie model. An additional 15 kips was added to each vertical tie to account for the tension induced by applying one-third of the prestressing force at each third of the development length. (see Section 2.3 and Fig 2.7). The vertical stirrups consisted of #4 closed hoops and #3 stirrups identical to those used through the middle of the beam.

No local shear reinforcement was required by this strut-and-tie model within the dap, but two #3 hoops were provided to carry the tension induced by the inclined prestressing strand.

The reinforcement layout for the OST detail is shown in Figure 3.12 and pictured in Figure 3.13.

**3.2.5 Inclined Strut-and-Tie Detail (IST).** Detailing of the final specimen was designed by combining two strut-and-tie models (Fig. 3.14). It was assumed that each model would carry half of the design load. The reinforcement requirements were then combined (Fig. 3.15).



Tie	Force (kips)	Area Required (in <sup>2</sup> )	Area Provided (in <sup>2</sup> )	Description of Reinforcement
1	85	1.42	1.44	Four #5 bars
2	115	1.91	2.0	Five #4 closed hoops
3	115	1.91	2.0	Five #4 closed hoops
5	115	1.91	1.98	Nine #3 stirrups
6	85	1.42	4.79	Two #5 bars Six #6 bars Eighteen 3/8" strands

Figure 3.11 OST Design Model

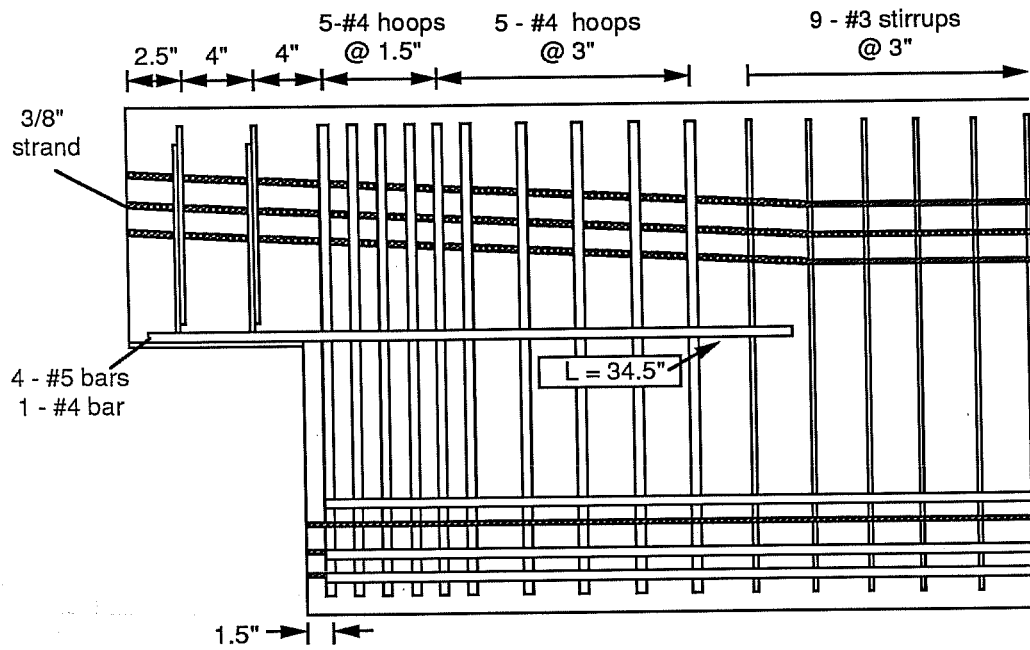


Figure 3.12 Reinforcement Layout for OST Detail

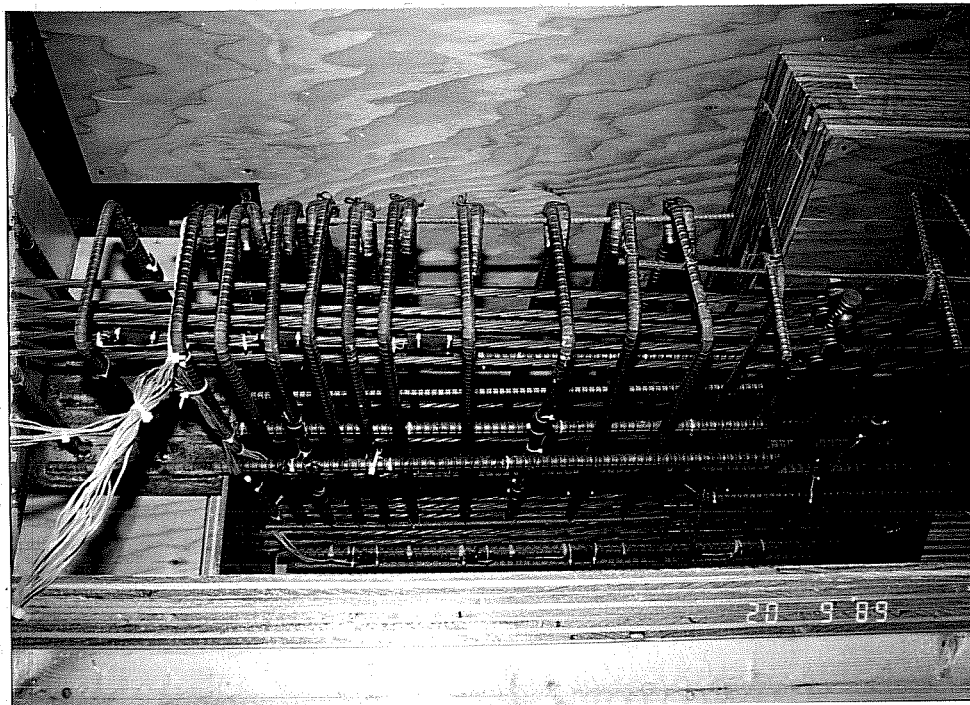


Figure 3.13 Photograph of OST Reinforcement Layout

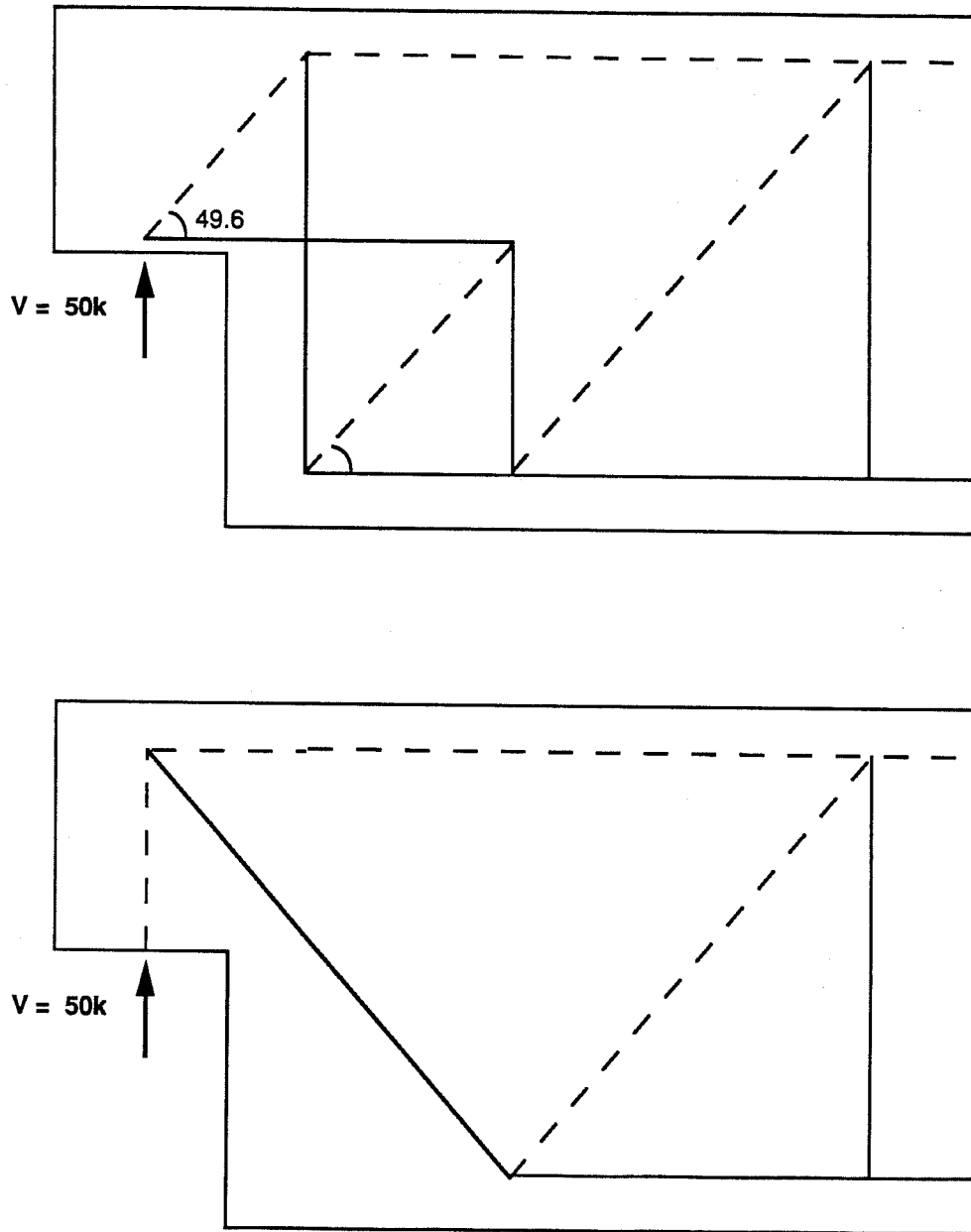
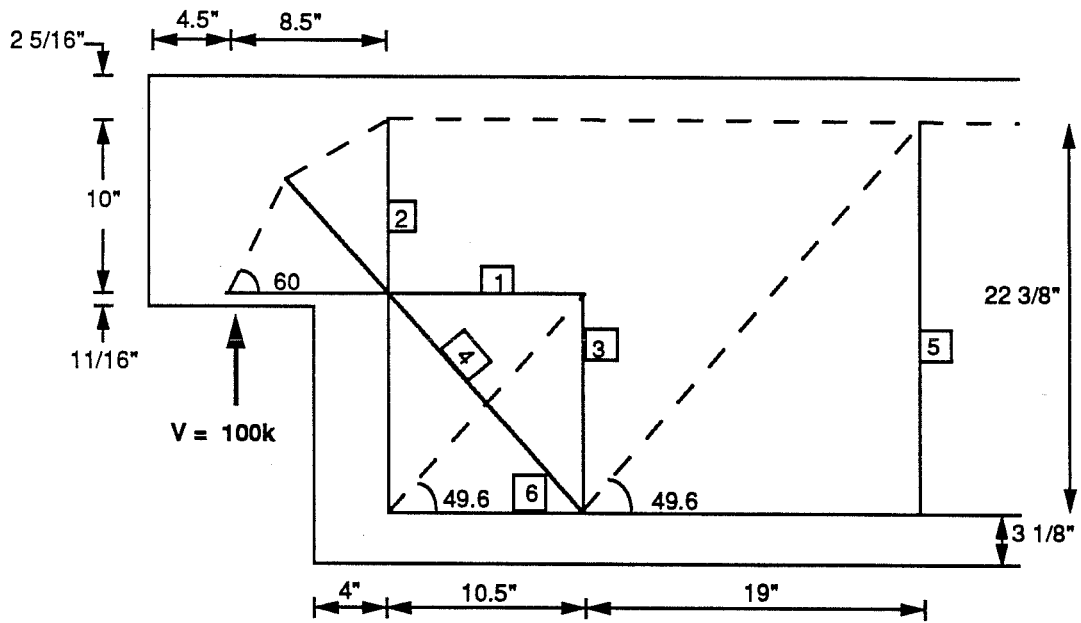


Figure 3.14 Strut-and-Tie Models Combined to Design IST Detail



Tie	Force (kips)	Area Required (in <sup>2</sup> )	Area Provided (in <sup>2</sup> )	Description of Reinforcement
1	42.5	0.71	0.88	Two #6 hooked bars
2	65	1.08	1.10	Five #3 closed hoops
3	65	1.08	1.10	Five #3 closed hoops
4	65.5	1.09	1.24	Four #5 hooked bars
5	115	1.91	1.98	Nine #3 stirrups
6	42.5	0.71	4.17	Six #6 bars Eighteen 3/8" strands

Figure 3.15 IST Detail Design Model

The diagonal tension tie across the corner of the dap consisted of four #5 hooked bars (Fig. 3.16). Two of these were continuous with the main flexural reinforcement and two were only extended longitudinally twelve inches to provide development length [1].

Horizontal tie 1 within the dap consisted of two #6 hooked bars. These were not welded to the bearing plate although the plate was still provided.

Horizontal tie 6 consisted of 18 prestressing strands and six #6 bars. The #5 bars in the IST end of the beam were bent up to provide reinforcement for tie 4.

An additional 15 kips was added to vertical ties 2, 3, and 5 to account for the tension applied by the prestressing strand as suggested by Bergmeister [3]. Vertical tie 2 reinforcement was #3 closed hoops like those in the OST detail. The same type of full height hoops were used for vertical tie 3 reinforcement. #3 stirrups identical to those used through the middle of the beam were used for tie 5 reinforcement. Two #3 hoops were placed vertically in the dap to carry the tension applied by the inclined prestressing strand.

Figure 3.16 shows the reinforcement layout for the IST detail and Figure 3.17 is a picture of the same.

### 3.3 Materials

The prestressing strand used in this study was 3/8" low-relaxation seven-wire strand with a yield strength of 270 ksi donated by Florida Wire and Cable Company. Tension tests performed on the strand resulted in an average modulus of elasticity of 27,900 ksi and an average yield stress of 242 ksi. Figure 3.18 shows the stress-strain curve for the strand.

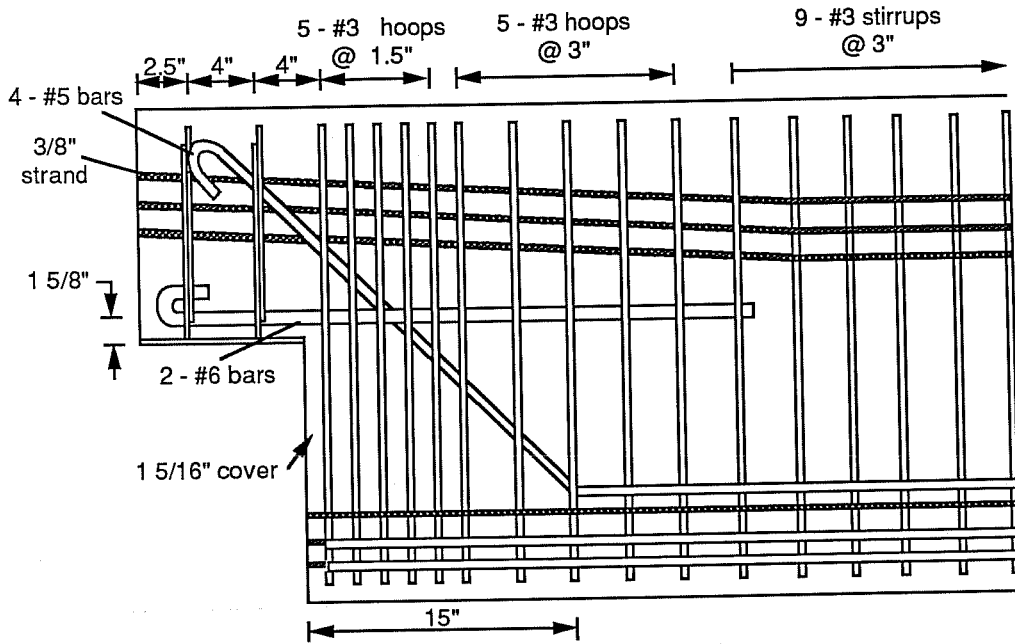


Figure 3.16 Reinforcement Layout for IST Detail

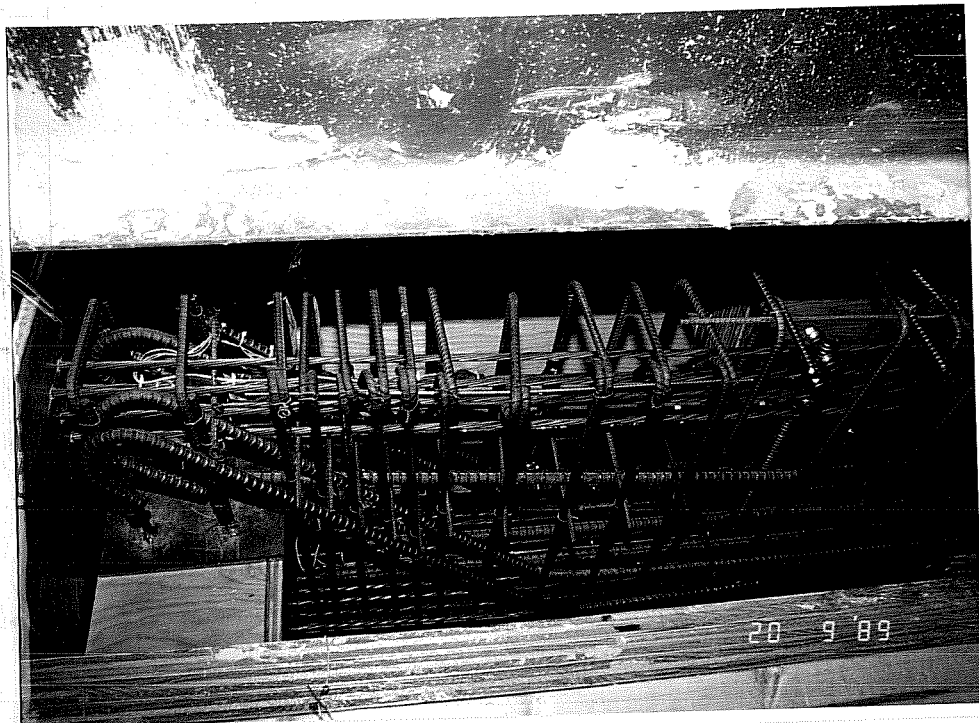


Figure 3.17 Photograph of IST Reinforcement Layout



Non-prestressed reinforcing bars used in this study were standard Grade 60 deformed bars with an average yield strain of 2900 microin/in. The stress-strain curve for #5 bars is shown in Fig. 3.19.

In the M/F detail a steel strap was constructed of steel bar stock with a yield strength of 54 ksi.

The concrete mix proportions are tabulated in Table 3.1. A slump of two inches was increased to ten inches using superplasticizer to gain the workability necessary for casting. Standard six by twelve inch cylinder tests were used to determine the compressive strength of the concrete at prestress release, seven day intervals, and each test day. A graph of concrete strength versus time is shown in Fig. 3.20. All beam specimens had a concrete strength of at least 7000 psi at time of testing.

#### 3.4 Fabrication

The two test beams were cast simultaneously in a fifty foot long prestressing bed. The prestressing strand was placed continuously throughout both beams and anchored behind steel plates (Fig. 3.21) with chucks donated by The Great Southwest Marketing Co, Inc. The draping hardware is shown in Figure 3.22. Prestressing strands were individually pretensioned to 50 ksi with a monostrand ram. After building the cage around the strand, the tension in the strands was increased to  $0.78f_{pu}$  or 212 ksi by moving the end plate shown in Fig. 3.21.

The M/F specimen was the most difficult to construct. Special precautions had to be taken to prevent the strap plates (Fig 3.8) from buckling during welding.

The IST specimen was the most difficult to assemble

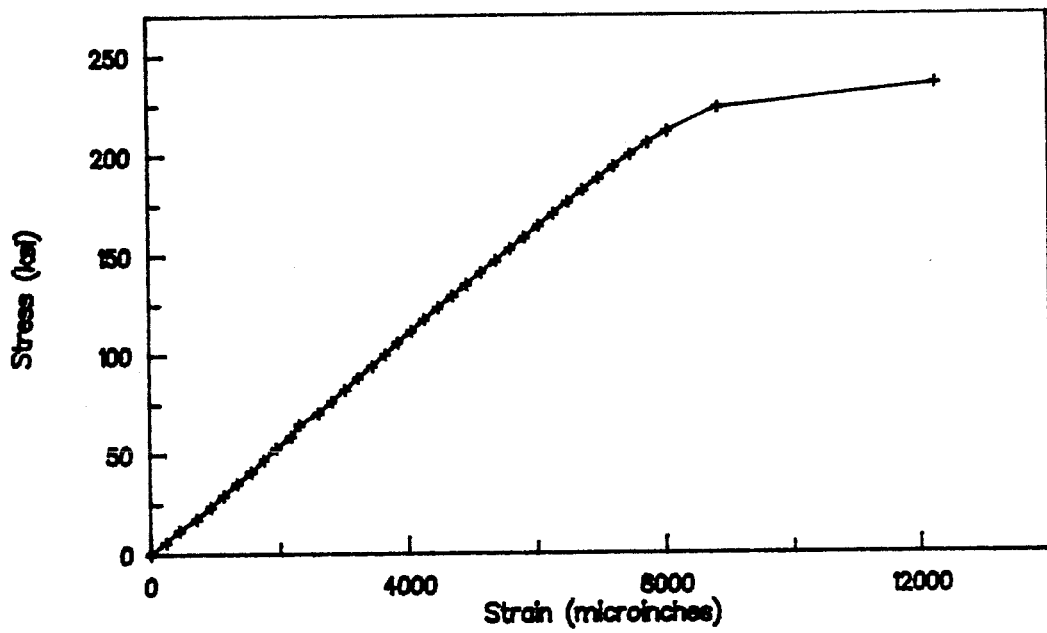


Figure 3.18 Stress-Strain Curve of Prestressing Strand

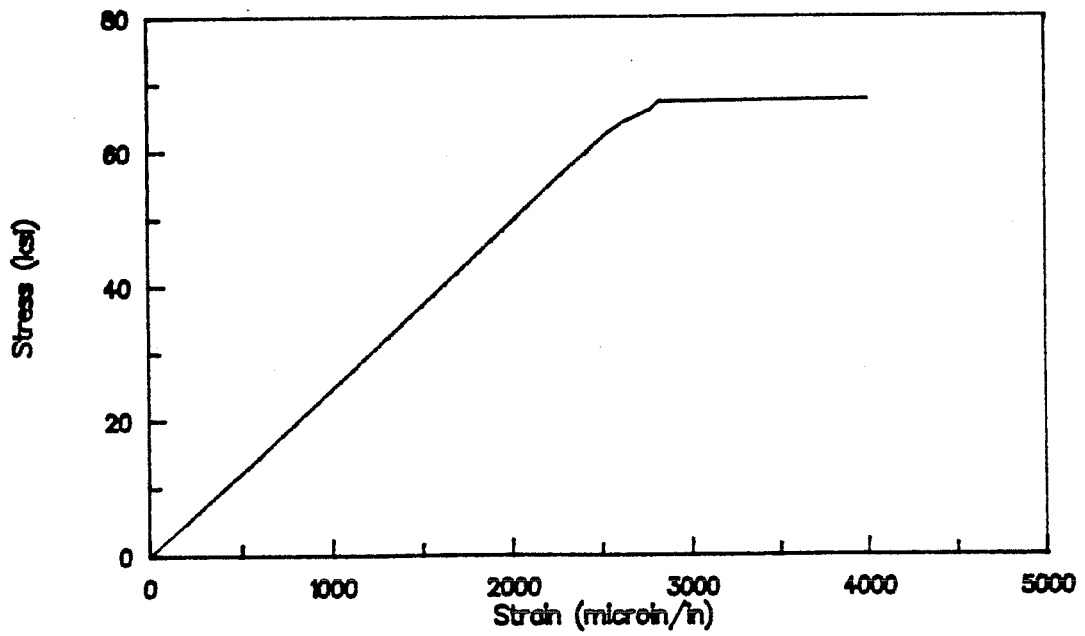
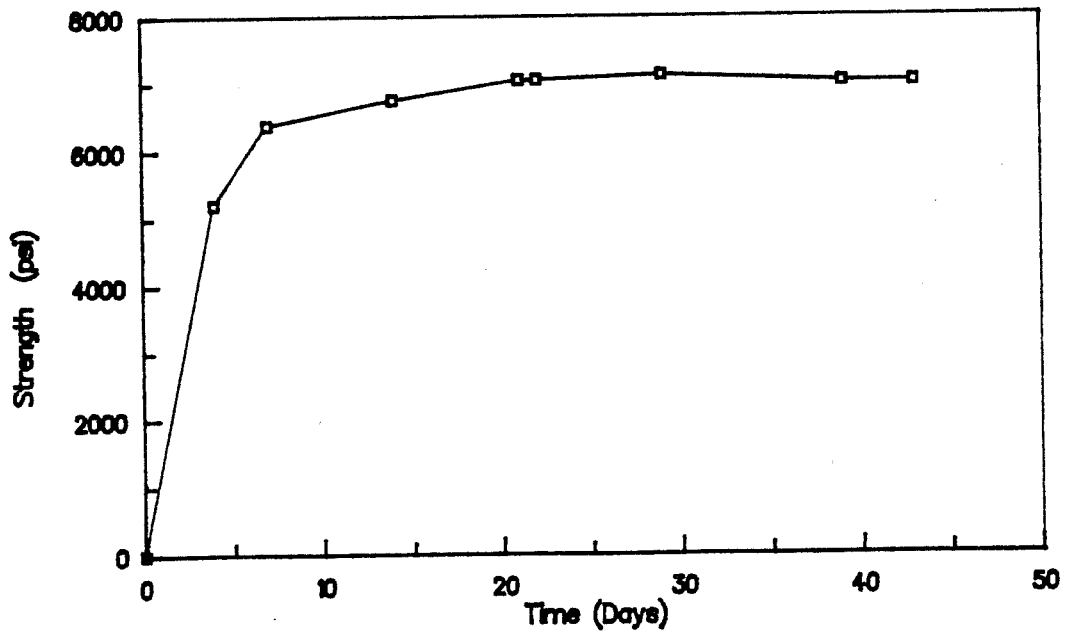


Figure 3.19 Stress-Strain Curve of #5 Reinforcing Bar

Cement	517 lb/yd
Coarse Aggregate	16801 lb/yd
Fine Aggregate	13551 lb/yd
Water	290 lb/yd
Retarder	37 lb/yd
Superplasticizer	77 oz/yd

**Table 3.1 Concrete Mix Proportions**



**Figure 3.20 Concrete Strength vs. Time**



Figure 3.21 End Plate of Prestressing Bed

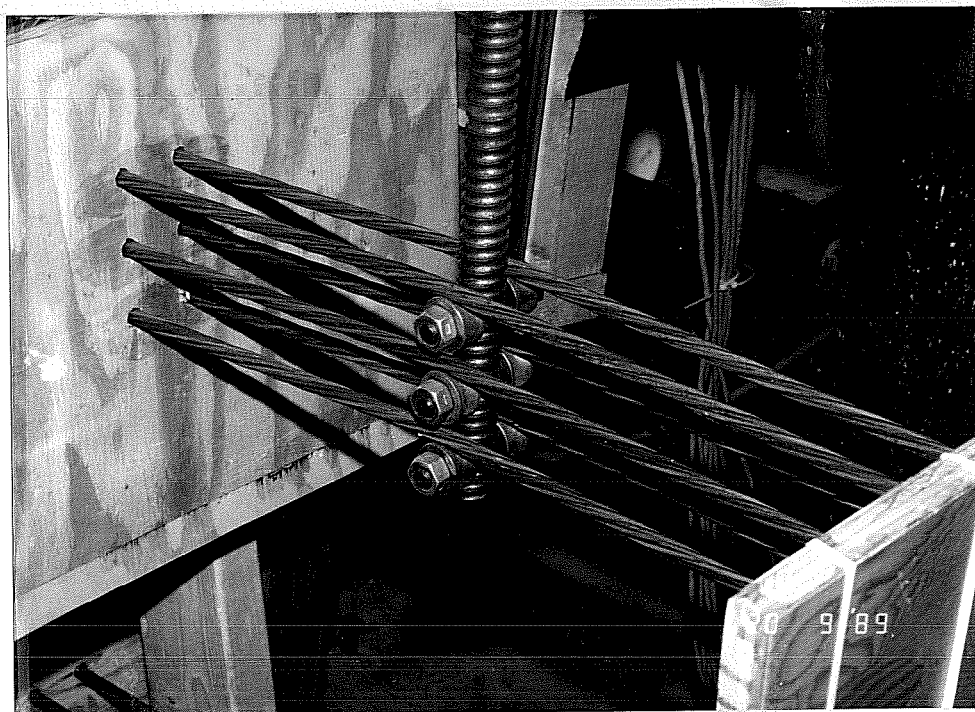


Figure 3.22 Draping Hardware

due to the large number of bars. Inclined #5 bars had to fit between both vertical and horizontal reinforcement. The two #5 bars which were continuous along the length of the beam for main flexural reinforcement were especially difficult to hold in place while tying the cage together.

### 3.5 Test Procedure

The test set-up consisted of a simply-supported beam with an overhang on one end (Fig 3.23a and b). The load was applied at one point only. The specimen was rotated 180 degrees to allow subsequent loading of the undamaged end.

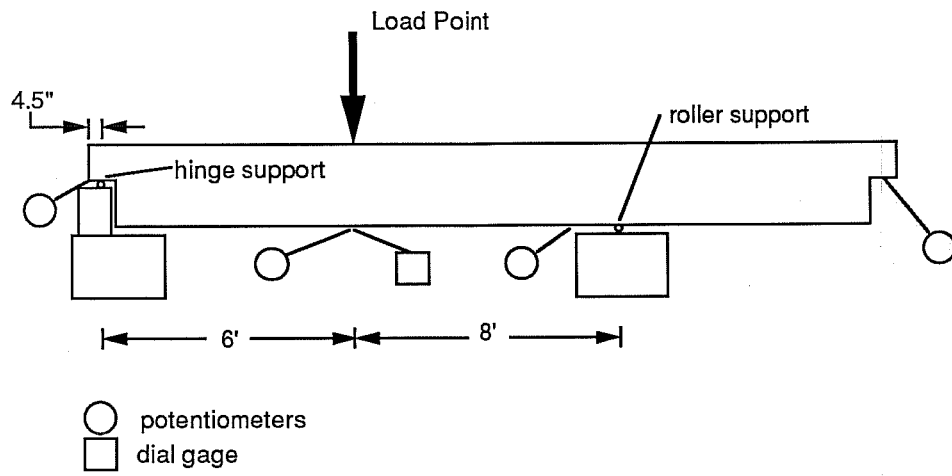
Each detail was individually loaded to failure using the same procedure:

1. Take initial readings on all gages
2. Apply a load increment
3. Scan all gages
4. Mark cracks
5. Apply another load increment.

Each specimen was loaded in increments to a shear of 50 kips, half of the design shear, then unloaded. Loads to this level were cycled twice before incremental loading to the ultimate design shear of 100 kips and then to failure. The PCI detail showed large cracks and some spalling at a shear of 46 kips so a maximum cyclic shear load of 45 kips was used.

### 3.6 Instrumentation

In order to monitor the stresses within the test beams, internal strain gages were placed on the reinforcement. The locations of all gages are shown in



a. Drawing of Test Set-Up



b. Photograph of Test Setup

**Figure 3.23 Test Set-Up**

Figures 3.24 through 3.27. Four linear potentiometers and one dial gage were used to measure vertical displacement of the beam. Their locations are shown in Figure 3.23a. Two dial gages were mounted on the ends of the prestressing strand to determine if the strand slipped into the beams.

Gages on the prestressing strands were initialized and monitored during initial and final prestressing. After prestress release, final strand strain readings were recorded. No readings were made of time dependent losses and the gages were reset on the day of testing. Due to oversight, strains in non-stressed reinforcement were not monitored during prestress release.

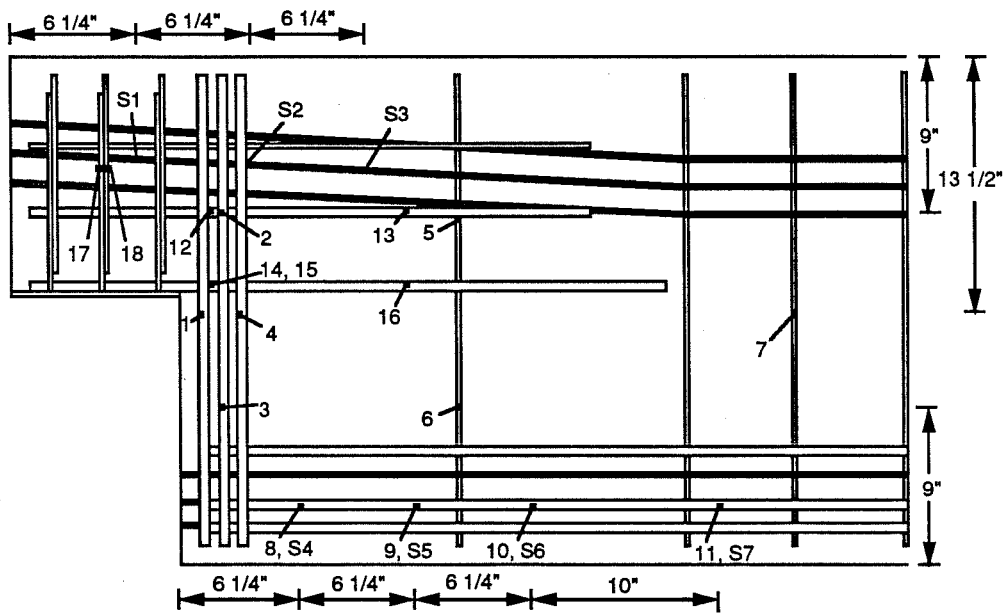


Figure 3.24 PCI Gage Location

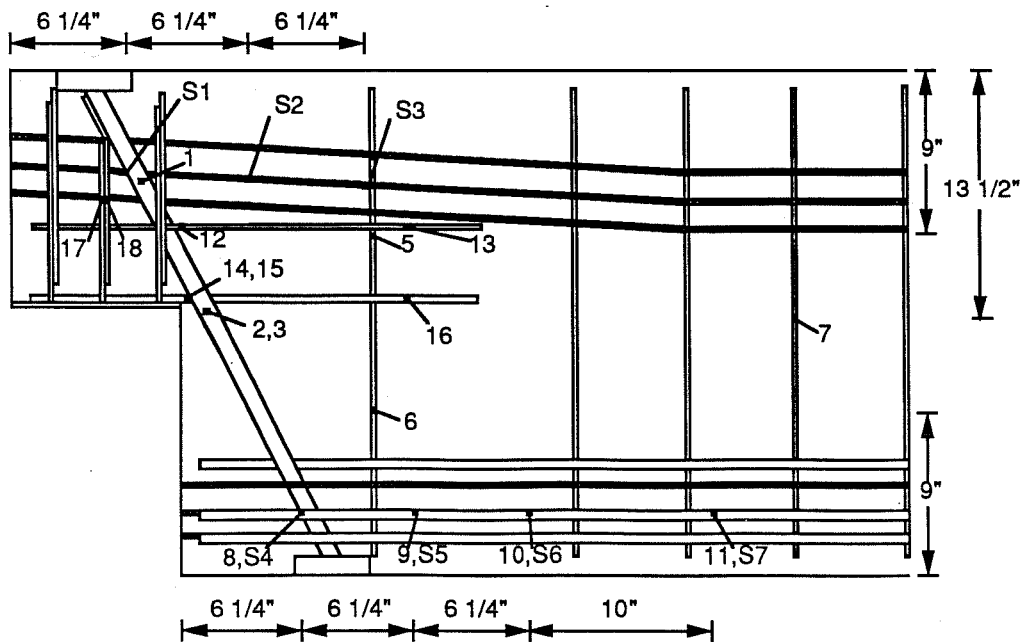


Figure 3.25 M/F Gage Location



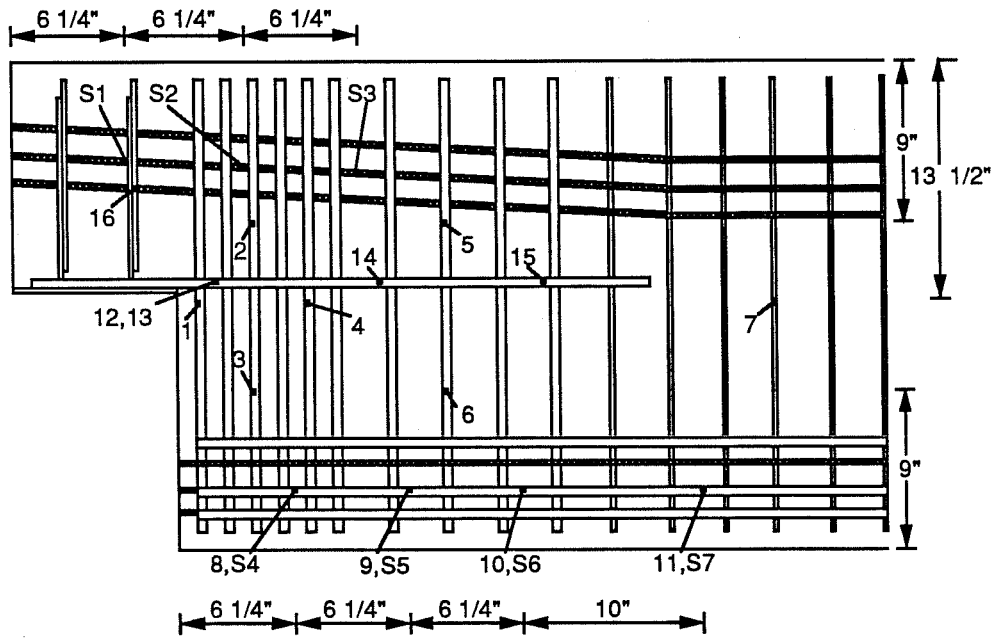


Figure 3.26 OST Gage Location

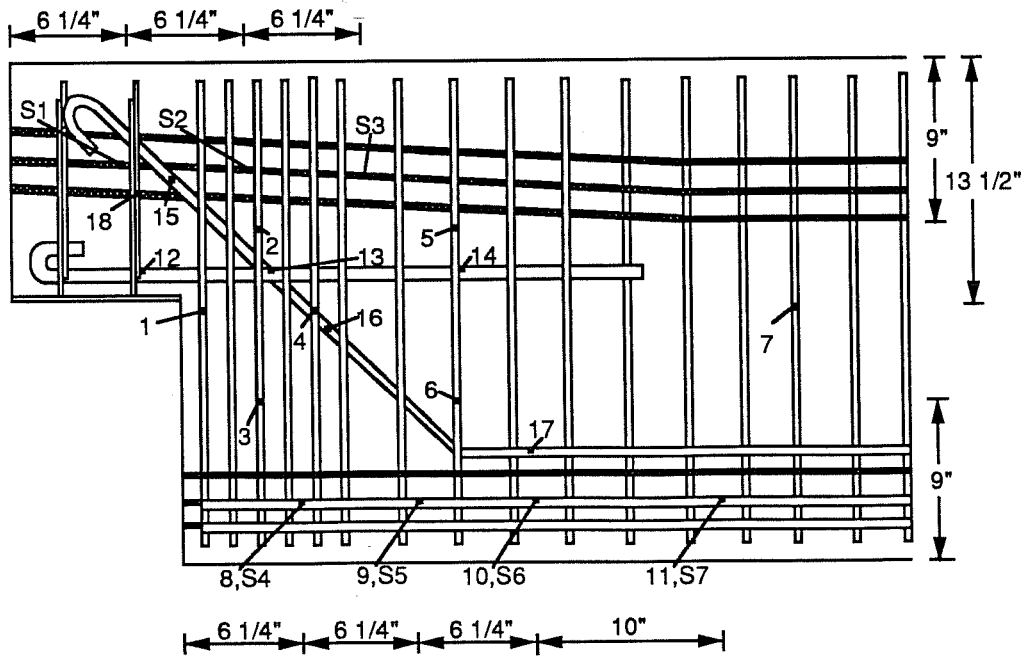


Figure 3.27 IST Gage Location

## CHAPTER 4 EXPERIMENTAL RESULTS

### 4.1 Introduction

Test results are presented in this chapter. The behavior of each specimen is evaluated and compared to the others. Additional data not covered in detail within this chapter are presented in Appendix A. Chapter 4 also includes design recommendations for future use of the strut-and-tie model.

### 4.2 Overall Specimen Behavior

**4.2.1 General.** With the exception of the PCI specimen, all test specimens carried loads higher than expected. Table 4.1 compares design loads, first cracking loads, predicted ultimate loads, and actual failure loads. The predicted failure load was based on the weakest link in the model.

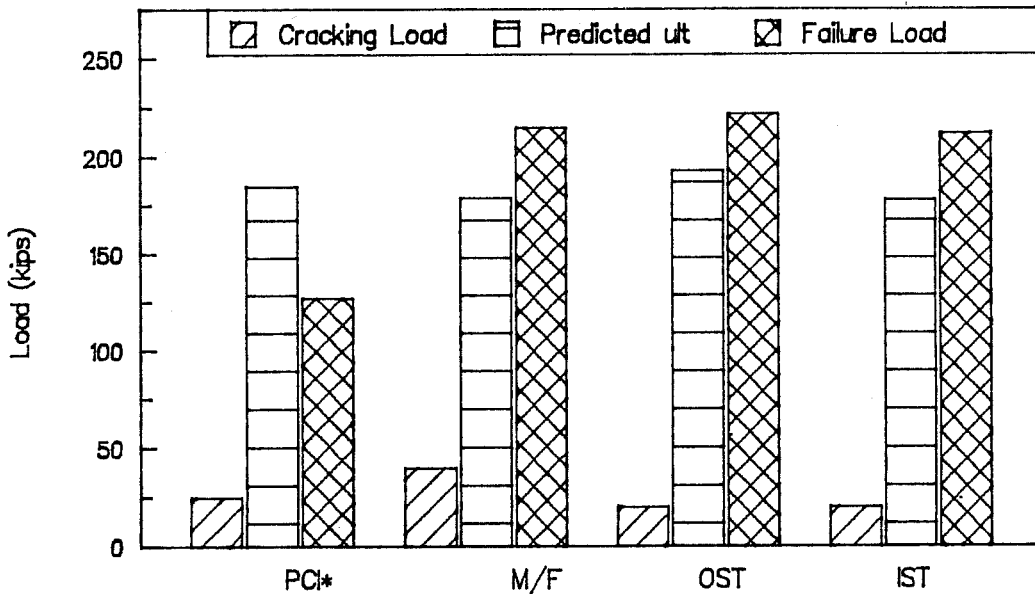
Figure 4.1 shows that all specimens showed visible cracks at very low loads. In all cases, the first crack appeared at the inside corner of the dap interface. The M/F detailing carried the highest load at first visible cracking because of the large steel strap placed immediately inside the interface corner.

The load on each specimen was cycled twice within the elastic region before loading to failure. In order to present data clearly, only the first cycle of loading is shown before the beams were loaded to failure. The load-deflection curves for all beam ends are shown in Figure 4.2.

Specimen	Design Load	First Cracking Load	Predicted Load	Failure Load	$P_{test} / P_{predicted}$
PCI*	175	25	185	127	0.69
M/F	175	40	179	215	1.20
OST	175	20	193	222	1.15
IST	175	20	178	212	1.19

\* PCI Specimen failed early due to poor detailing  
 Loads in kips

**Table 4.1 Design, Cracking, Predicted, and Failure Loads From all Tests**



\*PCI Specimen failed due to poor detailing

**Figure 4.1 Cracking, Predicted, and Ultimate Failure Loads For All Specimens**

**4.2.2 PCI Detail.** The first visible crack in the PCI specimen originated at the corner of the dap interface at a load of 25 kips. When the applied load reached 81 kips, large cracks suddenly occurred in the bottom end of the full depth beam. This corner region completely spalled off by the time ultimate load was reached. The vertical #5 reinforcing bars with bends to confine the prestressing strands in the end of the full depth section (Fig 3.4) straightened out causing the concrete cover to spall. The outermost strands in the bottom flange were no longer bonded to the concrete.

No cracks formed across the vertical #3 hoops within the dap. Cracks in the full depth section were closely grouped indicating formation of one major compression strut. This strut was inclined at an angle of 20 degrees toward the load point. Because the end of the beam failed at such a low load, only one shear crack formed in the web.

At an applied load of 127 kips, the PCI specimen could not carry any additional load so loading was stopped. It was impossible to maintain load while deflection continued to increase. Figure 4.3 shows the PCI specimen after failure.

The PCI specimen failed at such a low load due to the poor detailing of the end vertical reinforcement. Bending the stirrups outward to confine all the flexural reinforcement without providing a transverse tie at the bend points reduced their capacity. This reduced capacity could have been prevented by a cross tie as illustrated in Figure 4.4. A better detail would include restraining the #5 hoops at the bend as shown in Figure 4.4 or using closed hoops as in the OST and IST

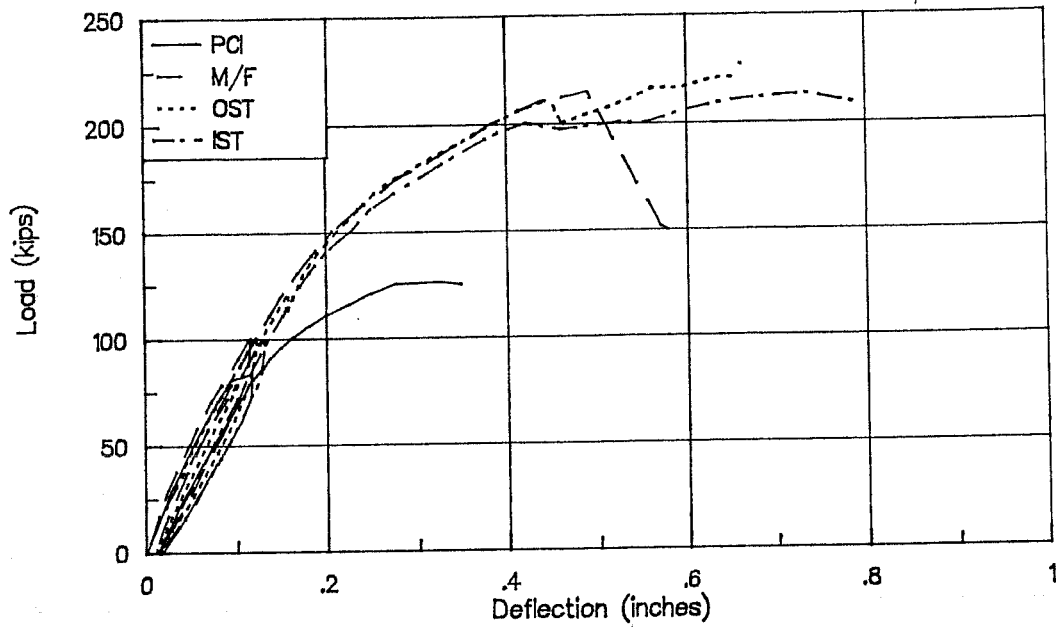


Figure 4.2 Load vs. Deflection Curve For All Specimens

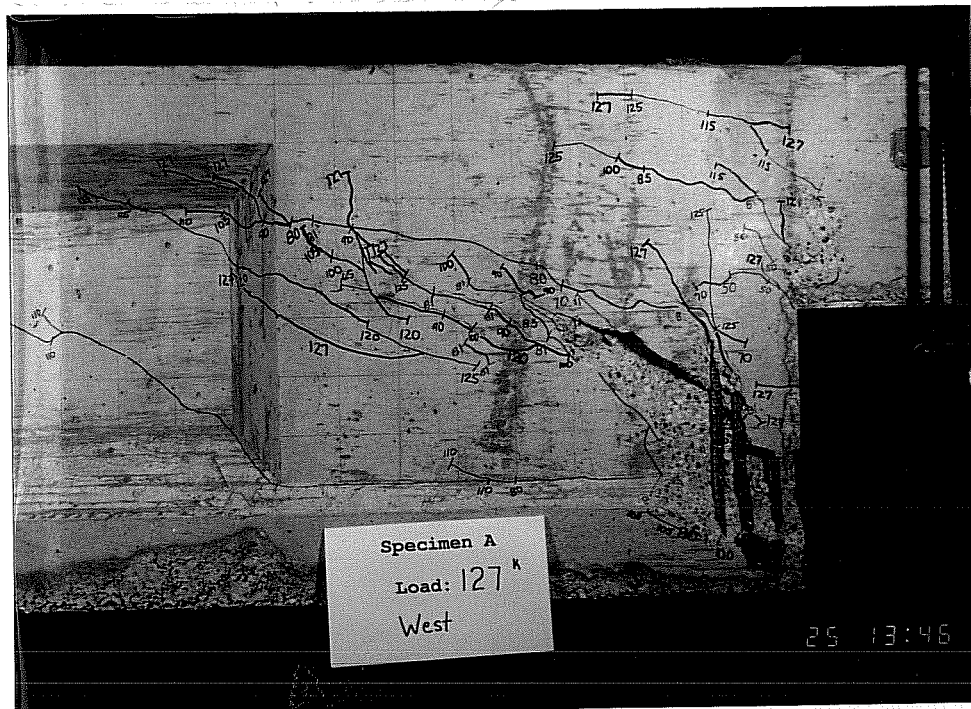


Figure 4.3 PCI Specimen at Failure

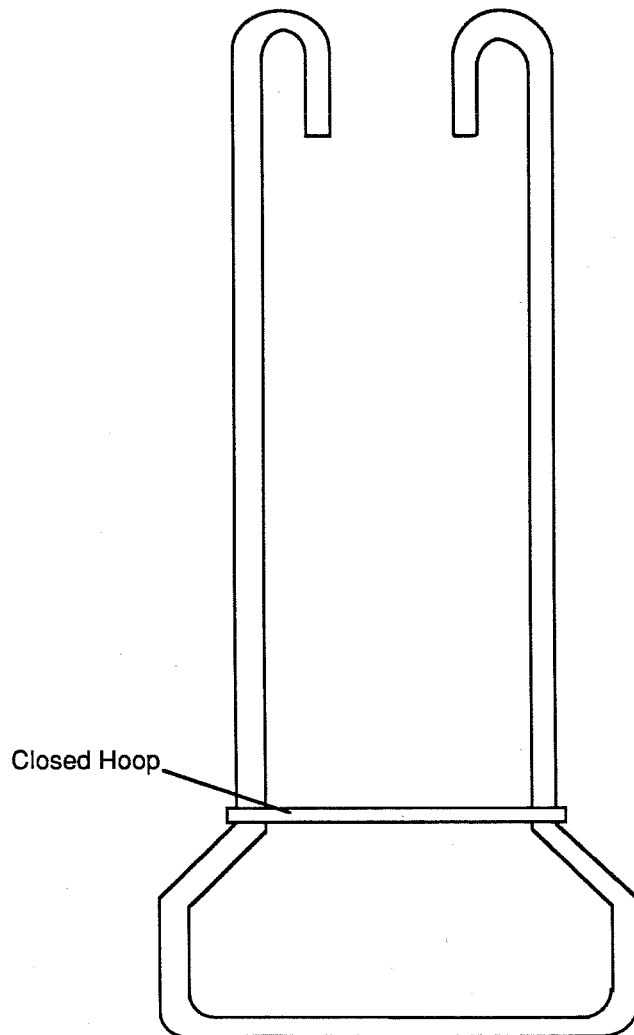


Figure 4.4 Restrained #5 Hoop

specimens.

**4.2.3 M/F Detail.** In the M/F specimen, the first crack appeared at a load of 40 kips originating from the dap interface corner. Throughout the first cycle of loading the cracks propagated almost horizontally. At loads above 100 kips, the cracks turned upward at angles between 50 and 60 degrees.

Web shear cracks occurred at a load of 160 kips. They extended through the bottom flange and to the end of the beam at an average angle of 29 degrees. One vertical crack formed through the middle of the dap from the strap plate downward indicating the formation of a vertical strut from the load point to the end plate on the strap.

When the applied load reached 215 kips cracks in the end of the beam opened very wide, the load dropped to 150 kips, a large displacement occurred under the load point and the load could not be recovered. A photograph of the M/F specimen at failure is shown in Fig 4.5.

**4.2.4 OST Detail.** The specimen designed using an orthogonal strut-and-tie model carried the highest load of 222 kips. At a load of 20 kips the first crack appeared at the dap interface and propagated horizontally. The cracks in this end were evenly distributed throughout the entire depth of the beam at an average angle of 45 degrees.

Cracks in the dap appeared at a load of 160 kips. They extended to the bearing plate and into the top flange at a 45 degree angle. Shear cracks formed in the web at a load of 175 kips. When the load reached 210 kips, large cracks opened up longitudinally along the top of the bottom flange.

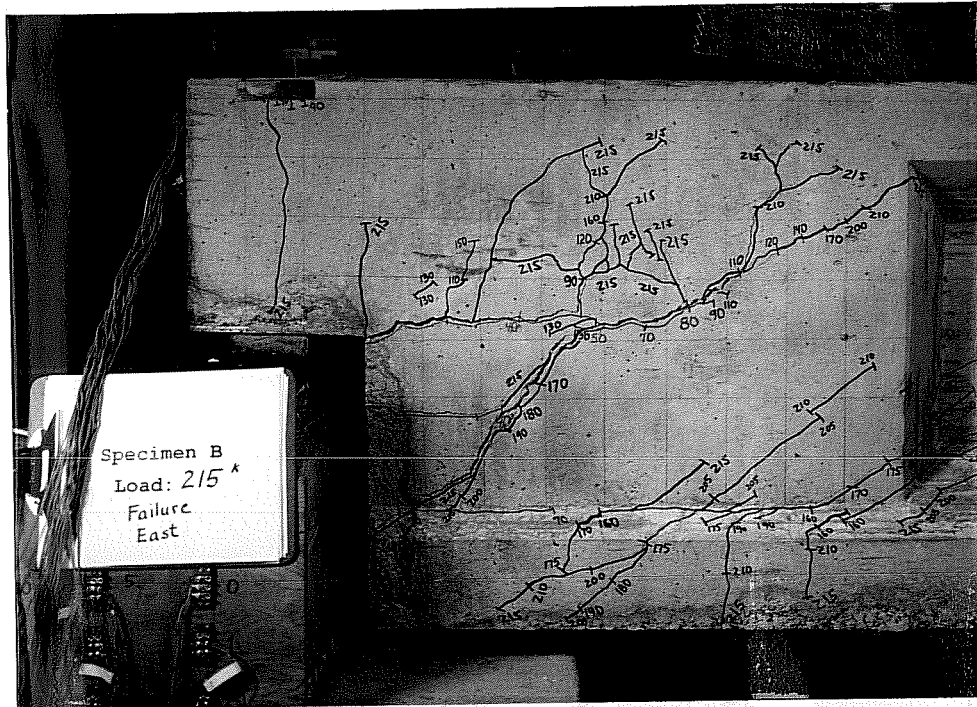


Figure 4.5 M/F Specimen at Failure

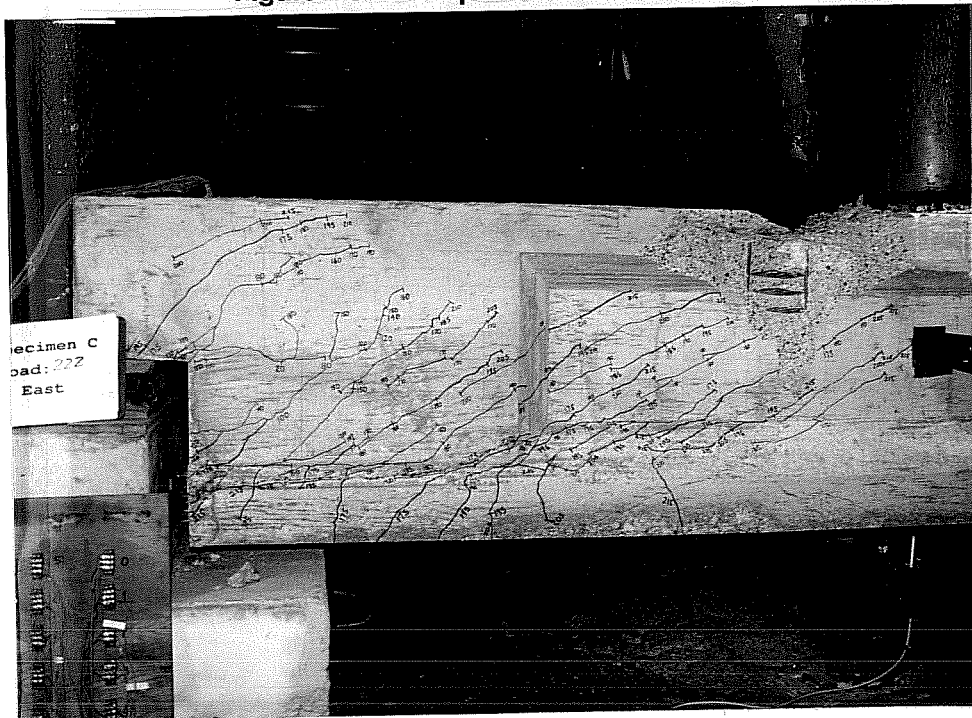


Figure 4.6 OST Specimen at Failure



When the dapped end could not carry additional load, but before the load was decreased, a compression failure occurred in the OST specimen well away from the dap. The top flange of the beam crushed immediately ahead of the loading plate. A photograph of the failed specimen is shown in Figure 4.6.

**4.2.5 IST Detail.** The first crack in the IST specimen appeared at a load of 20 kips at the dap interface. A crack also formed along the inclined #5 bars (see Fig. 3.16) which is the opposite direction to that expected. As the load increased above 40 kips, the cracks turned to the angle expected and propagated towards the load point.

Cracks inclined between 37 and 46 degrees were evenly distributed throughout the end section of the beam. The first web shear cracks appeared at a load of 150 kips. Small moment cracks originated from the bottom of the beam directly under the load point at a load of 185 kips.

At an applied load of 205 kips, large cracks opened up along the cross-section change in the bottom end of the full depth section. Additional load was carried by the beam until the applied load reached 212 kips. While marking cracks at this load, the load dropped and only 208 kips could be recovered while the deflection was still increasing. The IST specimen after failure is pictured in Figure 4.7.

### 4.3 Evaluation of End Reinforcement

The main vertical reinforcement corresponding to the full height hanger immediately adjacent to the dap (tension tie 2 (see Fig 3.12 and 15)) yielded in all four test specimens. In the M/F specimen, yielding occurred

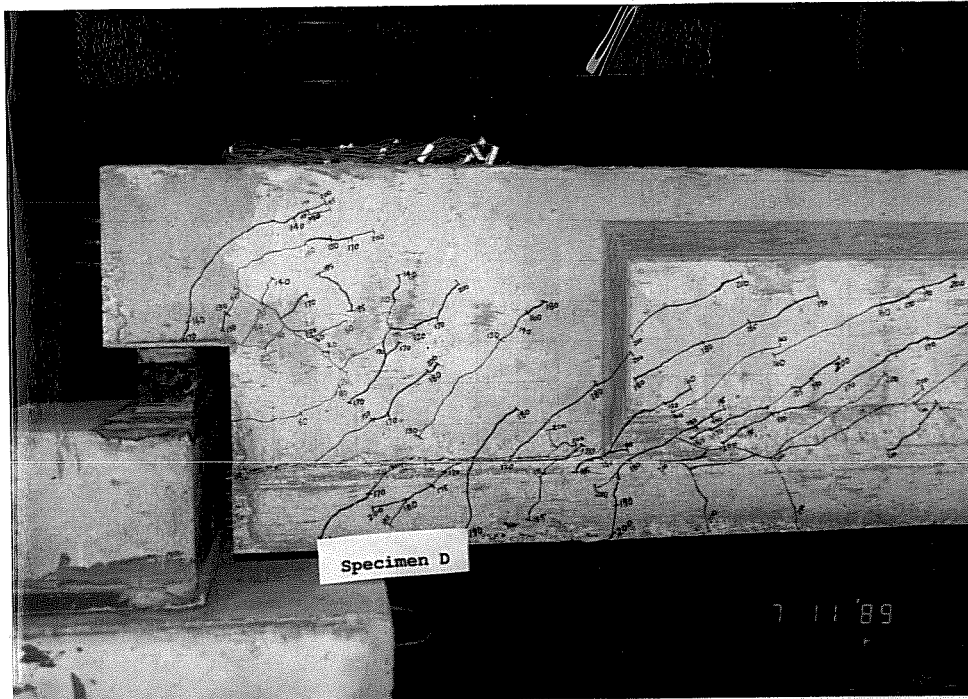


Figure 4.7 IST Specimen at Failure

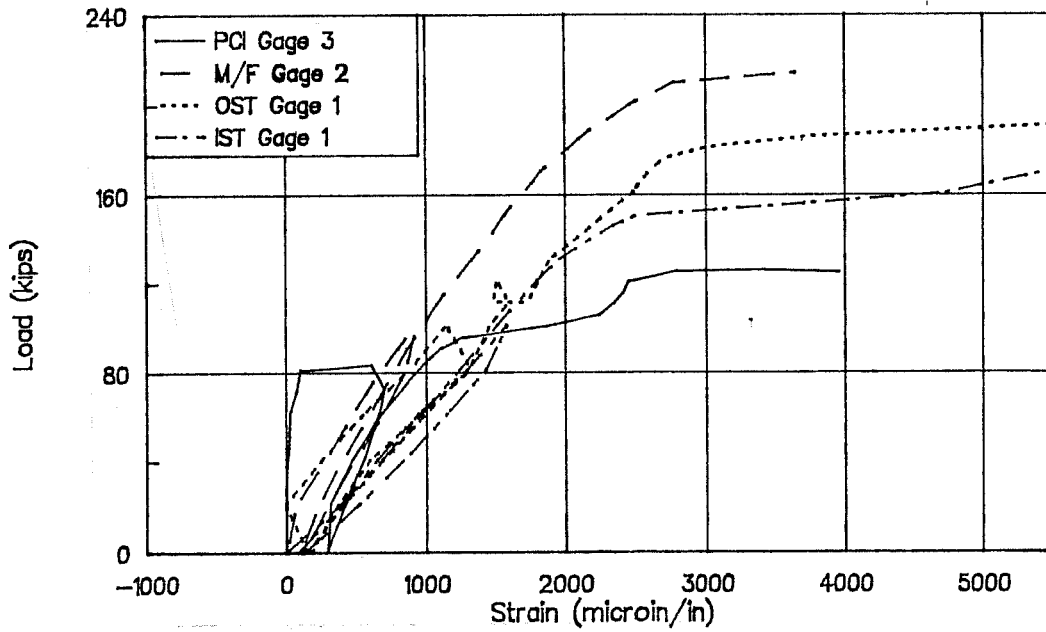


Figure 4.8 Applied Load vs. Strain in Yielded Vertical Reinforcement of All Tests

in the steel strap. The gage showing yielding was located just inside the dap interface in all specimens except in the specimen which was designed by the PCI procedure. During testing of the PCI specimen, gage 3 which was located 8 inches from the bottom of the full depth beam, registered strains above the yield strain of 2900 microin/in. A graph comparing the critical first yielding gage from all tests is shown in Figure 4.8. Other data from gages on the main vertical reinforcement is shown in Appendix A. Loads at first yielding are compared in Table 4.2. Steel in the PCI Specimen yielded at the lowest load of 127 kips. The M/F specimen carried the highest load, 210 kips, before yielding occurred.

The OST specimen was the only specimen in which horizontal reinforcement yielded. Horizontal tension tie 1 (Fig. 3.11) yielded just inside the dap interface at a load of 185 kips. Gages on horizontal reinforcement in the three other tests showed that no yielding occurred.

The IST specimen was the only specimen in which the main horizontal dap reinforcement was not welded to the bearing plate. The #6 bars in this specimen were hooked to provide the necessary anchorage (see Fig. 3.16). Strain readings showed that the steel-concrete bond was sufficiently developed and load was carried as expected. A comparison of horizontal reinforcement strains just inside the dap of each end is shown in Figure 4.9. Other gage readings on horizontal reinforcement are shown in Appendix A.

The IST specimen contained inclined #5 reinforcing bars across the dap interface. This reinforcement did not yield before failure (Fig. 4.10). The maximum strain

Specimen	Load at Yielding
PCI	127
M/F	210
OST	180
IST	145

Loads in kips

**Table 4.2 Load at First Measured Yielding**

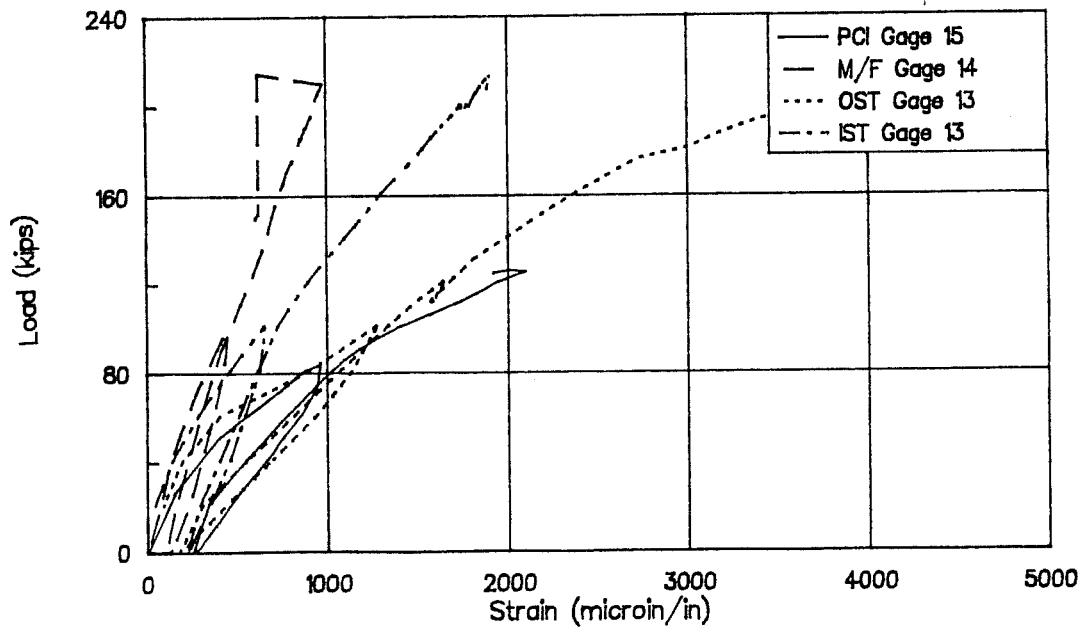


**Figure 4.9 Applied Load vs. Strain in Main Horizontal Dap Reinforcement of All Tests**

recorded was 2400 microin/in corresponding to a stress of 59 ksi. The total load carried by tie 4 at failure was 69.2 kips, 18% higher than the strut-and-tie model force of 58.6 kips.

Vertical tie 3 (Fig 3.15) was monitored by strain gages 5 and 6. In the two ends designed using strut-and-tie models these gages were on closed hoops located 24 inches from the end of the beam. The maximum strain recorded in both specimens was 1500 microin/in.

The corresponding gages in the specimens designed by the PCI and M/F methods were located at different distances from the end of the beam. Gage 5, 26 inches from the end of the PCI specimen, recorded large permanent strains at 81 kips when concrete spalled at the end of the full depth section. This stirrup, included to tie the end reinforcement into the shear reinforcement, carried a load of 16 kips at failure.

Neither gage 5 nor 6 showed yielding in the beam designed by the Menon/Furlong method. These gages were located 20 inches from the beam end. Test load versus strain curves for gages 5 and 6 from all tests are given in Appendix A.

All gages on vertical reinforcement within the dap measured strains below 450 microin/in. Negative strains only occurred in the M/F specimen due to the compressive forces applied by the steel strap. The IST specimen showed the largest strains in the nib (Figure 4.11).

#### 4.4 Behavior of Prestressing Strand

Internal strain gages were placed on one draped strand and one straight strand. Their location was determined using the  $50d_p$  transfer length suggested by

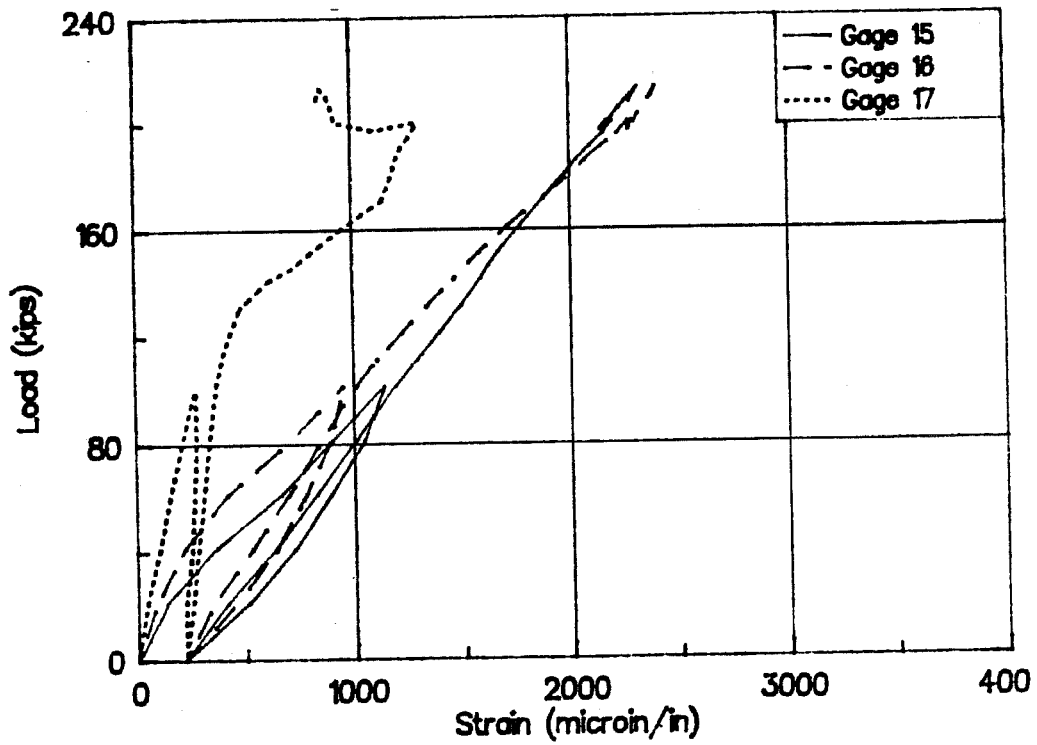


Figure 4.10 Applied Load vs. Strain in Inclined Bars of IST Test

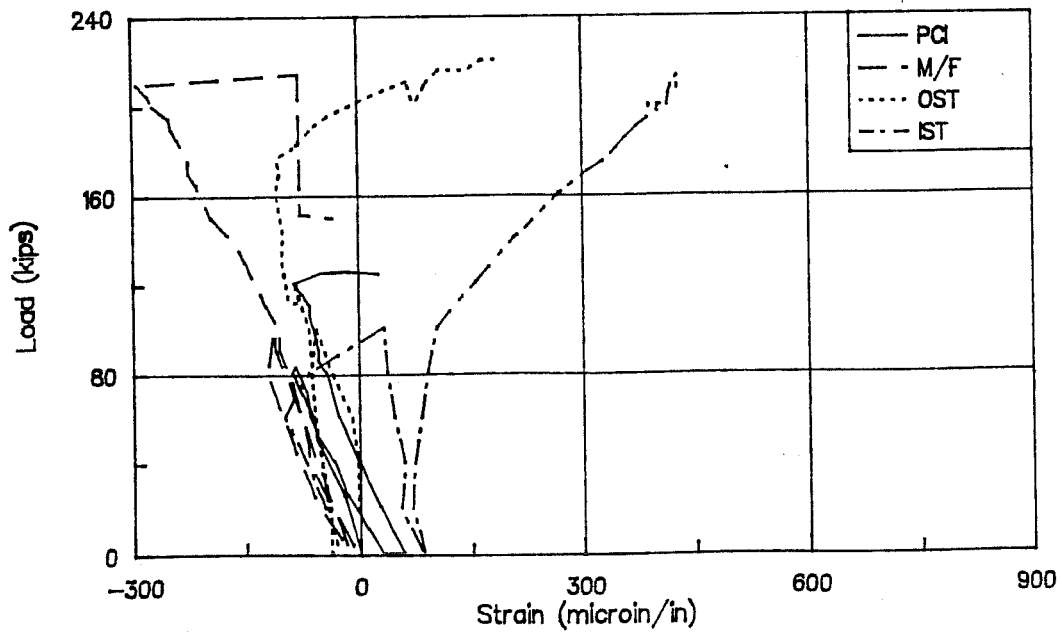


Figure 4.11 Applied Load vs. Strain in Local Vertical Dap Reinforcement of All Tests

Libby [6] divided into thirds. One additional gage was placed ten inches beyond the transfer length on the straight strand. In addition to the internal strain gages, one dial gage was mounted externally on the beam to record strand slip relative to the end of the beam.

All strands were pretensioned to an average strain of 8050 microin/in. After release, the strains remaining in gage S6 at the end of the transfer length, ranged from 5000 to 7000 microin/in. At approximately  $75d_b$  from the end, strains remaining in gage S7 after release were about 7000 microin/in in all specimens.

During all tests, increases in strand strain were very small. Most straight strand gages showed lower strains at failure than before loading began. In all tests except the PCI specimen, strand strains decreased significantly at the load which created longitudinal cracks along the cross section change in the end of the beam. These longitudinal cracks indicated that the concrete cover in the bottom flange was no longer providing anchorage for the outermost six prestressing strands. When the total prestressing force was reduced by the anchorage loss of six strands, the gaged strand in the middle of the beam showed a decrease in strain. The load-strain curve of the straight strands in the OST specimen is shown in Figure 4.12. Similar curves from the other tests are shown in Appendix A.

Increases in the draped strand strains were very small. The graphs of this data are presented in Appendix A.

Dial gages showed that the straight strands slipped more than the draped strands. The maximum recorded slip of the straight strand in the OST specimen (see Fig.

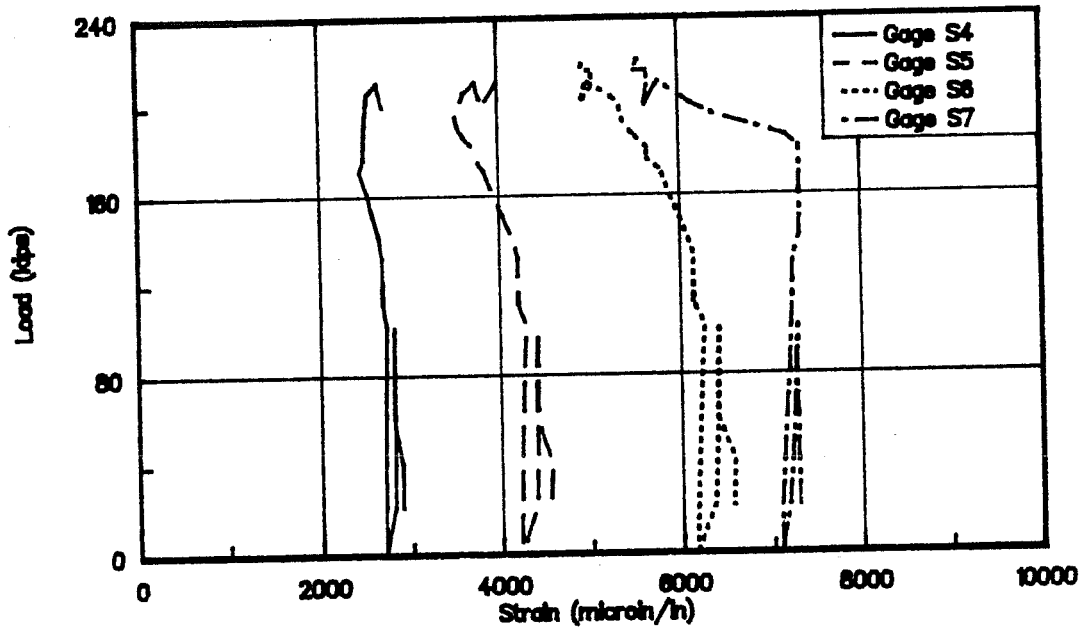


Figure 4.12 Applied Load vs. Strain in Straight Strand of OST Test

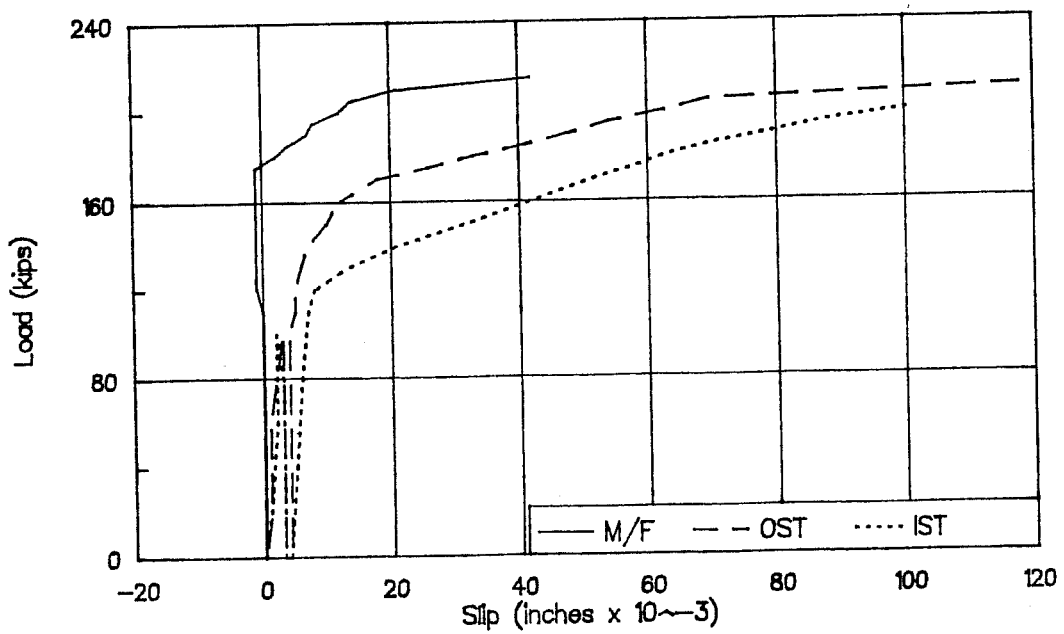


Figure 4.13 Applied Load vs. Straight Strand Slip of All Tests



4.13), was less than 1/8". During testing of the PCI Specimen the dial gages did not function properly so that data is unavailable.

#### 4.5 Behavior of Stirrups

In all four specimens the gaged stirrup was located 42 inches from the end of the beam. A graph comparing the behavior of this stirrup in three tests is shown in Figure 4.14. Gage 7 in the IST specimen malfunctioned during testing so it is not included in the data.

Using the ACI Building Code procedure [1], web shear cracking was predicted to occur at a load of 152 kips. Loads at which first web shear cracking actually occurred are given in Table 4.3. During the three tests from which data is available, no measurable stirrup strain was recorded until web shear cracking occurred. Once a crack crossed the stirrup, tension was carried by the steel. In all tests the end reinforcement yielded causing the beam to fail before the stirrup yielded.

#### 4.6 Behavior of Beam Flexural Reinforcement

In all tests, the main non-prestressed flexural reinforcement was initially under compression from prestress forces. The value of this initial compression strain was not measured due to oversight. Instead, measured strand strains were used to determine probable compressive bar strains at the same location due to release. These values were then added to the data recorded during testing. All data on main flexural reinforcement presented has been adjusted in this way to account for prestress forces.

The development length for #6 deformed bars in

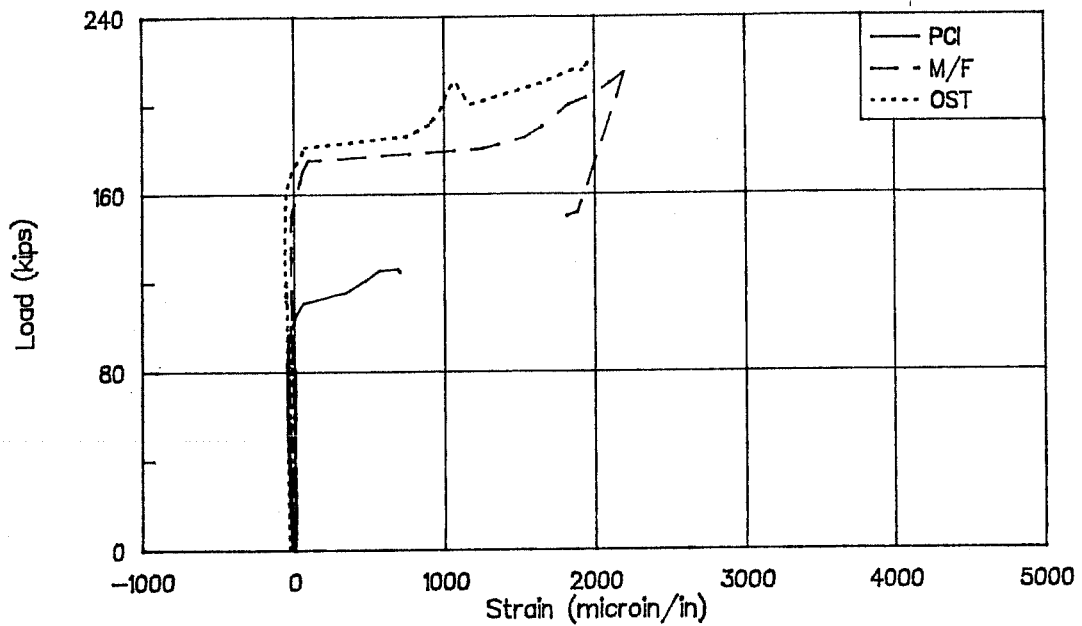


Figure 4.14 Applied Load vs. Stirrup Strain of All Tests

Specimen	Web Cracking Load	Test Crack Load/ACI Crack Load
PCI *	110	0.72
M/F	160	1.05
OST	175	1.15
IST	150	0.99

\*PCI Specimen cracked early due to poor detailing  
Loads in kips

Table 4.3 Load at First Web Crack

compression should be taken as not less than 13.5" according to the ACI Building Code [1]. Gage 8, located only 5 1/4" from the end of the bars registered the least increase in strain during all tests.

Lower strain increases occurred at gage 11 (located 28 3/4" from the end of the full depth section) than at gages 9 and 10, placed closer to the end of the beam (see Fig. 3.24-27). Crack patterns support this observation with cracks appearing at lower loads near the end of the beam. High loads were necessary to develop the few cracks around gage 11. Strains recorded by gage 10 in all tests are shown in Figure 4.15. Additional data from non-prestressed reinforcement is presented in Appendix A.

#### 4.7 Overall Comparison of End Details

In order to compare the efficiency of the design models, the volume of steel in the discontinuity zone of each end was determined. Because main flexure reinforcement, pretensioned and non-pretensioned, was the same in all four specimens, it was not included in the end volume of steel. The extent of the "D" or discontinuity zone at the beam ends was taken as 36 inches for all specimens (see Fig. 4.16). Only steel within the end 36" of the beam was included in the comparisons. In both strut-and-tie models, the #3 stirrups at 3" centers corresponding to tension tie 5 (Fig. 3.11 and 15) were placed beyond the end 36" of the beam and correspond to the ordinary shear reinforcement in the PCI and M/F beams. However, since the strut-and-tie model does not recognize any tensile concrete contribution ( $V_c$ ) to shear resistance, the shear

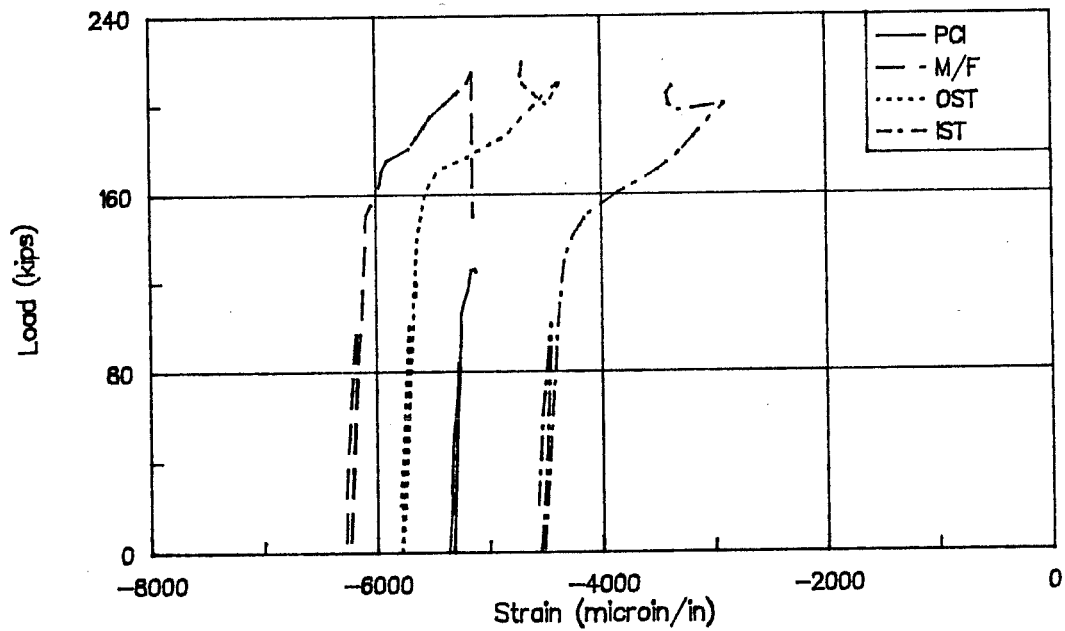


Figure 4.15 Applied Load vs. Strain in Main Flexural Reinforcement (Gage 10) of All Tests

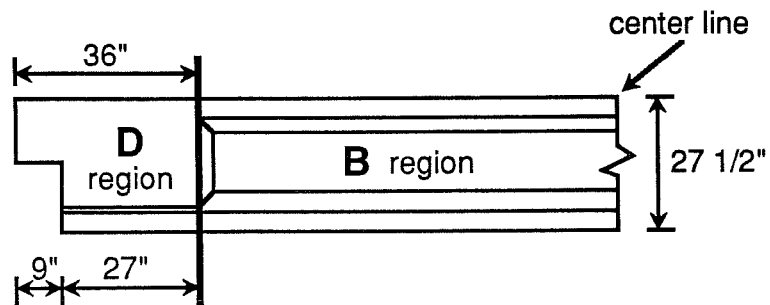


Figure 4.16 Discontinuity Zone at Beam End

reinforcement in the two strut-and-tie details is greater.

Steel volumes were divided into vertical and horizontal reinforcement. In the two specimens with inclined reinforcement (M/F and IST) the inclined reinforcement was considered to be vertical. The anchor plates of the steel strap in the M/F specimen were considered to be horizontal.

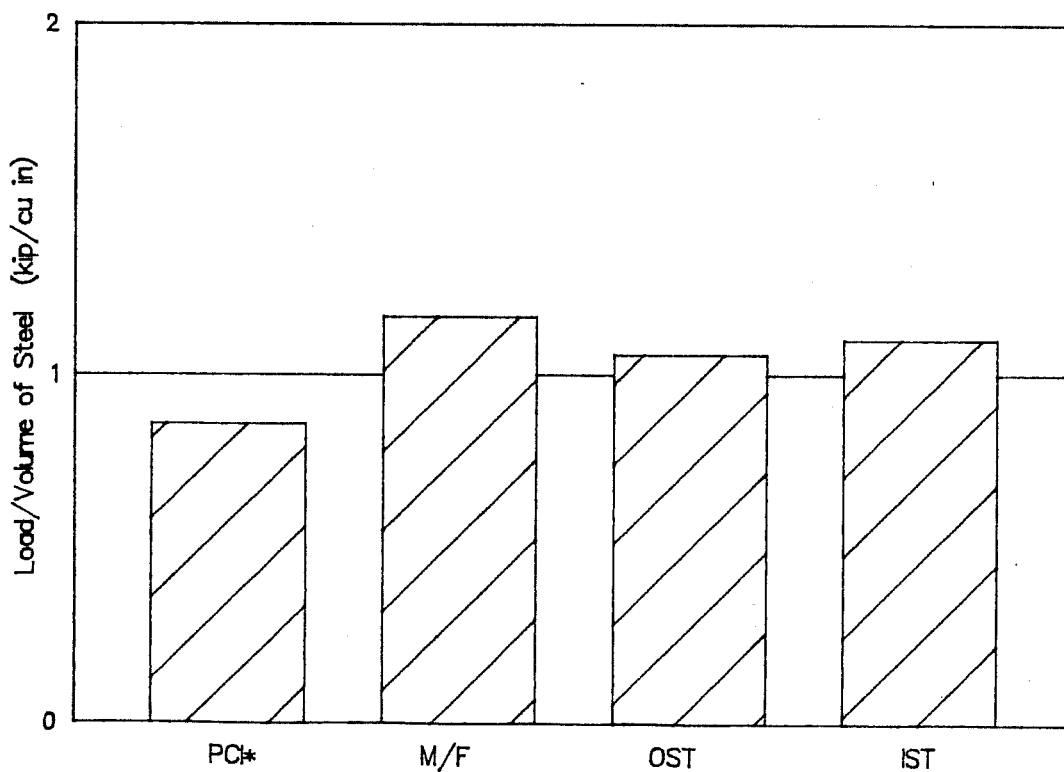
Total steel volumes for each specimen are presented in Table 4.4. The two strut-and-tie models contained more steel than either of the other two as an indication of efficiency. Ultimate load carried per cubic inch of steel is shown in Figure 4.17. The M/F specimen carried the largest load per unit of steel but was not very much more efficient than the two strut-and-tie models. The PCI specimen showed low load per unit of steel efficiency due to the poor detailing of the bent stirrups.

Construction efficiency of the four test specimens was also compared. Different construction tasks were rated according to their difficulty. These ratings reflect the time necessary to perform the task as well as the time necessary to assemble each piece in the cage. These "construction units" are presented in Table 4.5. The number of times a given task was performed in constructing each specimen was then multiplied by the rating for that task. Total construction units for each beam end were summed and are shown in Table 4.6. The M/F specimen required the most time and effort to construct while the PCI specimen required the least. The OST specimen carried the highest load per construction unit (Fig 4.18). Detailing of both strut-and-tie model specimens showed substantial construction efficiencies

Specimen	Ultimate Load (kips)	Vertical Steel (cu in)	Horizontal Steel (cu in)	Total Steel (cu in)	Load/Vol Steel (kip/cu in)
PCI*	127	94.2	53.6	147.8	0.86
M/F	215	84.7	99.7	184.4	1.17
OST	222	159.9	49.7	209.6	1.06
IST	212	155.5	37.2	192.7	1.10

\*PCI Specimen failed early due to poor detail

**Table 4.4 Volume of Steel in "D" Region of All Specimens (Excluding Main Flexural Reinforcement)**



\*PCI Specimen failed due to poor detailing

**Figure 4.17 Ultimate Load per Volume of Steel of All Tests**

Construction Process	Rating Units
Cut bar	0.25
Bend open hoops or stirrups	0.5
Bend closed hoop	1.0
Bend inclined bar	1.0
Weld bar to plate	1.0
Cut plate for strap	1.0
Weld strap plates	1.5
Bend #5 hoops for PCI	2.0

**Table 4.5 Cost Rating Units for Construction Tasks**

Specimen	Ultimate Load	Total Rating Units	Load/Unit
PCI	127	23	5.5
M/F	215	33	6.5
OST	222	29	7.7
IST	212	29	7.3

**Table 4.6 Total Construction Operation Cost Rating for all Specimens**

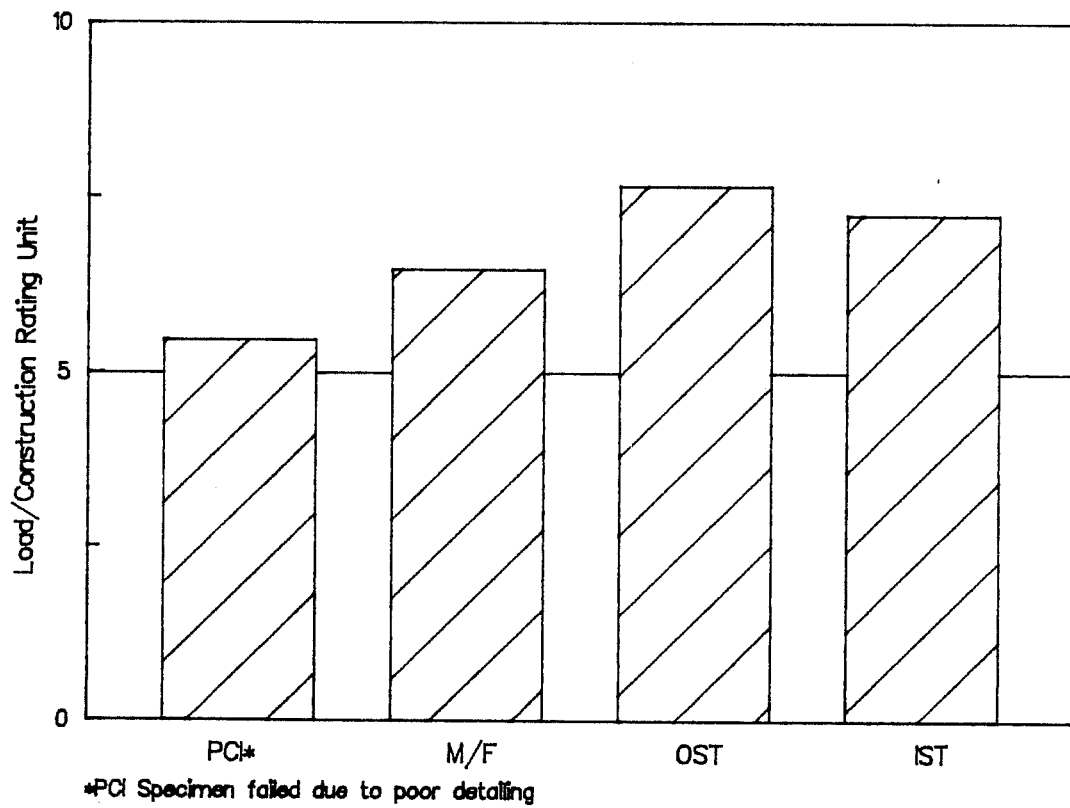


Figure 4.18 Ultimate Load per Construction Rating Unit of All Tests



over the other two methods.

#### 4.8 Design Recommendations for Implementing the Strut-and-Tie Model

**4.8.1 General.** The strut-and-tie models originally used to design the dapped end beams for this research project were not modified to distinguish between non-prestressed and prestressed beams except that the prestress force was used as an applied load and the reserve in the tendons above prestressing loads was considered as available for load resistance. After the test results were reviewed, new models were developed in which prestress forces were applied at nodes of the strut-and-tie model used for design. These models are described in the following sections. The calculated forces are based on measured prestress forces after losses and on actual failure loads.

**4.8.2 Orthogonal Strut-and-Tie.** All test specimens included draped prestressing strands in the top flange and straight strands in the bottom flange. Because only the draped strands extended through the dap, the two sets of tendons were considered separately. The final orthogonal strut-and-tie model is shown in Figure 4.19. Thin lines represent non-stressed reinforcement, medium lines show prestressing tendons, and thick lines represent compression struts and tension ties.

Horizontal forces from the six draped strands were applied in equal amounts at three points. The horizontal location of force application was taken as the average depth of the center of gravity of the draped strands over the development length. Varying the height of load points would complicate the model more than necessary

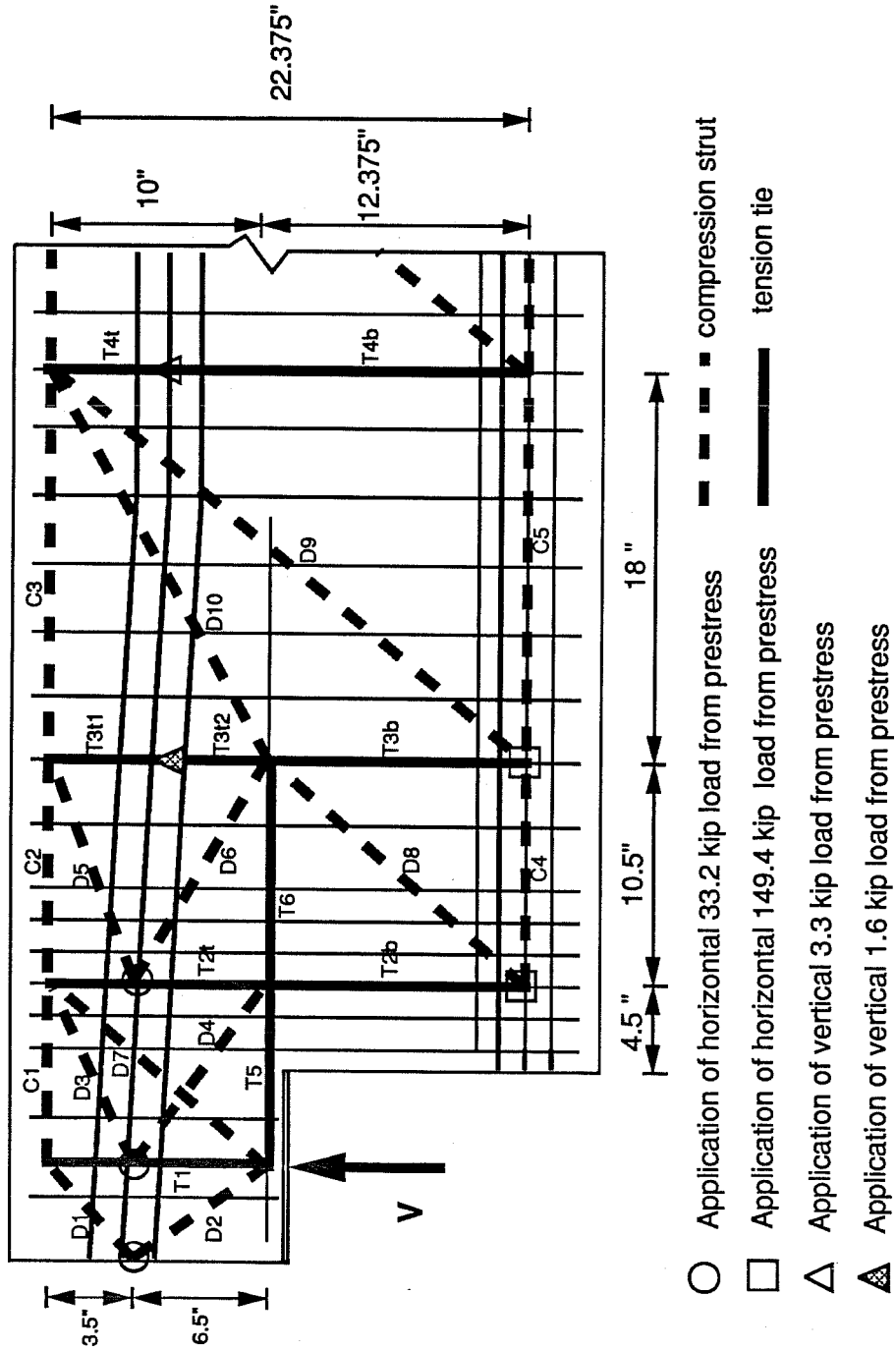


Figure 4.19 Final Strut-and-Tie model - Orthogonal

since the tendons are only draped 2.8 degrees. The horizontal prestress forces were assumed to transfer through the top of the beam using struts D1 through D6.

The vertical component of the draped prestressing strands was applied, in part, at both tension ties 3 and 4. Because the drape point did not fall directly on either vertical tie, the strand between these ties was modeled as a simply supported beam loaded at the drape point. Each tie was then loaded with its respective reaction force.

Geometric restrictions of the test specimen required forces from the straight strands to be applied at two points instead of three in the bottom of the full depth beam (see Fig. 4.19). Half of this force was induced at two locations along the center of gravity of the straight strands. These loads were transferred up through the beam by struts D8 and D9.

Compression strut D7 was assumed to carry the entire shear load as in the model without prestress. In Table 4.7 final compression forces and angles calculated using this model based both on the design shear of 100 kips and on the actual ultimate shear of 126.9 kips are presented.

Calculated and measured (from strain) tension forces are compared in Table 4.8. The force measured in tie T3t2 can be assumed to be in error based on how well all other values compare. The measured force in T4b compares the closest with the calculated value but is unconservative by 1%. All other ties carried forces at ultimate less than those calculated using the model. Measured forces in the five major ties ranged from -1% to 16% different from those calculated using the actual ultimate shear load (see Fig. 4.20). In general, the strut-and-

Compression Strut	Compression Force (kips)	Compression Force (kips)	Angle from Horizontal (degrees)
	V = 100	V = 126.9	
D1	27.4	27.4	37.9
D2	20.4	20.4	-55.3
D3	23.3	23.3	22.4
D4	14.6	14.6	-37.4
D5	22.7	22.7	18.4
D6	13.7	13.7	-31.8
D7	131.3	166.6	49.6
D8	131.3	166.6	49.6
D9	61.4	79.6	51.2
D10	110.6	136.8	29.1
C1	21.6	21.6	
C2	106.7	151.1	
C3	128.2	172.7	
C4	62.3	41.4	
C5	175.2	140.9	

**Table 4.7 Compression Forces and Angles for  
Orthogonal Strut-and-Tie Model**

Tension Tie	Measured Force at Ultimate	Calculated Force V = 100	$T_{meas} /$ $T_{calc}$ V = 100	Calculated Force V = 126.9	$T_{meas} /$ $T_{calc}$ V = 126.9
T1	5.3	16.8	0.32	16.8	0.32
T2t	74.4	108.9	0.68	135.8	0.55
T2b	109.9	100.0	1.10	126.9	0.87
T3t1	NA	7.2		7.2	
T3t2	37.2	8.8	4.23	8.8	4.23
T3b	79.3	47.9	1.66	94.9	0.84
T4t	NA	101.6		94.9	
T4b	98.2	104.9	0.93	97.4	1.01
T5	86.4	73.5	1.18	96.4	0.90
T6	78.5	61.9	1.27	84.8	0.93

Loads in kips

**Table 4.8 Calculated and Measured Tension Forces for  
Orthogonal Strut-and-Tie**

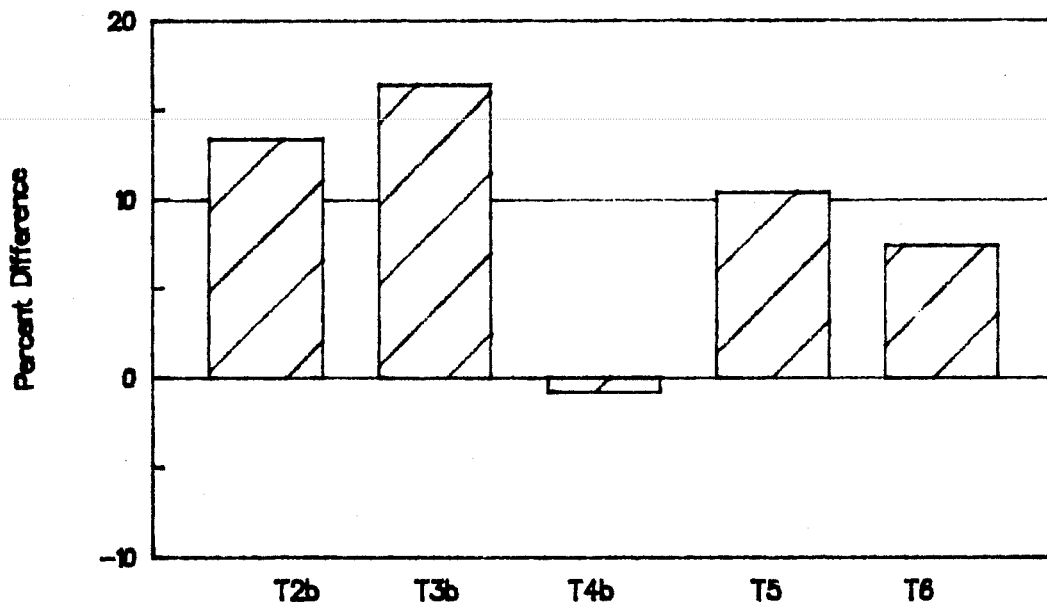


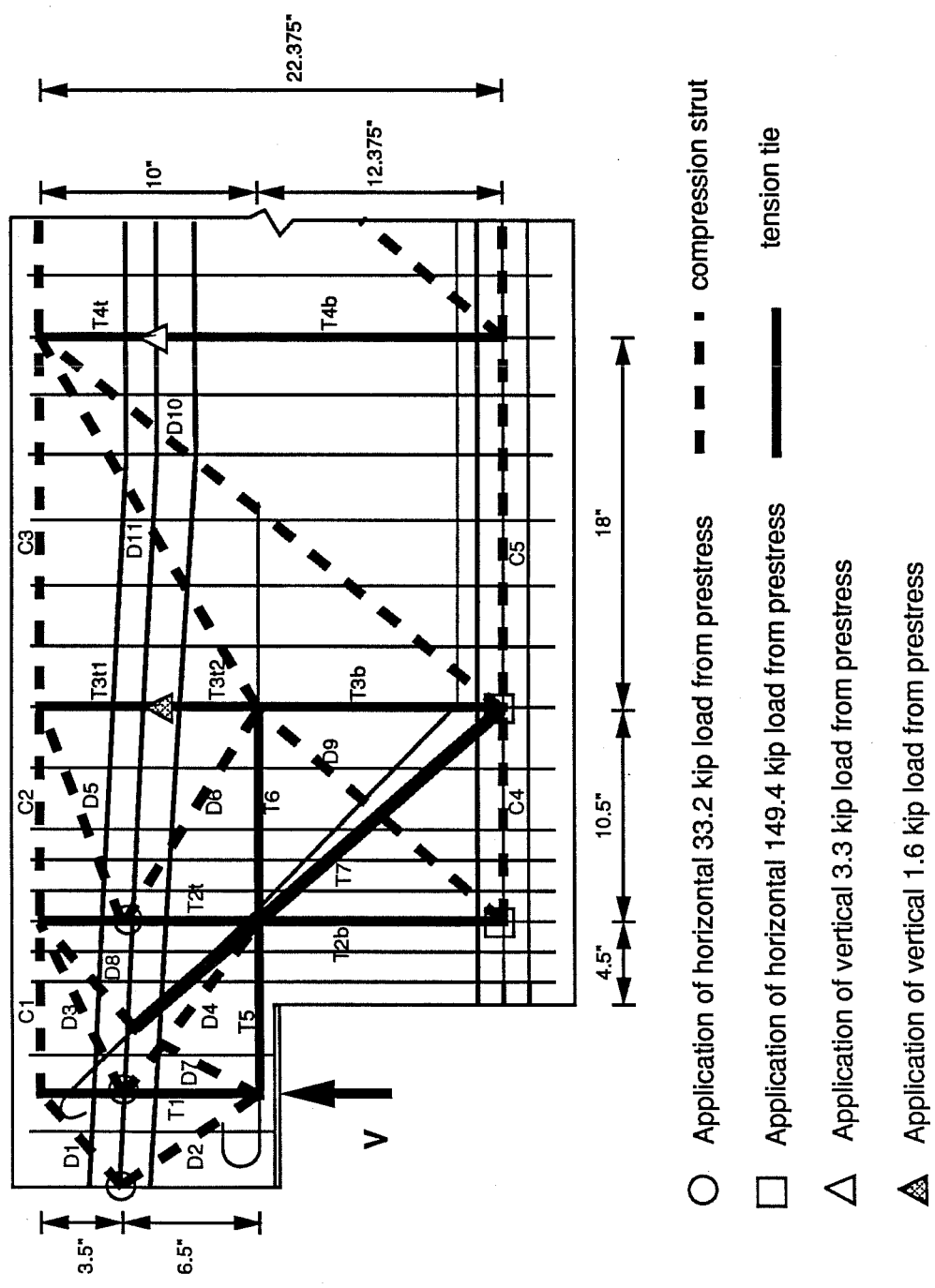
Figure 4.20 Percent Difference Between Measured and Calculated Tie Forces at Ultimate of OST Model

tie model shown in Figure 4.19 can be considered a conservative design model.

**4.8.3 Inclined Strut-and-Tie.** Prestress loads were incorporated into the inclined strut-and-tie model in the same manner as in the orthogonal model (see Fig. 4.21). Loads from draped strands were applied in thirds and transferred through the beam by struts D1 to D6. Straight strand loads were applied in halves and distributed up through the test specimen by struts D9 and D10.

Compression struts D7 and D8 were assumed to carry the shear load to the top of the beam. In Table 4.9 final compression forces and angles calculated using this combined model with a design shear of 100 kips and the actual ultimate shear of 121.1 kips are shown.

Calculated and measured tension forces are presented in Table 4.10. At the ultimate shear load, all measured tension forces were less than those calculated using the model of Figure 4.21. The force in tie T7 compared closest to the calculated force with a difference of less than 3%. Other tie forces were lower than the design force by up to 33% (see Fig 4.22). Based on the data collected during the IST test, the strut-and-tie model presented in Figure 4.21 can be considered a conservative design model.



- Application of horizontal 33.2 kip load from prestress
- Application of horizontal 149.4 kip load from prestress
- △ Application of vertical 3.3 kip load from prestress
- ▲ Application of vertical 1.6 kip load from prestress
- compression strut
- - - tension tie

Figure 4.21 Final Strut-and-Tie model - Inclined

Compression Strut	Compression Force (kips) V = 100	Compression Force (kips) V = 121.1	Angle from Horizontal (degrees)
D1	27.4	27.4	37.9
D2	20.4	20.4	-55.3
D3	23.3	23.3	22.4
D4	14.6	14.6	-37.4
D5	22.7	22.7	18.4
D6	13.7	13.7	-31.8
D7	115.5	139.9	60.0
D8	110.6	134.0	30.0
D9	72.6	87.9	49.6
D10	113.1	142.1	51.2
D11	27.7	24.7	29.1
C1	21.6	21.6	
C2	138.9	159.2	
C3	160.5	180.7	
C4	102.3	92.6	
C5	142.8	106.8	

**Table 4.9 Compression Forces and Angles for Inclined Strut-and-Tie Model**

Tension Tie	Measured Force at Ultimate	Calculated Force V = 100	$T_{meas}/T_{calc}$ V = 100	Calculated Force V = 121.1	$T_{meas}/T_{calc}$ V = 121.1
T1	9.8	16.8	0.58	16.8	0.58
T2t	47.7	64.2	0.77	75.9	0.63
T2b	49.1	55.3	0.89	67.0	0.73
T3t1	NA	7.2		7.2	
T3t2	5.5	8.8	0.63	8.8	0.63
T3b	42.3	43.4	0.98	56.6	0.75
T4t	NA	107.6		122.7	
T4b	NA	104.9		126.0	
T5	42.5	46.1	0.92	58.5	0.73
T6	31.6	34.5	0.92	46.9	0.67
T7	69.2	58.7	1.18	71.0	0.97

Loads in kips

**Table 4.10 Calculated and Measured Tension Forces for Inclined Strut-and-Tie**



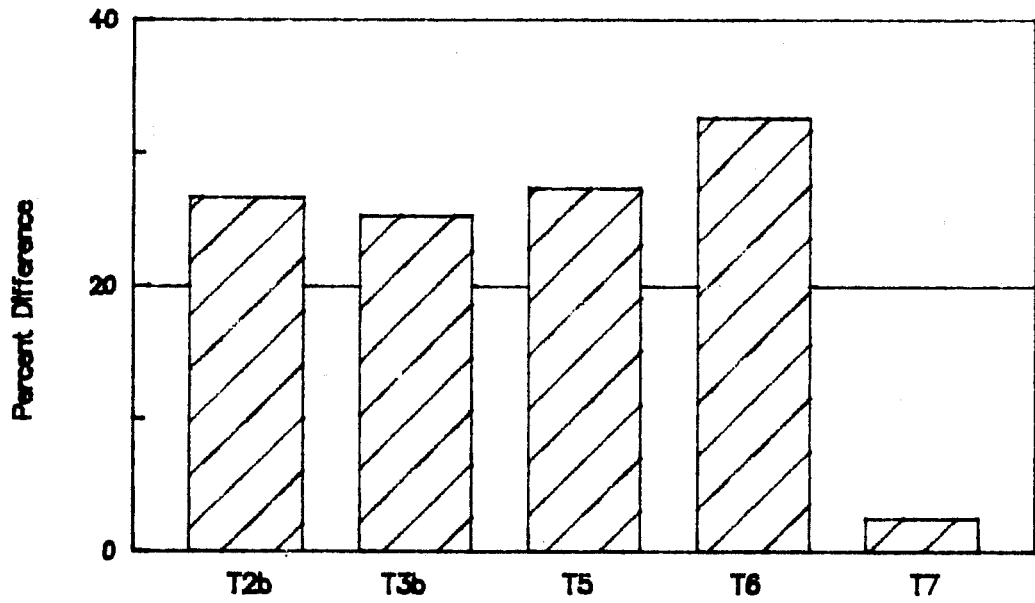


Figure 4.22 Percent Difference Between Measured and Calculated Tie Forces at Ultimate of IST Model

## CHAPTER 5

### SUMMARY AND CONCLUSIONS

#### 5.1 Summary

In the research described herein, the behavior of specimens designed with four different models for detailing the discontinuity region in the ends of dapped pretensioned beams was compared. The four different design methods were: 1) Prestressed Concrete Institute Method, 2) Menon/Furlong Method (currently used by the TSDHPT), 3) Orthogonal Strut-and-Tie Model (using only vertical and horizontal reinforcement), and 4) Inclined Strut-and-Tie Model (using a combination of vertical, horizontal, and inclined reinforcement). Each specimen was individually loaded in increments to failure. Strains in the reinforcement bars and strand, strand end slip, cracking loads, and deflections were observed.

A secondary objective was to determine how pretensioning forces can be incorporated into strut-and-tie models of dapped ends. After testing, the strut-and-tie models were revised to permit application of prestressing forces at nodes. Measured tie forces were compared to those calculated using the revised models.

#### 5.2 Conclusions

Based on observed behavior, the following conclusions can be made concerning the design of pretensioned dapped beams.

### **5.2.1 Ultimate Capacity.**

- 1) All design methods resulted in beam ends that carried loads 15-20% higher than predicted except for the PCI design method. This specimen failed at a load lower than predicted due to poor local detailing of vertical hoop bars.

### **5.2.2 Cracking Patterns.**

- 1) First cracking occurred at very low loads at the dap interface corner in all specimens.
- 2) Cracks were more evenly distributed across the depth of the beam in the specimens designed using strut-and-tie models than in the two other specimens.

### **5.2.3 Efficiency.**

- 1) The M/F specimen carried 6 to 10% more load per cubic inch of steel reinforcement within the beam end than the strut-and-tie models.
- 2) The OST specimen carried the most load per unit cost of construction based on estimated construction operation units.
- 3) Strut-and-tie model specimens were 11 to 29% more efficient than the PCI and M/F models based on load carried per construction operation unit.
- 4) Standard hooks in the main horizontal reinforcement within the dap provided adequate anchorage so that welding could be avoided in the IST specimen.

### **5.2.3 Comparison of Strut-and-Tie Models to Observed Behavior.**

- 1) Calculated ultimate loads based on strut-and-tie models were 15 and 19% less than measured loads at failure for two tests.

- 2) At failure, forces measured in the major ties of the OST specimen were less than their predicted values.
- 3) At failure, forces measured in the major ties of the IST specimen were less than their predicted values.
- 4) Since the strut-and-tie model is supposed to be a lower bound plasticity solution, the conservative results verify that it is such a lower bound solution.

## APPENDIX A

This appendix contains plots of applied load versus strains measured by electronic strain gages. One plot of applied load vs. strand slippage measured by a dial gage is also included. Strain gage numbers refer to numbers in Figures 3.24 through 3.27. Tension tie numbers refer to Figures 3.11 and 3.15.

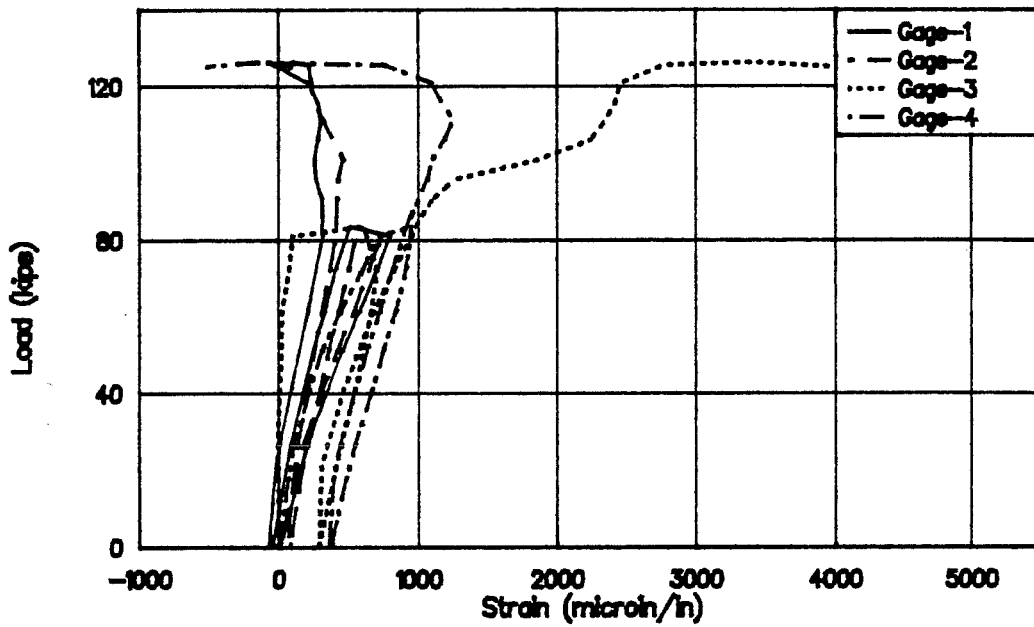


Figure A.1 Applied Load vs. Strain in Tie 2 of PCI Test

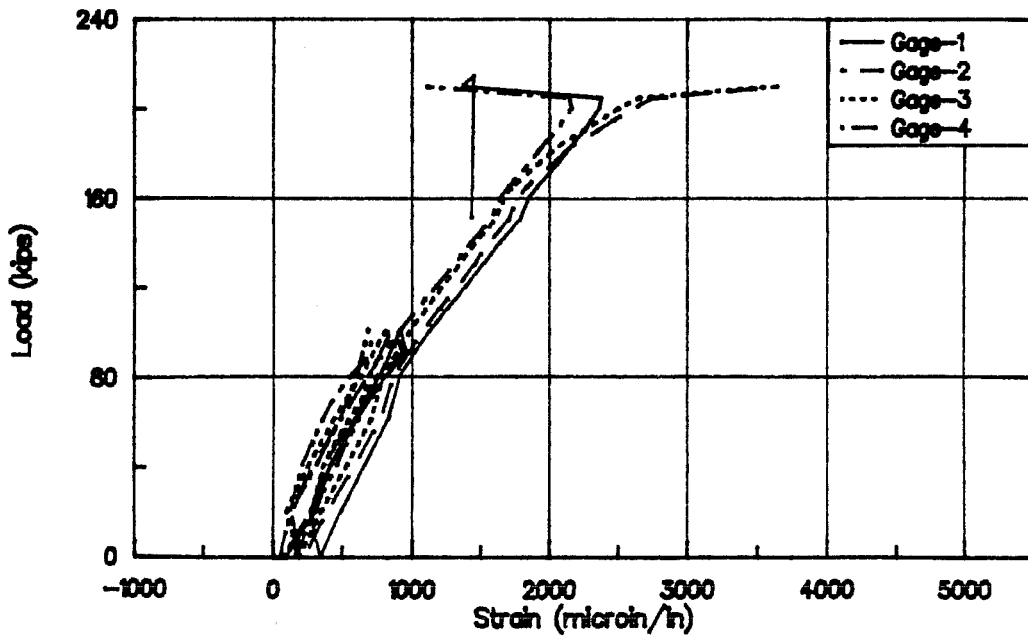


Figure A.2 Applied Load vs. Strain in Tie 2 of M/F Test

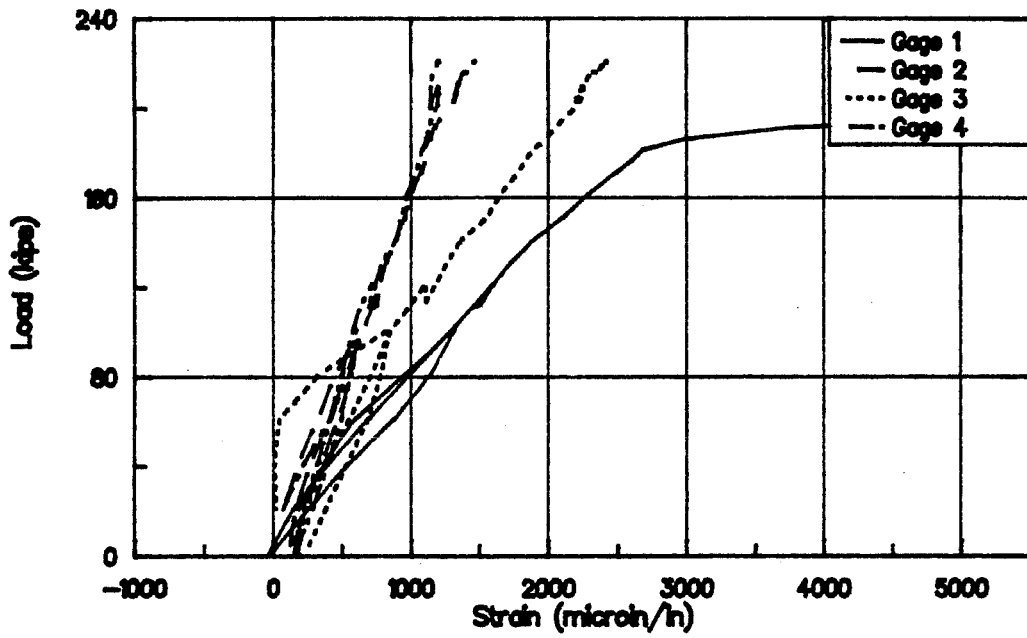


Figure A.3 Applied Load vs. Strain in Tie 2 of OST Test

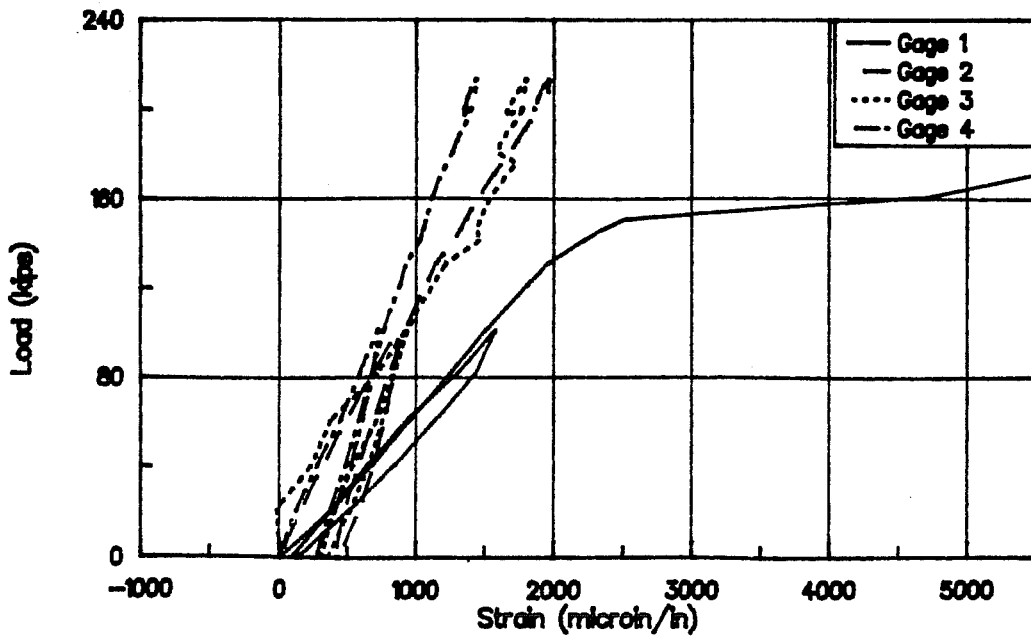


Figure A.4 Applied Load vs. Strain in Tie 2 of IST Test

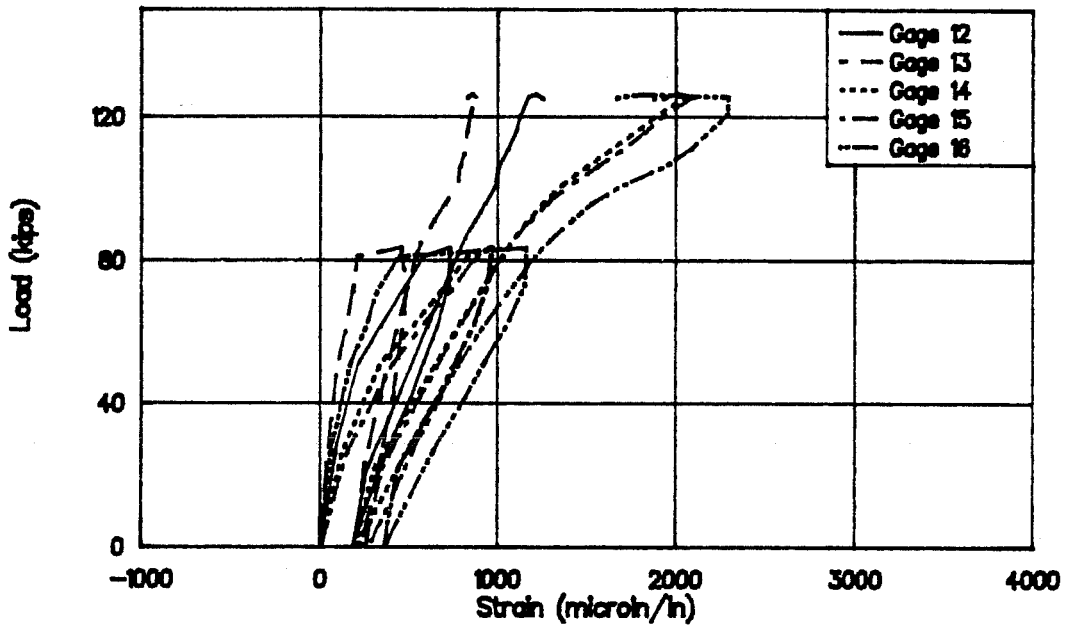


Figure A.5 Applied Load vs. Strain in Horizontal Dap Reinforcement of PCI Test

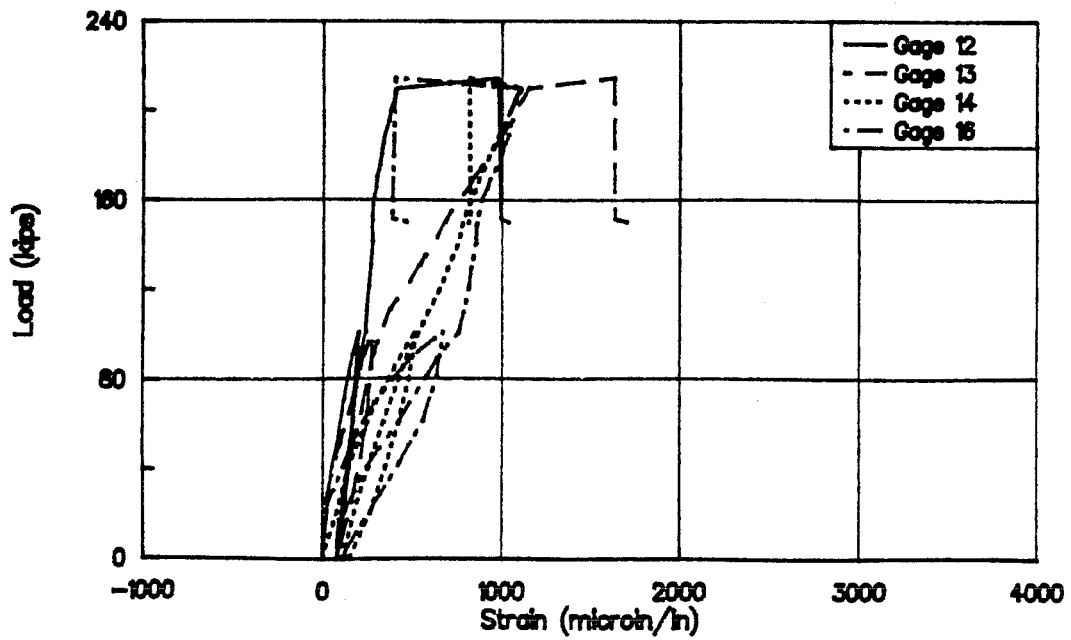


Figure A.6 Applied Load vs. Strain in Horizontal Dap Reinforcement of M/F Test



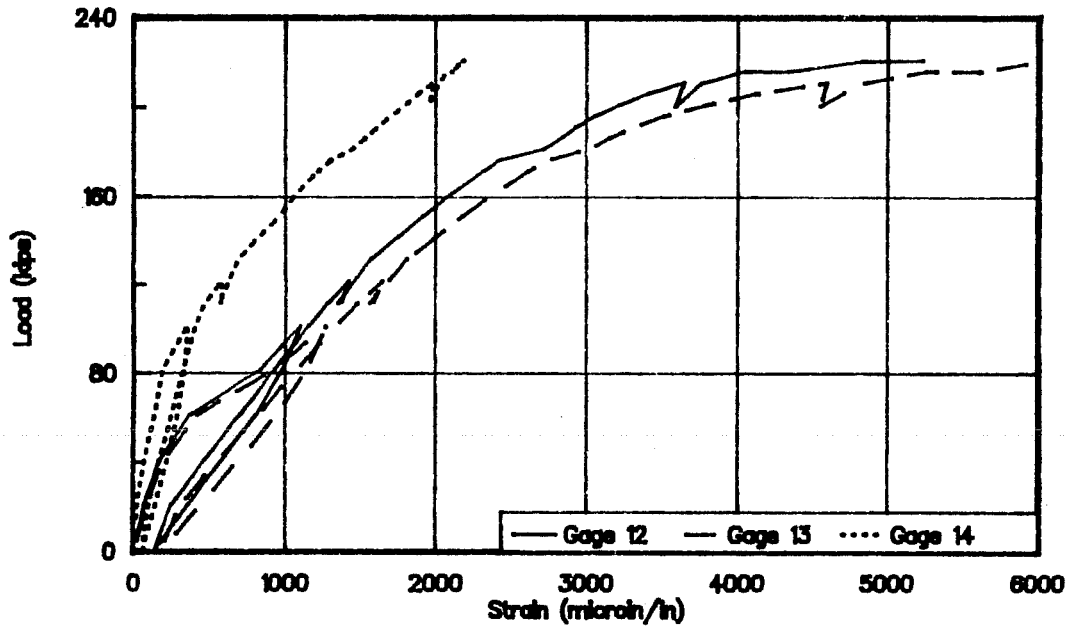


Figure A.7 Applied Load vs. Strain in Horizontal Dap Reinforcement of OST Test

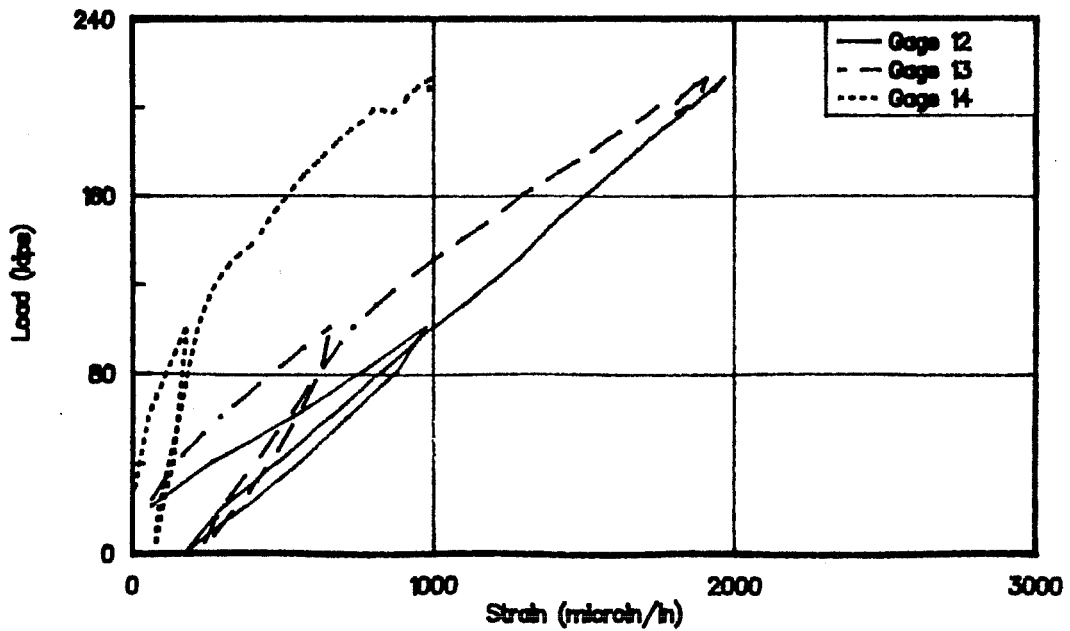


Figure A.8 Applied Load vs. Strain in Horizontal Dap Reinforcement of IST Test

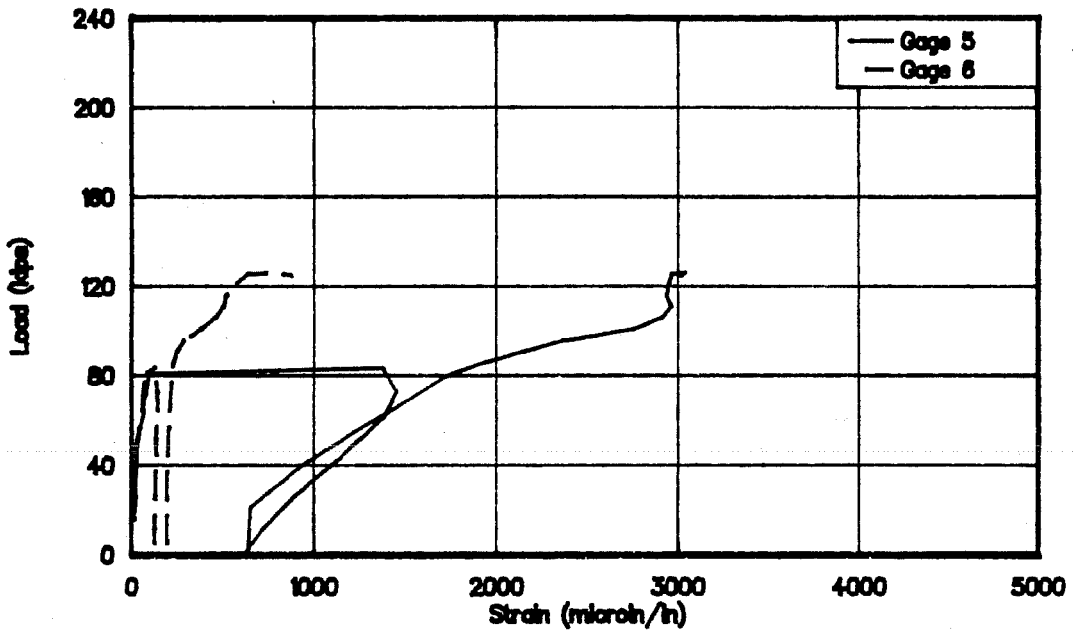


Figure A.9 Applied Load vs. Strain in Tie 3 of PCI Test

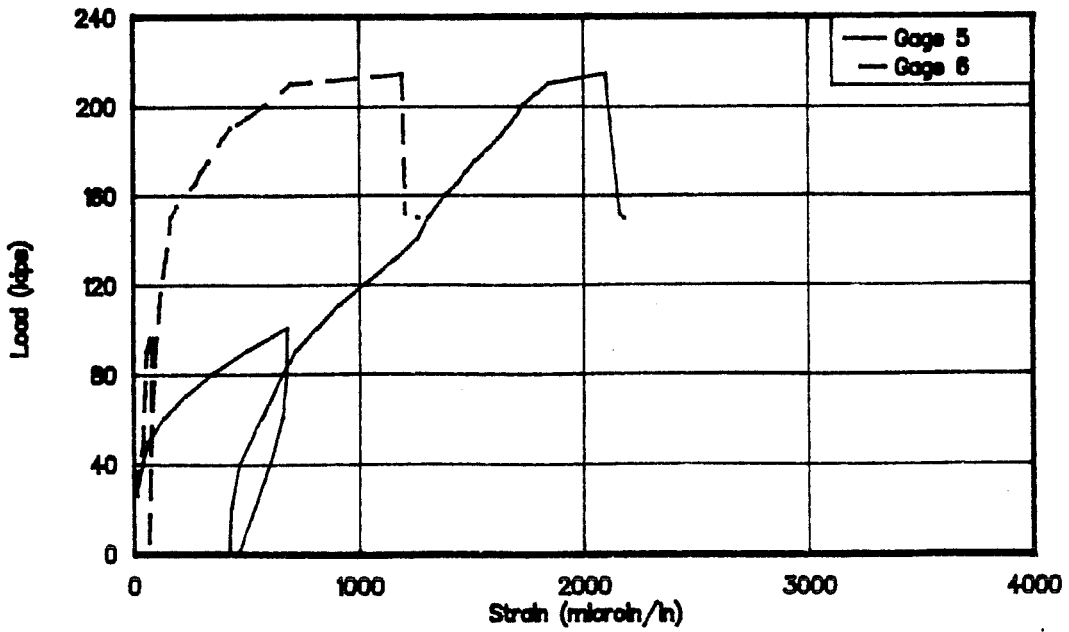


Figure A.10 Applied Load vs. Strain in Tie 3 of M/F Test

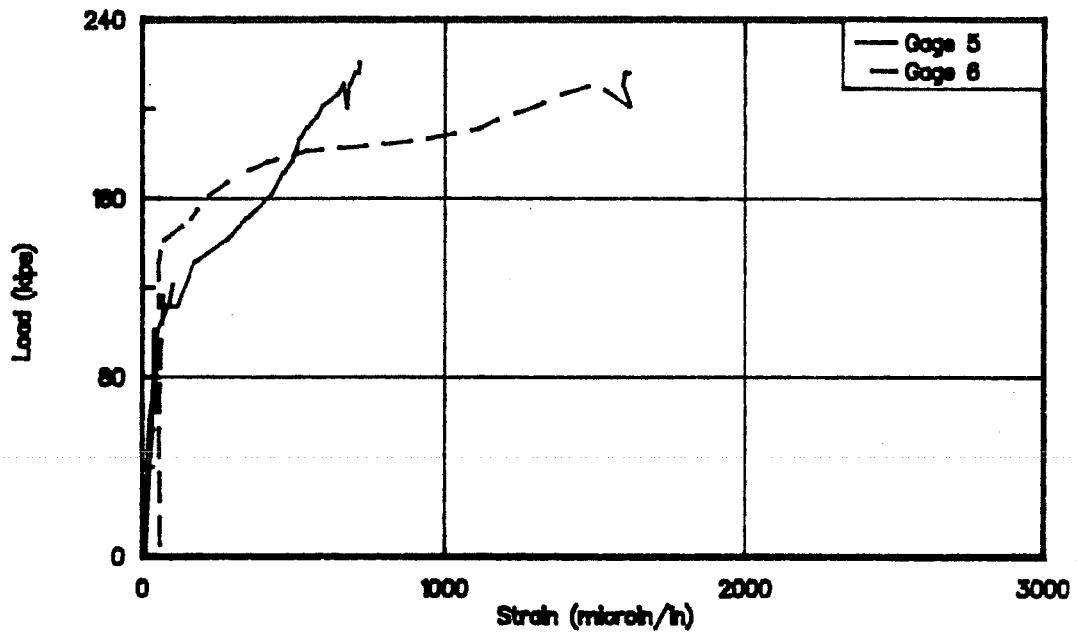


Figure A.11 Applied Load vs. Strain in Tie 3 of OST Test

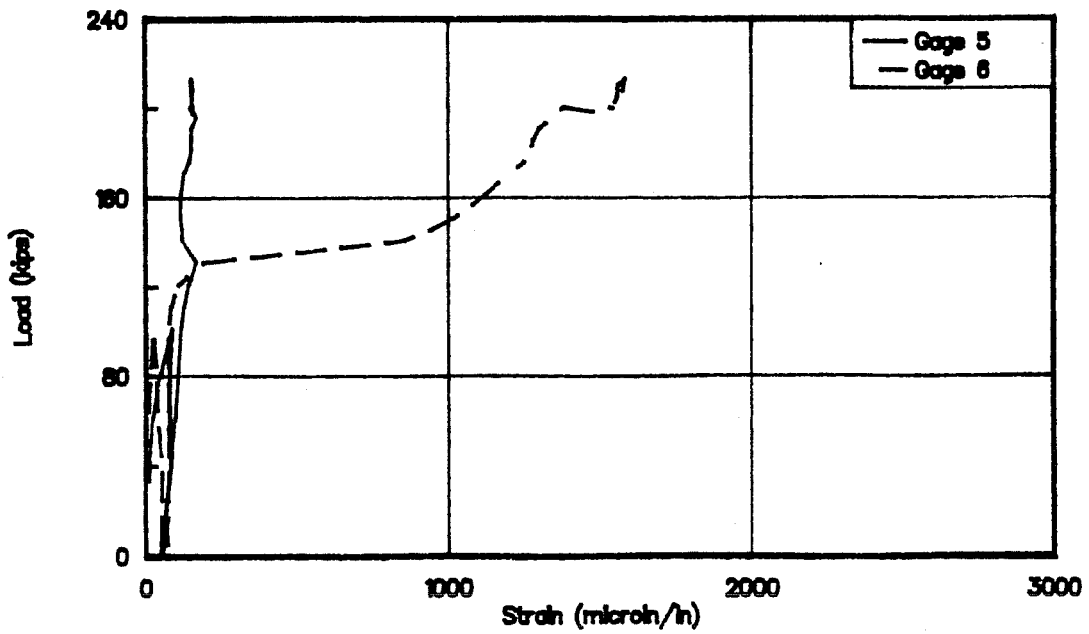


Figure A.12 Applied Load vs. Strain in Tie 3 of IST Test

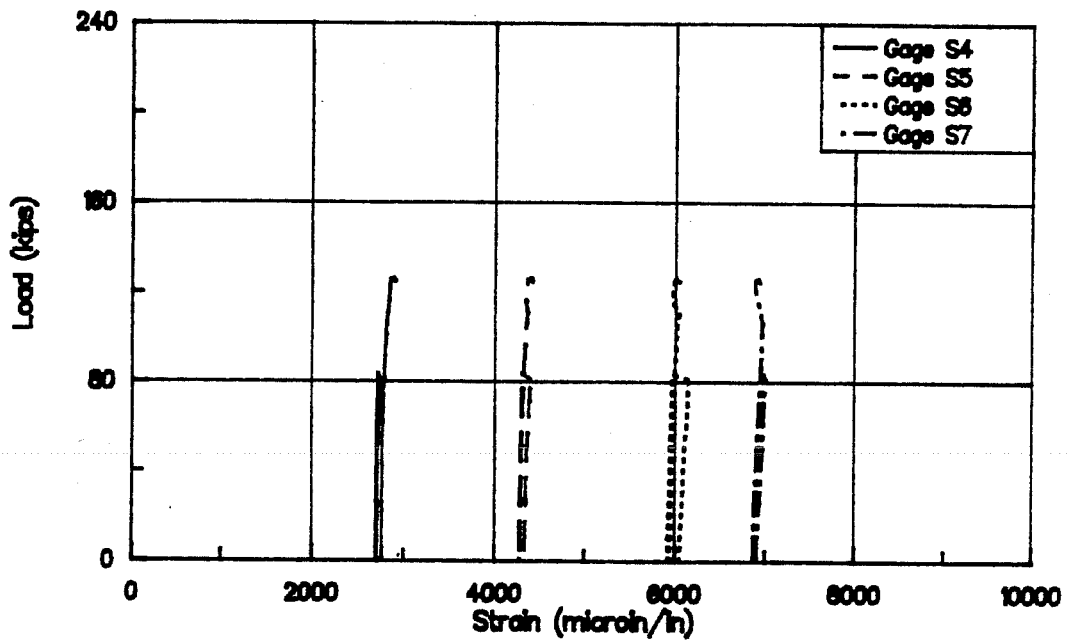


Figure A.13 Applied Load vs. Straight Strand Strain of PCI Test

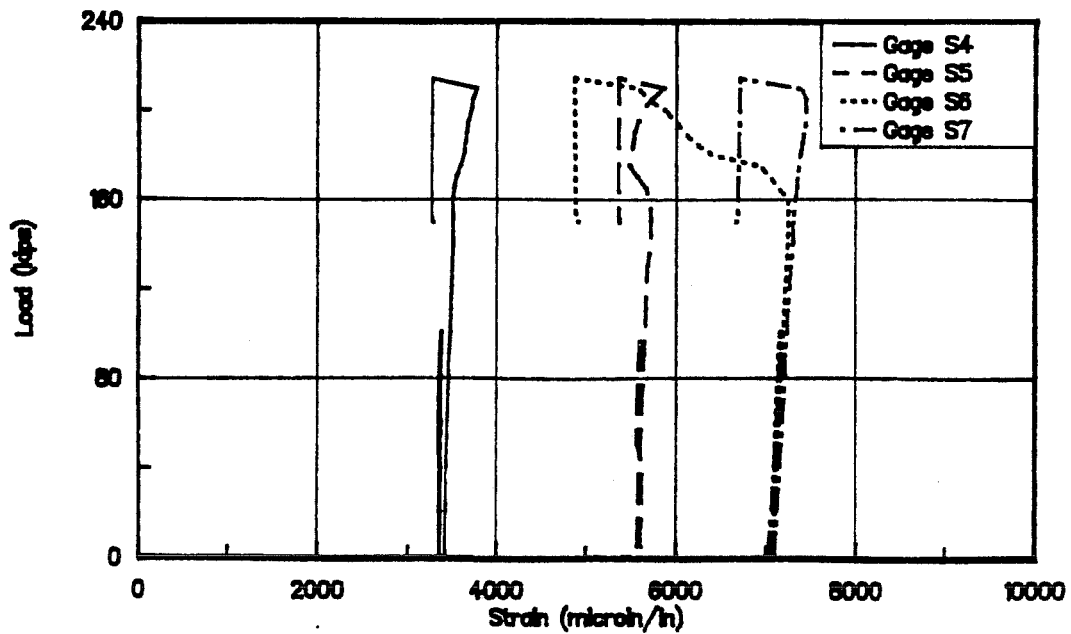


Figure A.14 Applied Load vs. Straight Strand Strain of M/F Test

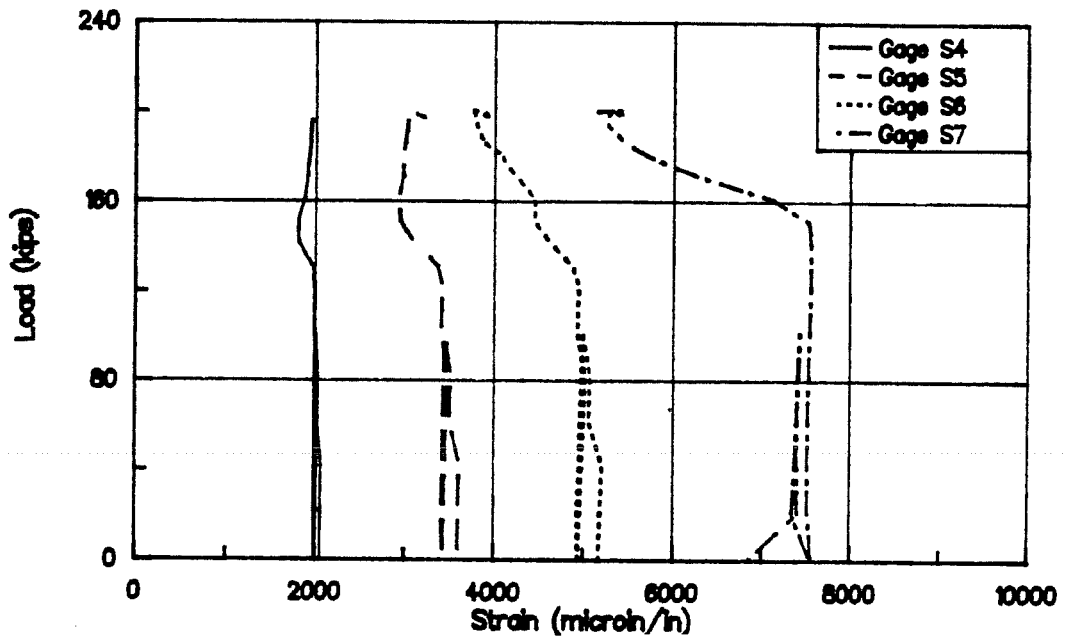


Figure A.15 Applied Load vs. Straight Strand Strain of IST Test

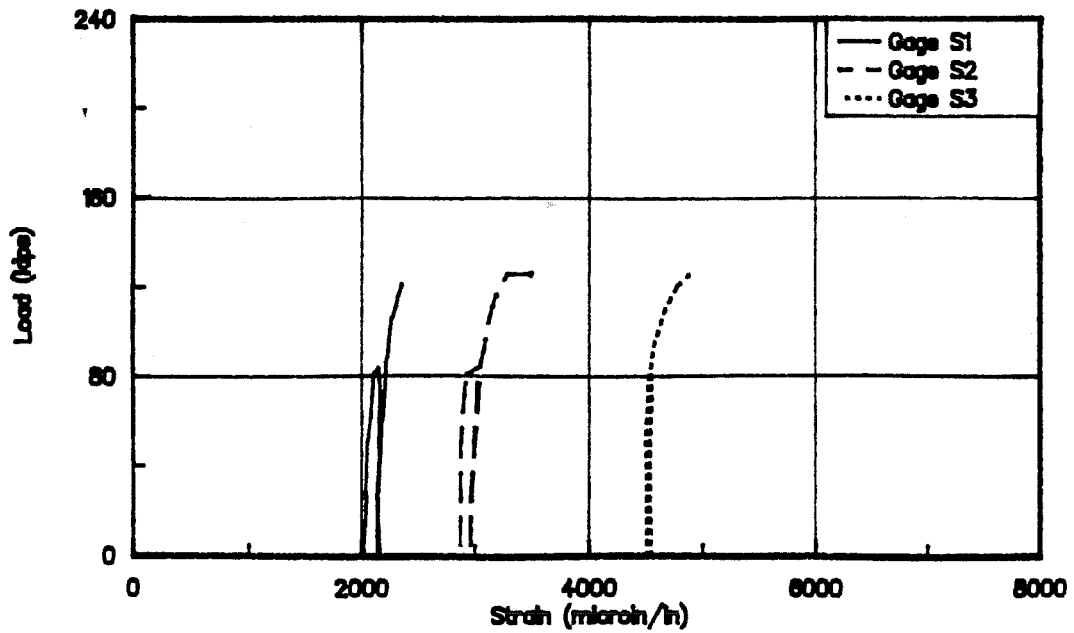


Figure A.16 Applied Load vs. Draped Strand Strain of PCI Test

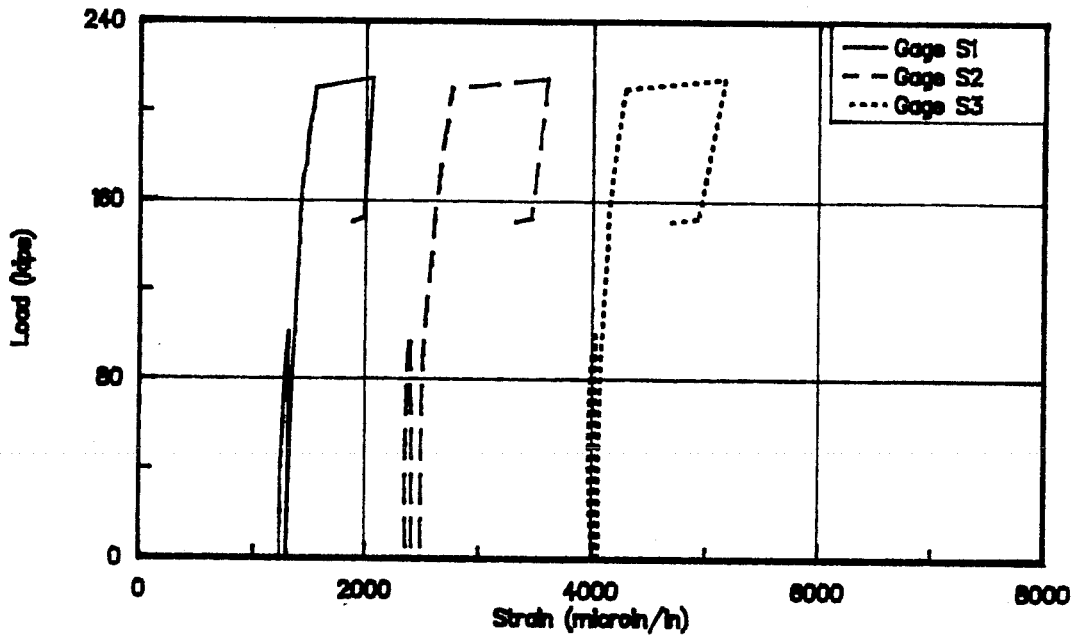


Figure A.17 Applied Load vs. Draped Strand Strain of M/F Test

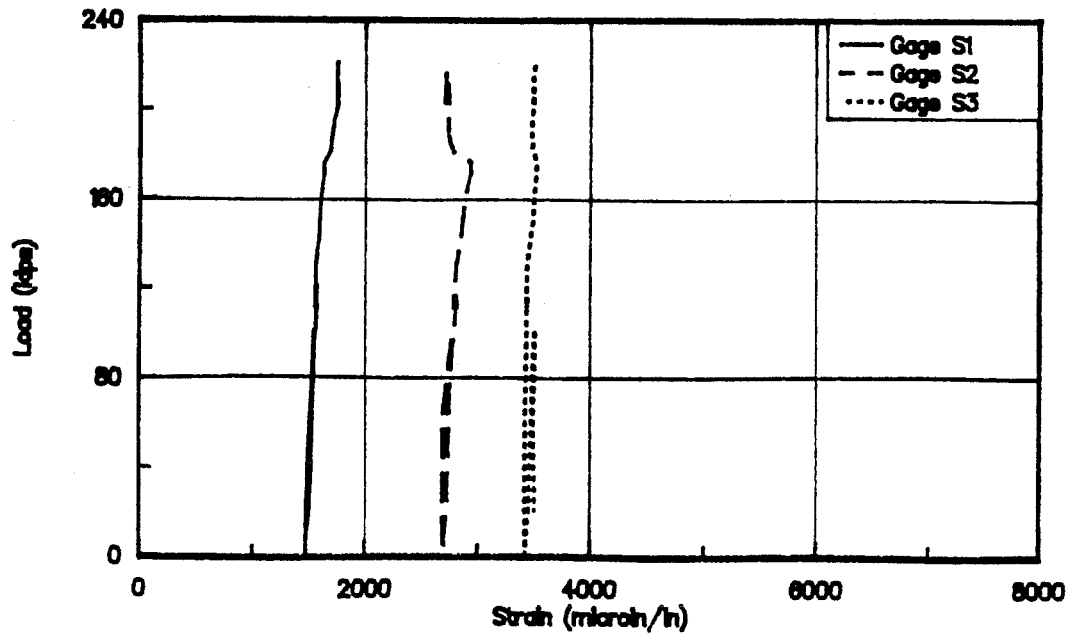


Figure A.18 Applied Load vs. Draped Strand Strain of OST Test

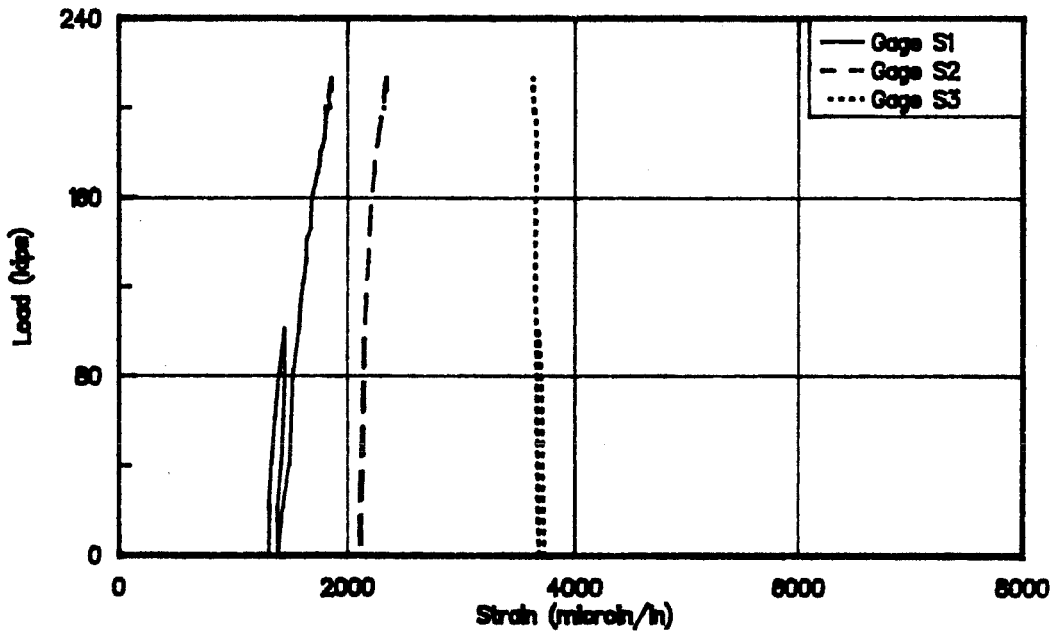


Figure A.19 Applied Load vs. Draped Strand Strain of IST Test

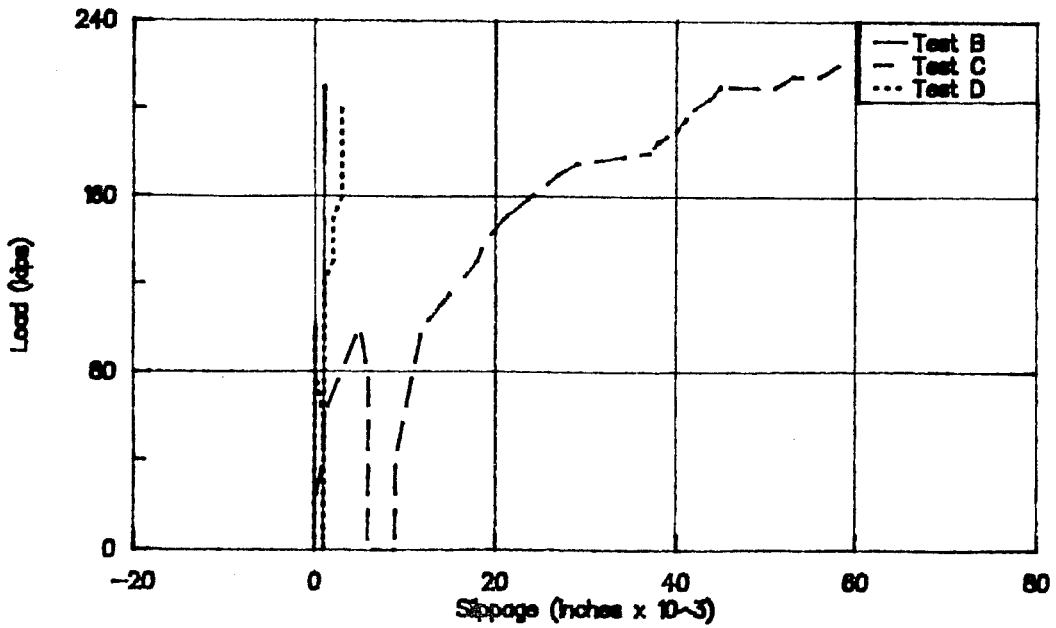


Figure A.20 Applied Load vs. Draped Strand Slippage of All Tests

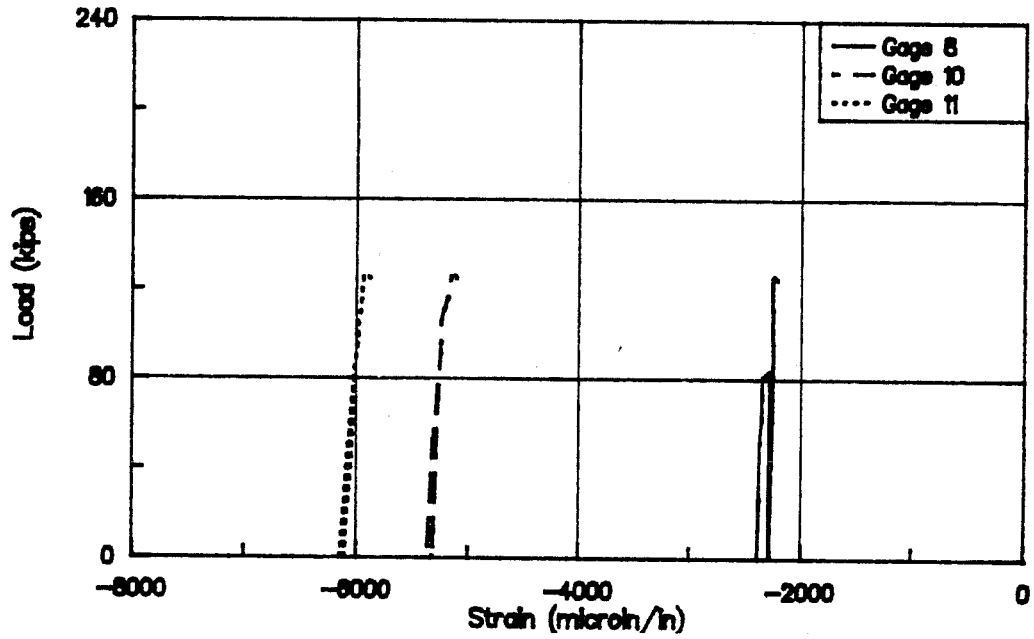


Figure A.21 Applied Load vs. Main Flexural Reinforcement Strain of PCI Test

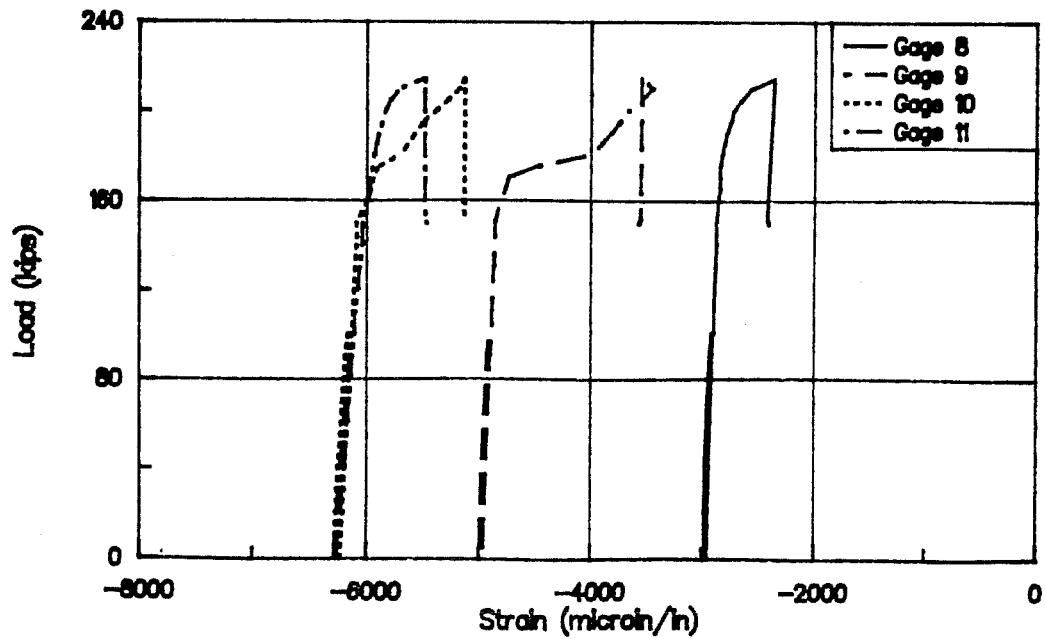


Figure A.22 Applied Load vs. Main Flexural Reinforcement Strain of M/F Test



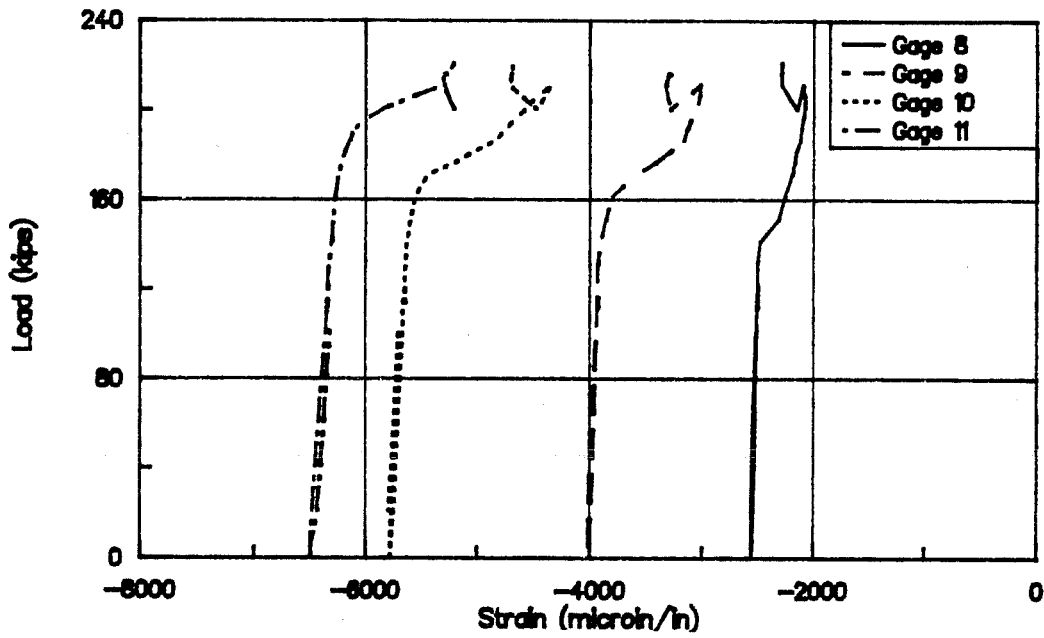


Figure A.23 Applied Load vs. Main Flexural Reinforcement Strain of OST Test

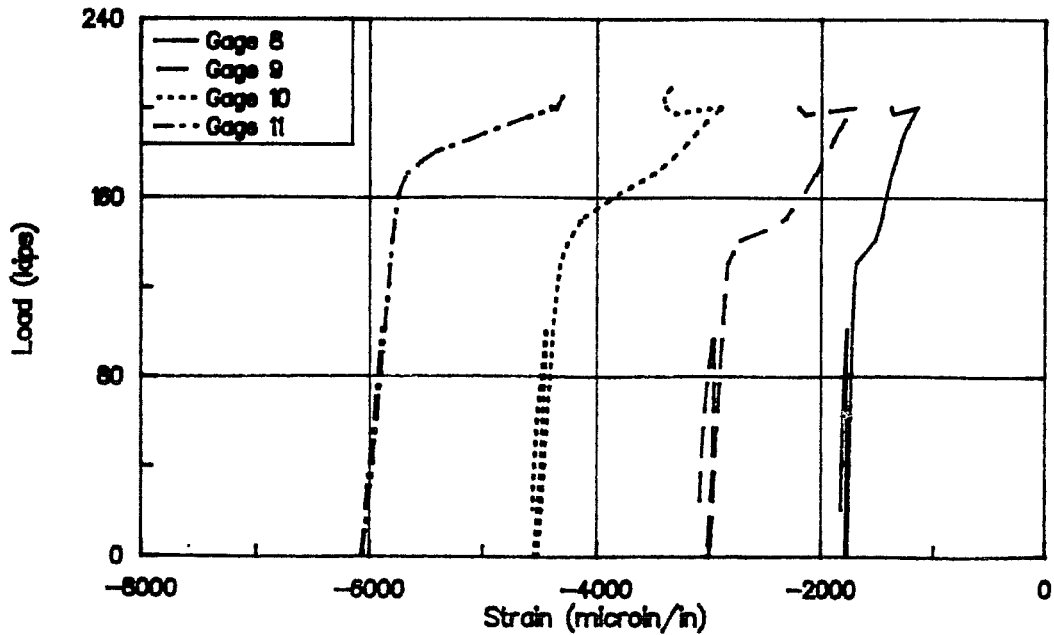


Figure A.24 Applied Load vs. Main Flexural Reinforcement Strain of IST Test

## REFERENCES

1. American Concrete Institute, Building Code Requirements for Reinforced Concrete (ACI 318-83), Detroit, 1983, 111 pp.
2. Barton, D.L., "Detailing of Structural Concrete Dapped End Beams", Unpublished Master's Thesis, The University of Texas at Austin, Dec. 1988.
3. Bergmeister, K., Breen, J.E., Jirsa, J.O., and Kreger, M.E., "Detailing for Structural Concrete" - Draft Report, Research Report 1127-3F, Center for Transportation Research, The University of Texas at Austin, Sept. 1989.
4. CEB-FIP, Model Code for Concrete Structures, CEB-FIP International Recommendations, Third Edition, Comite Euro-International du Beton, Paris, France, 1978, 348 pp.
5. Collins, M.P., and Mitchell, D., "Shear and Torsion Design of Prestressed and Non-Prestressed Concrete Beams", PCI Journal, Vol. 25, No. 5, Sept./Oct. 1980, pp. 32-100.
6. Libby, J.R., Modern Prestressed Concrete: Design Principles and Construction Methods, Third Edition, Van Nostrand Reinhold Company, New York, 1971, pp. 166-171.
7. Marti, P., "Truss Models in Detailing", Concrete International, Dec. 1985, pp. 66-73.
8. Marti, P., "Staggered Shear Design of Simply Supported Concrete Beams", ACI Journal, Jan./Feb. 1986, pp. 36-42.
9. Mattock, A.H., and Chan, T.C., "Design and Behavior of Dapped-End Beams", PCI Journal, Vol. 24, No. 6, Nov.-Dec. 1979, pp. 28-44.

10. Mattock, A.H., and Theryo, T., "Strength of Members with Dapped Ends," PCI Research Project No. 6 Report, University of Washington, Seattle, 1986.
11. Menon, G., and Furlong, R.W., "Design of Reinforcement for Notched Ends of Prestressed Concrete Girders," Research Report 196-1F, Center for Transportation Research, Bureau of Engineering Research, The University of Texas at Austin, 1977.
12. Nielsen, M.P., Braestrup, M.W., Jensen, B.C., and Bach, F., "Concrete Plasticity, Beam Shear -- Shear in Joints -- Punching Shear", Special Publication, Danish Society for Structural Science and Engineering, Technical University of Denmark, Lyngby, 1978, 129 pp.
13. Powers, A.C., "Shear Strength of Pretensioned Concrete Girders in Negative Moment Regions", Unpublished Master's Thesis, The University of Texas at Austin, May 1990.
14. Prestressed Concrete Institute, PCI Design Handbook (Third Edition), Chicago, Illinois, 1985, pp. 6.28-6.32.
15. Ramirez, J., "A Truss Analysis of the Shear and Torsional Strength of Beams", PhD Thesis, The University of Texas at Austin, 1984.
16. Rogowsky, D.M., and MacGregor, J.G., "Design of Reinforced Concrete Deep Beams", Concrete International, Aug. 1986, pp. 49-58.
17. Schlaich, J., Schafer, K., and Jennewein, M., "Special Report: Toward a Consistent Design of Structural Concrete", PCI Journal, May/June 1978, pp. 74-150.
18. Thurlimann, B., "Shear Strength of Reinforced and Prestressed Concrete Beams -- CEB Approach", Presented at ACI Symposium 1976, Philadelphia, PA 33 pp.

## VITA

Donna June Mader was born in Garnett, Kansas to Clair and Agnes Mader. She received a Bachelor of Science in Civil Engineering from the University of Kansas in May, 1988. In August, 1988, she entered The Graduate School of The University of Texas.

Permanent address: RR3 Box 210  
Garnett, KS 66032

This thesis was typed by Donna J. Mader.